ASSESSING THE UTILIZATION OF REMOTE SENSING AND GIS TECHNIQUES FOR FLOOD STUDIES AND LAND USE/LAND COVER ANALYSIS THROUGH CASE STUDIES IN NIGERIA AND THE USA.

by

Dorcas Idowu

A thesis submitted to the Faculty and the Board of Trustees of the Colorado School of Mines in partial fulfillment of the requirements for the degree of Doctor of Philosophy (Geological Engineering).

Golden, Colorado

Date ----------

Signed: ----------

Dorcas Idowu

Signed: ----------

Dr. Wendy Zhou
Thesis Advisor

Golden, Colorado

Date ----------

Signed: ----------

Dr. Wendy Bohrson
Professor and Head
Department of Geology and Geological Engineering

ABSTRACT

Globally, there has been a rise in geologic hazards such as flooding. A rise, which has often been attributed to climate change. First world countries especially the United States of America have well-structured ground and space-based flood monitoring systems through which data are obtained to provide real-time flood prediction and warnings to stakeholders. However, developing regions of the world mostly suffer the devastating effect of flooding due to a lack of adequate flood monitoring systems to provide accurate flood warnings. Land-use changes associated with an increase in impervious surface resulting from vegetation loss and/or replacement of flood plains and wetland with pavements are known to increase flood intensity. Hence, knowing how land cover changes affect floods in an area is therefore crucial to mitigating it and so is knowing the flood hazard level for these areas. In this study, we evaluated the effectiveness of the Gravity Recovery and Climate Experiment data (GRACE) storage-based Flood Potential Index (FPI) at correctly predicting floods in Nigeria with a focus on its efficacy at predicting past floods in the country. A newly derived Water Budget-based FPI was assessed and compared to the GRACE-FPI in terms of its capability to predict floods in the Mississippi River basin in the USA. Finally, the influence of changes in LULC on flooding was assessed for Lagos State using satellite datasets.

TABLE OF CONTENTS

LIST OF FIGURES

LIST OF TABLES

LIST OF SYMBOLS

ds/dt …….Monthly change in terrestrial water storage *(cm)*

P ……Precipitation *(cm)*

R ……..Runoff *(cm)*

ET …… ….Evapotranspiration *(cm)*

SM ……. …..Soil moisture *(cm)*

GW …….....Groundwater

TWSC ……..Terrestrial Water Storage Capacity *(cm)*

(t-1) ……Represent previous month

t ……Time (months)

Sdef …….Storage deficit

Smax …….Historic maximum storage capacity *(cm)*

TWSA ……Terrestrial Water Storage Anomaly *(cm)*

Pmon ……..Monthly precipitation

F …….....Flood potential

FPI ……...Flood Potential Index

Ef ……..Efficiency Index

n ……..Number of samples

X ……. …..Observation value

Y ……...Simulated value

Z …….....Observed data

∞ ……. …...Infinity

NSE ……Nash-Sutcliffe Efficiency

r ……..Pearson's correlation coefficient

R^2 ……Coefficient of determination

TP ……True Positive

FP …….....False Positive

FN ……... False Negative

TN ……True Negative

TPR ……True Positive Rates

FPR ……False Positive Rates

Y_t ……LULC map product from the past and recent years

Y_{t1} …….....LULC map from previous year

Y_{t2} …….....LULC map from recent year

CD ……Change detection

W_j ……..Hybrid weight *(%)*

X_j ……AHP weight *(%)*

Y_j …….....Entropy weight *(%)*

FHI …….....Flood Hazard Index

C_i ……i^{th} Criterion

w_i …….....Criteria weights *(%)*

LIST OF ABBREVIATIONS

National Aeronautics and Space Administration…….....NASA

Gravity Recovery and Climate Experiment Follow-On……..GRACE-FO

Terrestrial Water Storage……. ……TWS

Terrestrial Water Storage Anomaly……TWSA

Flood Potential Index…….....FPI

Lower Niger River Basin……. …….....LNRB

Water Budget…….....WB

Land Use and Land Cover…….....LULC

Dartmouth Flood Observatory……. ……..DFO

United States……US

Moderate Resolution Imaging Spectroradiometer……. ……...MODIS

Land Information System…….....LIS

Niger River Basin……...NRB

National Emergency Management Agency…….....NEMA

GeoforschungsZentrum…….....GFZ

Center for Space Research……..CSR

Jet Propulsion Laboratory…….....JPL

Global Precipitation Climatology Centre…….GPCC

National Oceanic and Atmospheric Administration…….....NOAA

Land-Surface Model……..LSM

North American Land Data Assimilation System…….NLDAS

Modelling, Analysis, Prediction and Projections…….MAPP

United States Geological Survey……..USGS

Receiver Operative Characteristics…….....ROC

Multiple-Criteria Decision-Making……...MCDM

Geographic Information System……..GIS

Analytic Hierarchy Process……AHP

Enhanced Thematic Mapper Plus…….....ETM+

Operational Land Imager…….OLI

Shuttle Radar Topography Mission…….....SRTM

Digital Elevation Model……DEM

ACKNOWLEDGEMENT

I would like to thank my thesis advisor – Dr. Wendy Zhou for her invaluable supervision, support, and tutelage during my pursuit of the doctoral degree. Her immense knowledge, guidance and plentiful experience have encouraged me in all the time of my academic research and daily life. My gratitude extends to the American Association of University Women (AAUW), Chevron International Fellowship and the Geological Society of America for the funding opportunities to undertake my studies at the Department of Geology and Geological Engineering, Colorado School of Mines. My thanks go out to the member of my thesis committee for their kind and constructive criticism and guidance. I would like to thank Dr. Zhou's research group past and present for a cherished time spent together and for their contributions over the course of my program. My appreciation also goes out to my parents and friends for their encouragement and support all through my studies. Finally, I would like to express my gratitude to my darling husband and daughter. Without their tremendous understanding and encouragement in the past few years, it would be impossible for me to complete my study. Thanks for being there always!

To God be the Glory.

CHAPTER 1

GENERAL INTRODUCTION

1.1 Research Motivations

Longer lead-time flood prediction could significantly lessen flood-related hazards. It is not enough to know only rainfall intensities and durations. Still, accurate flood prediction requires knowledge of antecedent conditions and the hydrological responses of events for a spectrum of antecedent states. Especially important is information on the hydrologic state of an entire river basin before catastrophic rainfall events. Unfortunately, such detailed measurements are difficult to acquire with current hydrological networks, primarily providing flood stages. Land use can also play a critical role in flood hazards. It is well known that land-use changes that cause faster runoff and less temporary storage enhance flood risks, but how much has not been quantified. Remotely sensed imagery could provide valuable synoptic information on vegetative covers and changes over time, along with topographic data. We hypothesize that we can use a forensic approach to evaluate past catastrophic flooding events using the contributions of land-use changes and changes in water storage from GRACE and other satellite data. We are also interested in analyzing and determining the contributions of land-use changes and antecedent moisture conditions to observed flooding.

1.2 Research Objectives and Questions

This research aims to improve early flood warning by applying Reager and Famiglietti [1] methodology to Nigeria and evaluate the efficacy of the GRACE-based FPI using the catastrophic 2012 flooding as ground truth. The result is assessed by comparing Water-budget derived FPI and the Dartmouth Flood report. Thereby demonstrating the importance of the integration of remotely sensed data for flood predictions in Nigeria [2].

However, one major limitation of the GRACE data is its low spatial resolution (1° x 1°). A study area needs to be greater than 200,000 km^2 to enable the extraction of meaningful information relevant for hydrologic studies from the GRACE data. Hence, the second objective is to apply the Water-Budget-based FPI at a higher spatial resolution of 0.25° x 0.25° in a flood

warning study. This approach is demonstrated through a case study of predicting the 2019 Mississippi River flooding in the US. The predicting accuracy is evaluated using GRACE-based FPI, which could further strengthen the use of Water Budget-based FPI to supplement GRACE-based FPI [3].

The third objective was to evaluate and quantify Land Use and Land Cover (LULC) changes in Lagos state Nigeria and how it relates to flooding by creating a flood hazard map. This study demonstrates how (1) satellite data can be used for flood hazard mapping and (2) LULC changes, urban expansion, and population growth influence flooding in Lagos State, Nigeria. Ultimately, we want to answer the questions: Can the flood potential in Nigeria be evaluated effectively and correctly using remotely sensed data? Can GRACE-based Flood Potential Index (FPI) effectively predict past floods in Nigeria? How does a Water Budget-based FPI with higher spatial resolution compare to GRACE-derived FPI? How is the new FPI performance at predicting historical floods in the Mississippi River Basin? How much has the Land Use and Land Cover changed in Lagos State over the past three decades? How have these changes impacted the annual flooding in the State?

1.3 Background of Study

In Nigeria, Flooding is a major natural disaster resulting from high rainfall intensity. The country's riverine and coastal areas are mostly affected by devastating floods with the annual occurrence and leading to loss of lives and properties. Pluvial flooding is another typical type of flooding uniquely to most urban cities in Nigeria. There has been an alarming rise in the areas exposed to flooding in large cities of the country. Apart from the Ogunpa Stream in Ibadan that killed several people and completely grounded socio-economic activities in 1980, there has been an increase in economic losses due to flooding in the country. However, this systematic rise reached a crescendo with the floods of 2012 (the worst flooding in 50 years), claiming over 400 lives across 30 affected states, displacing about 2 million people, while a total loss of about 2.29 trillion Naira (7.26 billion US Dollars) was estimated (Figure 1.1). In 2018, there was a presidential declaration of national disaster for Kogi, Niger, Anambra, and Delta states. The September 2020 flooding in the Northern part of Nigeria resulted in 21 deaths, destroyed thousands of homes, and displaced 51,000 families. Large areas of rice farmland worth billions of Naira were also flooded [4]. The number of people vulnerable to a devastating flood is expected to rise due to large-scale urbanization and population

growth in flood-prone areas, deforestation, climate change, and rising sea levels. As a result, the rise in incessant flooding in the country needs to be assessed in terms of early warning systems.

Figure 1.1: Imagery from the Moderate Resolution Imaging Spectroradiometer (MODIS) on NASA's Terra Satellite showing the swelling of Rivers Niger and Benue from heavy rainfall captured on the 16th of October 2012 [5]. Photo: LANCE MODIS Rapid Response Team at NASA GSFC.

Many developed countries have created systems to continually monitor rainfall events, rivers, and streams water levels directly and indirectly by combined ground/satellite-based techniques [6 – 9]. Among all these methods, the Gravity Recovery and Climate Experiment (GRACE) mission is unique in its ability to provides an idea of water storage change in the ground, which is known to be a precursor to flooding [10]. The GRACE satellite mission, a joint mission of the US National Aeronautics and Space Administration (NASA) and the German Aerospace Center (DLR), was launched in March 2002. The GRACE data present an avenue to study monthly variations in terrestrial water storage within large (>200,000 $km^{2)}$) drainage basins based on

estimates of changes in Earth's gravity field: The gravity signal in an area increases when the water storage in the area increases and is captured by the GRACE mission with enormous accuracy. GRACE-based flood potential can predict flood compared to other flood prediction models that use conventional data sources such as snow amounts, river heights, and soil moisture [10]. When combined with other traditional methods of satellite-based precipitation, the GRACE-based storage deficit method could be useful for assessing flood likelihood. However, their reliability for applications in developing countries needs to be evaluated due to the sparse availability of ground measurement data.

Reager and Famiglietti [11] proposed the Flood Potential Index (RFPI) to estimate flood risks worldwide based on GRACE Total Water Storage Anomaly (TWSA) and precipitation records. A qualitative comparison of FPI with a record of observed floods from the Dartmouth Flood Observatory (DFO) data set suggested that the proposed RFPI product is useful for flood risk assessment in most regions [1]. Researchers (e.g., [12]) tested the RFPI in the USA, where a dense network of flood gauges has been established. It was reported that, potentially, greater use of this method is in developing countries, where floods tend to cause significant damage and the most loss of life due to inadequate monitoring capability. Additionally, Tatiana et al. [12] reported that floods in developing countries, as found through the DFO database, are mainly caused by massive rainfall events. The RFPI seems to perform well in predicting flood potential.

Several studies have linked changes in LULC, population, and urbanization to flooding [13 - 17]. Urbanization leads to the loss of existing drainage capacity and vegetative cover. An increase in the impervious surface has been the leading cause of urban flooding [18]. Satellite imageries are an essential source of data to monitor LULC [19, 20]. Geographic Information Systems (GIS) and remote sensing, in combination, are effective techniques for flood hazard delineation. They are also used to assess the spatial variability of flood hazards [21, 22]. Flood hazard mapping prevents loss of human life and minimizes property damage and social disruption [23]. In a coastal city such as Lagos state, the land area is surrounded by lagoons and wetlands. LULC change rapidly alters the hydrologic process with an increase in urbanization. When heavy rainfall coincides with high intensity, the existing drainage system losses its capacity, thereby resulting in flooding.

In this dissertation, we aim to evaluate the usability of the GRACE-based FPI for flood prediction in Nigeria and evaluate how changes in LULC and Urban expansion affect flooding in Lagos State

1.4 Research Challenges

For our research, the major challenge was the minimum adequate study area due to the GRACE satellite data's low spatial resolution. There has been some debate among researchers about the adequate study size to obtain mass changes from GRACE after some signal post-processing. Vishwakarma et al. [24] argued that for hydrological studies, the adequate catchment size is approximately 63,000 km^2 and also that the error in GRACE data increases as the catchment area decreases in size. Other researchers [25 - 27] argued for minimum catchment areas of approximately 200,000 km^2, 150,000 km^2, and 52,000 km^2, respectively, while Lorenz et al. [28] showed that most watersheds smaller than these limits were captured by GRACE based on strong seasonal cycles of water storage changes. In our work, we ensured that the ancillary data have a similar spatial resolution as GRACE data. We went further to apply the GRACE resolution to the entire area of Nigeria.

1.5 Research Scope

The focus of this work was to investigate the effectiveness of remote sensing data for flood prediction in developing countries where annual flooding is a major issue partly because of inadequate and no ground flood monitoring systems and where in most places, the issue of security and sabotage prohibits the installation of these systems. Therefore, this research is centered on flood prediction and impacts of LULC, urban development, and high population on flooding using satellite data.

1.6 Study Sites

The research methods developed were applied to three study areas, including the Lower Niger River Basin (LNRB) in Nigeria (Figure 1.2), Mississippi River Basin in the United States of America (Figure 1.3), and Lagos State, Nigeria (Figure 1.4). These areas were chosen based on data availability. GRACE data were downloaded from the NASA JPL website, while other data were sourced from the USGS and other open-source portals.

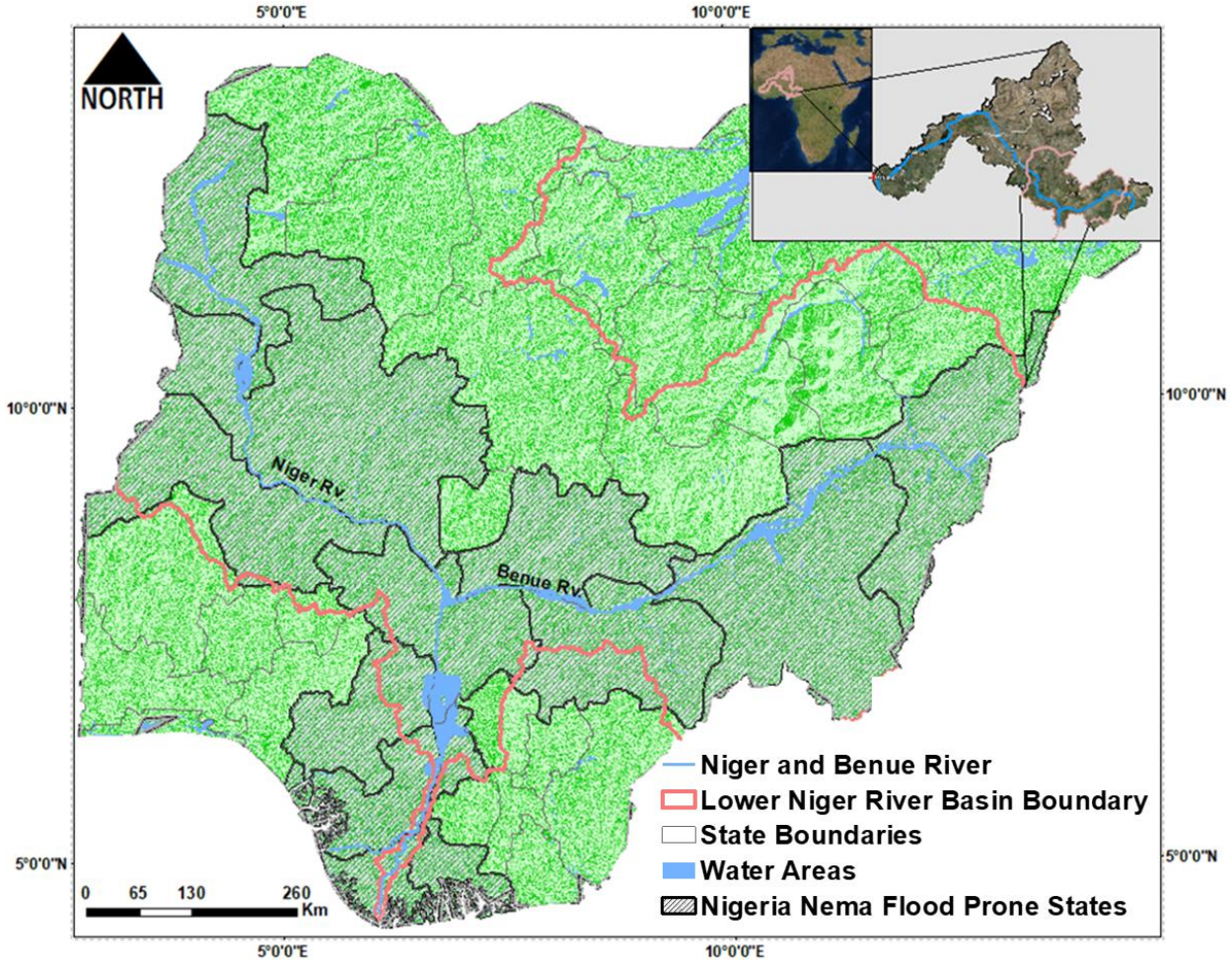

Figure 1.2: Map showing the boundaries of the Lower Niger River Basin in Nigeria with the states prone to Flooding (Nigeria National Emergency Management Agency) [2].

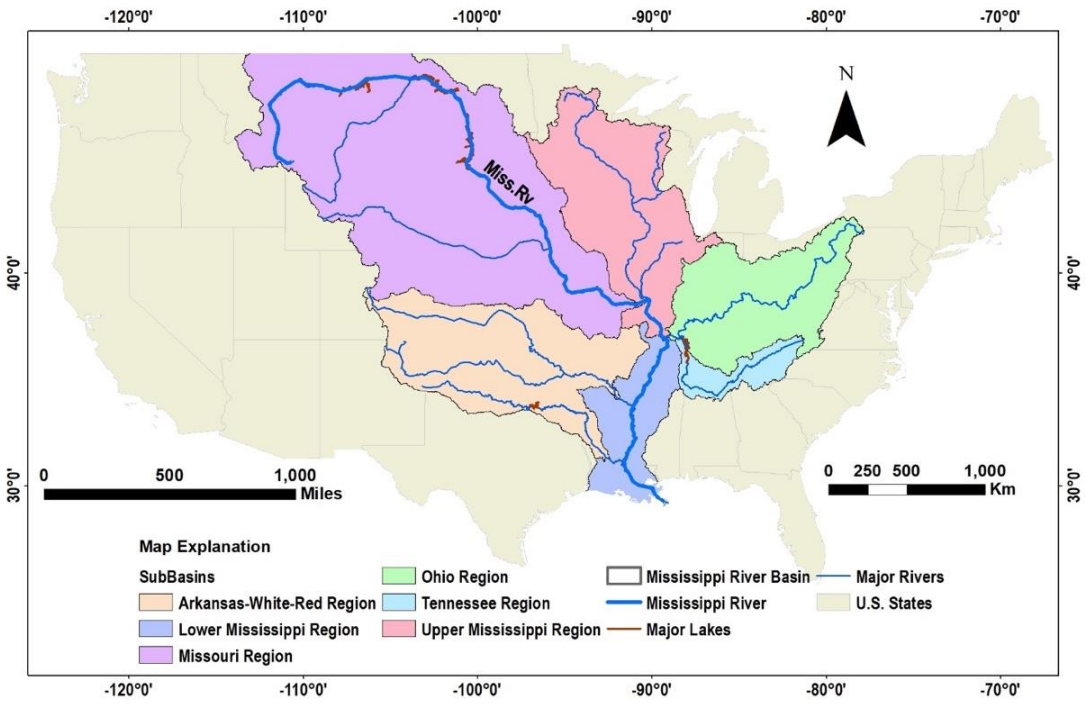

Figure 1.3: Map of the United States of America showing the Mississippi River and its major drainage basins [3].

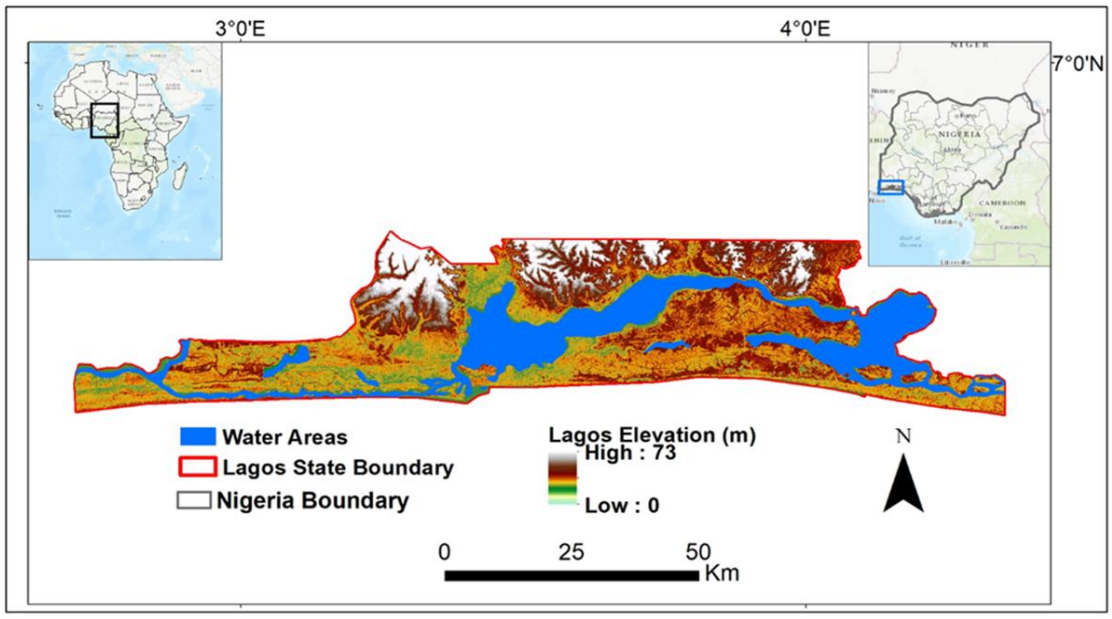

Figure 1.4: Map showing the boundary, water areas and elevations of the Lagos State, Nigeria [28].

1.7 Dissertation Organization

In this research, we tested the application of the Flood Potential Index to predict past floods in the Lower Niger River Basin (LNRB) in Nigeria, where annual flooding is mainly due to heavy rainfall. We also derive a new FPI using the traditional water budget methodology. All the water budget variables are remotely sensed and compared to GRACE FPI in the Mississippi river basin in the USA. Furthermore, we assessed the impacts of LULC changes in Lagos State, Nigeria, and how those changes impact flooding in the area. The following chapters have been structured to address the scope and research outcomes mentioned above.

Chapter 2 is a paper published in Remote Sensing [2]. It focused on evaluating the efficacy of the GRACE FPI at predicting past flood events in the Lower Niger River basin in Nigeria. The predictive ability of the GRACE–FPI was compared against the Dartmouth Flood Observatory report and the Water Budget FPI (WB-FPI). Chapter 3 presents a paper accepted for publication in Environmental and Engineering Geosciences [3]. It focuses on further evaluating WB-FPI using data with a finer spatial resolution to predict past floods in the Mississippi River Basin, USA. Its predictive ability was compared to the GRACE FPI statistically. The study concludes with a new WB FPI that could supplement the GRACE data for flood prediction in developing countries. Chapter 4 is a paper published in Water [29]. The study aims to assess the effect of changes in LULC in the context of flood hazards in Lagos State, Nigeria [30].

The dissertation closes with a final chapter on the summary of notable findings from previous sections and an overview of future work to be done.

1.8 References

[1] Reager J. T. and Famiglietti J. S. (2009). Global terrestrial water storage capacity and flood potential using GRACE. Geophys. Res. Lett. 36, L2340.

[2] Idowu, D. and Zhou, W. (2019). Performance Evaluation of a Potential Component of an Early Flood Warning System—A Case Study of the 2012 Flood, Lower Niger River Basin, Nigeria. Remote Sens. 11(17), 1970; https://www.mdpi.com/2072-4292/11/17/1970.

[3] Idowu, D., and Zhou W. (accepted, Paper no - EEG-D-20-00056), Spatio-temporal Evaluation of Flood Potential Indices for Watershed Flood Prediction in Mississippi River Basin, USA, Environmental and Engineering Geoscience.

[4] Nigeria - Floods (DG ECHO, NIMET, FloodList, NOAA-CPC, media) (ECHO Daily Flash of 08 September 2020), https://reliefweb.int/report/nigeria/nigeria-floods-dg-echo-nimet-floodlist-noaa-cpc-media-echo-daily-flash-08-september. (Accessed 09/28/2020).

[5] NASA Earth Observatory: https://earthobservatory.nasa.gov/images/79404/flooding-in-nigeria. (Accessed 05/18/2021)

[6] Liang, X., Lettenmaier D. P., Wood E. F., and Burges S. J. (1994). A Simple hydrologically Based Model of Land Surface Water and Energy Fluxes for GSMs, J. Geophys. Res., 99(D7), 14,415-14,428.

[7] Huffman, G. J., Adler R. F, Bolvin D. T. and Nelkin E. J. (2010): The TRMM Multi-satellite Precipitation Analysis (TMPA). Chapter 1 in Satellite Applications for Surface Hydrology, F. Hossain and M. Gebremichael, Eds. Springer Verlag, ISBN: 978-90-481-2914-0, 3-22.

[8] Wu, H., Adler R. F., Hong Y., Tian Y. and Policelli, F. (2012). Evaluation of Global Flood Detection Using Satellite-Based Rainfall and a Hydrologic Model. J. Hydrometeor, 13, 1268.1284.

[9] Wu, H., Kimball J. S., Li, H., Huang, M., Leung, L. R. and Adler, R. F. (2013). A new global river network database for macroscale hydrologic modeling, Water Resour. Res., 48, W09701, doi:10.1029/2012WR012313.

[10] Wasko, C., Nathan, R., and Peel, M. C., (2020). Trends in Global Flood and Streamflow Timing Based on Local Water Year, Water Resources Research, 10.1029/2020WR027233, 56, 8.

[11] Reager J. T., Thomas B.F. and Famiglietti J.S. (2014). River basin flood potential inferred using GRACE gravity observations at several months lead-time. Nature Geoscience, 2014, 7, 588-592.

[12] Molodtsova, T., Molodtsov S., Kirilenko A., Zhang X. and VanLooy J. (2016). Evaluating flood potential with GRACE in the United States, Nat. Hazards Earth Syst. Sci., 2016, 16, 1011-1018.

[13] Kundzewicz Z. W., Krysanova V., and Dankers R. (2016) Differences in flood hazard projections in Europe—their causes and consequences for decision making. Hydrol Sci J. https://doi.org/10.1080/02626667.2016.1241398.

[14] Chen, Y. and Yu, B. (1999) Impacts of climate and land-use changes on floods in an urban catchment in southeast Queensland, Australia. Griffith School of Engineering, Griffith University, Nathan, pp 1–7.

[15] Huong H. T. L., and Pathirana, A. (2013). Urbanization and climate change impacts on future urban flooding in Can Tho city, Vietnam. Hydrol Earth Syst Sci 17:379–394. https://doi.org/10.5194/hess-17-379-2013.

[16] Mitsova, D. (2014). Coupling land use change modeling with climate projections to estimate seasonal variability in runoff from an urbanizing catchment near Cincinnati, Ohio. ISPRS Int J Geo-Inf 3:1256–1277. https://doi.org/10.3390/ijgi3041256.

[17] Choi. W., Pan, F. and Wu, C. (2016). Impacts of climate change and urban growth on the streamflow of the Milwaukee River. Reg Environ Change. https://doi.org/10.1007/s10113-016-1083-3.

[18] Konrad, C.P. (n. d.) Effects of Urban Development on Floods; Fact Sheet 076-03; U.S. Geological Survey: Tacoma, WA, USA, 2016. Available online: https://pubs.usgs.gov/fs/fs07603/ (accessed Feb 25, 2021).

[19] Coppin, P. R. and Bauer, M. E. (1996). Digital change detection in forest ecosystems with remote sensing imagery Remote Sens. Rev., 13 (3–4), pp. 207-234.

[20] Galford G. L., Mustard J. F., Melillo J., Gendrin A., Cerri C. C. and Cerri C. E. P. (2008). Wavelet analysis of MODIS time series to detect expansion and intensification of row-crop agriculture in Brazil Remote Sens. Environ., 112 (2), pp. 576-587.

[21] Pramojanee P., Tanavud C., Yongchalermchai C. and Navanugraha C. (1997). An application of GIS for mapping of flood hazard and risk area in Nakorn Sri Thammarat Province, South of Thailand. In Proceedings of the International Conference on Geo Information for Sustainable Land Management, En Schede. The Netherlands, pp. 198-207.

[22] Qi H. and Altinakar M. S. (2011). A GIS –based decision support system for integrated flood management under uncertainty with two dimensional numerical simulations Environ. Model. Softw.

[23] Alaghmand S., Abdullah R. B., Abustan I., Vosoogh B. (2010). GIS-based river flood hazard mapping in urban area (a case study in Kayu Ara River Basin, Malaysia) Int. J. Eng. Technol.

[24] Vishwakarma B. D., Devaraju B. and Sneeuw N. (2018). What Is the Spatial Resolution of GRACE Satellite Products for Hydrology? Remote Sens. 2018, 10, 852.

[25] Long, D., Longuevergne, L., Scanlon, B.R. (2015). Global analysis of approaches for deriving total water storage changes from GRACE satellites. Water Resour. Res. 2015, 51, 2574–2594.

[26] Rowlands, D. D., Luthcke S. B., Klosko S. M., Lemoine F. G. R., Chinn D. S., McCarthy J. J., Cox C. M. and Anderson O.B. (2005). Resolving mass flux at high spatial and temporal resolution using GRACE intersatellite measurements. Geophys. Res. Lett. 2005, 32, L04310.

[27] Tourian, M., Elmi, O., Chen, Q., Devaraju, B., Roohi, S. and Sneeuw, N. A. (2015). Spaceborne multisensor approach to monitor the desiccation of Lake Urmia in Iran. Remote Sens. Environ. 2015, 156, 349–360.

[28] Lorenz, C., Tourian, M.J., Devaraju, B., Sneeuw, N. and Kunstmann, H. (2015). Basin-scale runoff prediction: An Ensemble Kalman Filter framework based on global hydrometeorological data sets. Water Resour. Res. 2015, 51, 8450–8475.

[29] Idowu, D.; Zhou, W. (2021) Land Use and Land Cover Change Assessment in the Context of Flood Hazard in Lagos State, Nigeria. Water 2021, 13(8), 1105; https://doi.org/10.3390/w13081105.

[30] Idowu, D., and Zhou W., (in press), Land use land cover assessment and flood hazard mapping in Lagos State (Nigeria) using optical remote sensing data, 3rd Conference of the Arabian Journal of Geosciences (CAJG), 2-5 November 2020, Sousse Tunisia.

CHAPTER 2

PERFORMANCE EVALUATION OF A POTENTIAL COMPONENT OF AN EARLY FLOOD WARNING SYSTEM— A CASE STUDY OF THE 2012 FLOOD, LOWER NIGER RIVER BASIN, NIGERIA

Reproduced from a publication in the Remote Sensing[1]

Dorcas Idowu[2]*, Wendy Zhou*[3]

2.1 Abstract

Floods frequently occur in Nigeria. The catastrophic 2012 flood in Nigeria claimed 363 lives and affected about seven million people. A total loss of about 2.29 trillion Naira (7.2 billion US Dollars) was estimated. The effect of flooding in the country has been devastating because of sparse to no flood monitoring, and a lack of an effective early flood warning system in the country. Here, we evaluated the efficacy of using the Gravity Recovery and Climate Experiment (GRACE) terrestrial water storage anomaly (TWSA) to evaluate the hydrological conditions of the Lower Niger River Basin (LNRB) in Nigeria in terms of precipitation and antecedent terrestrial water storage prior to the 2012 flood event. Furthermore, we accessed the potential of the GRACE-based flood potential index (FPI) at correctly predicting previous floods, especially the devastating 2012 flood event. For validation, we compared the GRACE terrestrial water storage capacity (TWSC) quantitatively and qualitatively to the water budget of TWSC and Dartmouth Flood Observatory (DFO) respectively. Furthermore, we derived a water budget-based FPI using Reager's methodology and compared it to the GRACE-derived FPI quantitatively. Generally, the GRACE TWSC estimates showed seasonal consistency with the water budget TWSC estimates with a correlation coefficient of 0.8. The comparison between the GRACE-derived FPI and water budget-derived FPI gave a correlation coefficient of 0.9 and agreed well with the flood reported by the DFO. In addition, the FPI showed a marked increase with precipitation that implies that rainfall is the main cause of flooding in the study area. Additionally, the computed GRACE-based storage

[2]Graduate student, department of Geology and Geological Engineering, Colorado School of Mines. Leading author
[3]Department of Geology and Geological Engineering, Colorado School of Mines. Thesis advisor and corresponding author

deficit revealed that there was a decrease in water storage prior to the flooding month while the FPI increased. Hence, the GRACE-based FPI and storage deficit when supplemented with water budget-based FPI could suggest a potential for flood prediction and water storage monitoring respectively.

2.2 Introduction

Flooding is a major disaster in Nigeria, especially along the Niger and Benue Rivers. In Nigeria, it occurs in three main forms: Coastal floods which occur in mangrove and delta coastlines; river floods which occur on the flood plains of large rivers; and flash floods which are short-lived events developing in less than 6 hours from rainfall to the onset of flooding [1,2].

In 2012, heavy rainfall during the wet season combined with the release of water from Ladgo Dam in Cameroon led to a catastrophic flooding event that affected 30 states out of the 36 states of the country. The flooding which was described by the Nigeria National Emergency Management Agency as the worst in 40 years, claiming 363 lives, affecting about 7 million people, while a total loss of about 2.29 trillion Naira (7.2 billion US Dollars) was estimated.

The developed countries are still affected by disasters resulting from floods but have flood alert systems (such as the European Flood Alert System [3] and the US National Weather Service Automated Flood Warning System [4]) in place which are effective in providing a monitoring and warnings service. A significant portion of the economic losses caused by floods occur in developing countries where ground flood monitoring and management programs are still inefficient, and the costs of building water control infrastructure such as dams, weirs, embankments and gauging stations can be prohibitive [5]. Also, ground-based methods used to monitor floods are based on hydro-meteorological data such as discharge and precipitation which are time-consuming in terms of collection and processing and are also affected by varying weather conditions. Furthermore, worthy of mentioning is the recent problem of security in Nigeria which may also inhibit the installation of these systems.

Over the years, there have been novel advances on remote sensing for forecasting and monitoring hydrological extremes such as floods and droughts. Victor [6] studied the use of satellite data for flood delineation, monitoring and prediction. Nasreddine et al. [7] developed a new flood forecasting approach for flood disaster management in poorly or totally ungauged watersheds

using precipitation measurements. Sheffield et al. [8] and Zhang et al. [9] applied satellite data to monitoring and forecasting drought.

In recent decades, satellite data availability has improved dramatically and to complement the ground-based observations, flood monitoring has increasingly relied on the products obtained with space-borne sensors such as National Aeronautics and Space Administration (NASA) advanced microwave scanning radiometer for EOS (AMSR-E) [10] and moderate resolution imaging spectroradiometer (MODIS) [11]. Zhan et al. [12] explored the marginal benefit of incorporating space-borne soil moisture measurements into a hydrologic model for improved streamflow and flood prediction. They incorporated the surface soil moisture data from the AMSR-E into the Noah land surface model within the Land Information System (LIS). Their findings suggested the potential for improving flood forecasting through the assimilation of remotely sensed soil moisture data into a hydrologic model. Among the remote sensing products that have been used for flood monitoring, prediction and forecasting, data from the Gravity Recovery and Climate Experiment (GRACE) [13,14] are unique in that the changes in the amount of terrestrial water can be directly measured.

The GRACE satellite mission was launched in March 2002. It presents a means to observe monthly variations in total/terrestrial water storage within large (>200,000 km^2) river basins based on measurements of changes in Earth's gravity field [15]. These changes result when the amount of water stored in a region increases or decreases, which produces a ripple effect leading to the gravity signal in that region increasing or decreasing proportionately. The predictive ability of a GRACE-based flood potential has been compared to flood prediction models that use traditional input data sources such as river heights, snow amounts and the wetness of surface soils [16]. The method of GRACE storage deficit estimates could be used in combination with traditional remote sensing methods of precipitation forecasting to help assess the likelihood for flooding [16]. However, their reliability and efficacy for applications in developing countries need to be assessed due to the sparse availability of ground measurement data.

Reager and Famiglietti [17] proposed the flood potential index (FPI) to estimate flood risks worldwide based on GRACE terrestrial water storage anomaly (TWSA) and precipitation records. A qualitative comparison of FPI with a record of observed floods from the Dartmouth Flood Observatory (DFO) data set suggested that the proposed FPI product is useful for flood risk

assessment in most regions [17]. Molodtsova et al. [18] tested the FPI in the United States where a dense network of flood gauges has been established, and reported that, potentially, a greater use of this method is in developing countries, where due to inadequate monitoring capability, floods tend to cause significant damage and the most loss of life. Additionally, they reported that floods in African countries, as found through the DFO database, are mainly caused by heavy rainfall events, for which the FPI seems to perform well in predicting flood potential.

Molodtsova et al. [18] went further to study the Juba–Shabelle River Basin, a 783,000 km^2 watershed shared between Somalia and Ethiopia, and found an increasing FPI was in the watershed one month prior to the flood and during the month of the flood, where both predictions agreed well with the actual flood extent area reported by the DFO. Based on their analysis, they inferred that developing countries with sparse or inadequate flood monitoring networks are potential beneficiaries of this approach.

Sun et al. [19] evaluated the GRACE FPI over the Yangtze River Basin (YRB) in China and suggested that estimates of terrestrial water storage based on GRACE, measured as FPI, are critical for understanding and predicting flooding. Thus, they concluded that GRACE data can be effectively used for monitoring and examining large floods in the YRB and elsewhere.

For our study, we chose the Lower Niger River Basin, Nigeria (Figure 2.1) as our area of interest, and the flooding event in 2012 as our case study (Table 1) because it was the worst in 40 years. We investigated the capacity of the GRACE TWSA (terrestrial water storage capacity, TWSC) in accurately capturing and predicting the 2012 flood event, and other flood years within the basin. We also evaluated the hydrological condition of the basin in terms of the available storage and predisposition to flooding. The GRACE-derived FPI was validated using the DFO report and compared to a water budget-derived FPI.

2.3 Data and Methods

2.3.1 Study Area

The Lower Niger River Basin (LNRB) is so termed because of its location within the Niger River Basin (NRB). Located in West Africa, the NRB covers 7.5% of the continent and cuts across ten countries. With a total area of approximately 2.2 million km^2 and a total length of 4100 km, the NRB is the third-longest river in Africa. It is divided into four parts, the Upper Niger River System,

the Inner Delta, the Middle Niger River System and the LNRB. The major river within the basin is the Niger River which starts in the highlands of Guinea (upstream) threading eastwards mainly through Mali, Niger and Nigeria (downstream) before entering the Gulf of Guinea to the Atlantic Ocean. Its unusual crescent shape takes it inland towards the Sahara before turning south-west to the Gulf. Along its route, the river hydrology changes from its rain-fed headwaters, it loses flow and volume as it nears the Sahara where it forms an inland delta. The inland delta is an area of high evaporation that is composed of a number of slow-moving channels. Only after the Benue River joins the river in Nigeria does it become a large river once more. The Benue River (Figure 2.1) which is the major tributary that feeds the Niger River Basin in Nigeria meets the Niger River (Figure 2.1) to form a confluence in Lokoja, Nigeria. Rivers Niger and Benue (Figure 2.1) are the two largest rivers in West Africa. The water in the Niger River is partially regulated through dams.

Table 2.1**:** Statistics for the most devastating flood disasters in 2012 (compiled by authors based on [20]).

Country	Date	Death Toll	Number of People Affected	Number of People Displaced	Cause(s)	Cost of Damage
Pakistan	September	455	>5,000,000	350,000	Heavy monsoon rains	N/A
Nigeria	July–October	363	7,000,000	2,100,000	Heavy rains and water release from Dam	US $7.2 billion
North Korea	July–September	330	N/A	241,547	Torrential rains and tropical storm Khanun	N/A
Russia	July	171	30,000	13,000	Heavy rainfall	N/A
Philippines	August	95	1,230,000	15,134	Torrential rains	US $14.31 million
China	July	79	>1,600,000	56,933	Heavy rainfall	US $1.6 billion
India	August	35	>12000	N/A	Monsoon rainfall	US $ 89 million
Nepal	May	26	N/A	N/A	Flooding from the outburst of a landslide dam	N/A

.

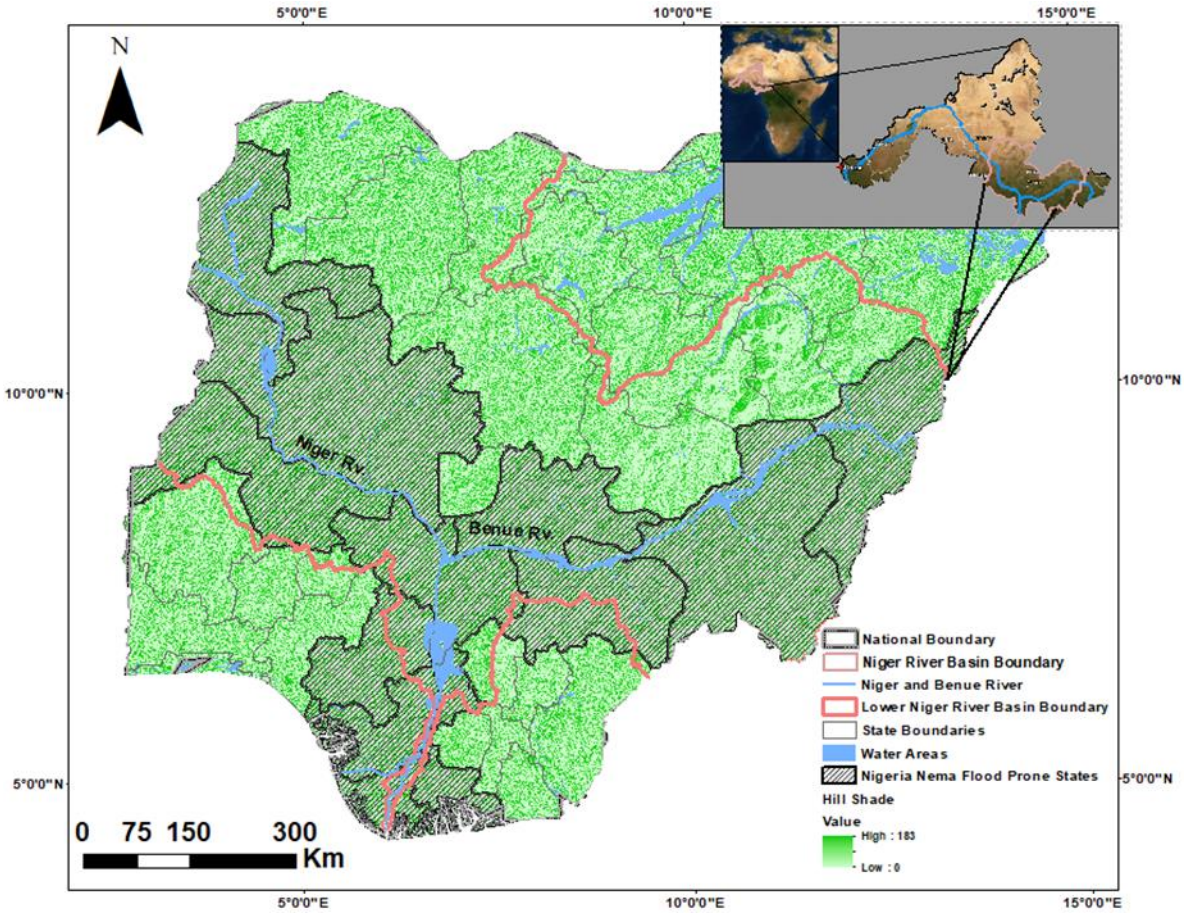

Figure 2.1: Map showing the boundaries of the Lower Niger River Basin in Nigeria with the states prone to Flooding (Nigeria National Emergency Management Agency).

The Benue reaches its flood level in September. It begins to fall in October and falls rapidly in November, continuing slowly over the next three months to reach its lowest level in March and April. Annually, these rivers experience flooding as a result of the annual heavy rainfall which coincides with the wet season in Nigeria [21] and because of poor urban planning, settlements located within the floodplains and in the proximity of the river get flooded [22] (Figure 2.2).

In 2012, the flooding was devastating and in spite of the increasing awareness in combating flood hazard in along the rivers, the menace had recurred. This is because past flood control strategies have not achieved the desired result due to a lack of understanding of the hydrological variables that influence the persistence of these floods. The Nigerian National Emergency Management Agency (NEMA), in 2012 listed the flood-prone states in the country. Most of these states are within the LNRB and along the Niger and Benue Rivers (Figure 2.1).

Figure 2.2: NASA's Terra (Moderate Resolution Imaging Spectroradiometer) satellite images showing the pre flood (normal river geometry) and post flood river geometry of the Benue River and Niger and Benue confluence point. Post – flood image was captured in 2012. (Modified after [23]).

2.3.2 Datasets

2.3.2.1 GRACE Terrestrial Water Storage Anomaly Products

The three official solutions (spherical harmonics solutions), the JPL (Jet Propulsion Laboratory), GFZ (GeoforschungsZentrum Potsdam) and CSR (Center for Space Research at University of Texas, Austin) of the GRACE RL05 TWSA product [24] were downloaded (http://grace.jpl.nasa.gov), from January 2004 to December 2012. The workflow in Figure 3 was applied to the datasets to derive the TWSA for the baseline of the study. The scaling factor suggested by the GRACE Tellus data portal [24] was applied to the GRACE data to account for the attenuation of small-scale surface mass variations [25]. For some years within our baseline of our study, some monthly TWSA data were missing. This is because, since early 2011, the GRACE instruments were periodically turned off due to active battery management. Those months were not considered in our study.

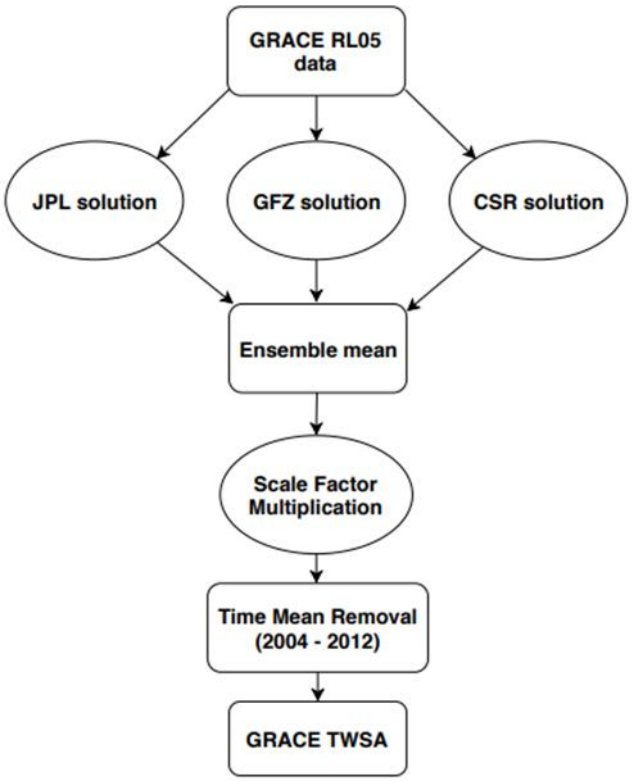

Figure 2.3: The basic workflow for the gravity recovery and climate experiment (GRACE) RL05 processing.

2.3.2.2 Evaluation of GRACE and Water Budget Terrestrial Water Storage Change (TWSC)

The GRACE TWSA was evaluated against the traditional water balance estimates before being used in generating the FPI. First, we calculated the TWSC from GRACE TWSA, then from the traditional water budget equation. The following water balance equation was used:

$$\frac{ds}{dt} = P - R - ET - SM - GW \qquad (2.1)$$

where $\frac{ds}{dt}$ is the monthly change in terrestrial water storage, P is monthly precipitation, R is a monthly runoff, ET is monthly evapotranspiration, SM is soil moisture and GW is groundwater.

The change was calculated for our time steps using Equation (2).

$$ds/dt = TWSC(t) - TWSC(t-1) \;/\; t \qquad (2.2)$$

For this study, the water balance data (P, R, ET, SM and GW) were obtained from the eartH2Observe water cycle integrator (WCI) [26].

2.3.2.3 Global Precipitation Climatology Centre (GPCC)

The 1 × 1 GPCC precipitation data, provided by the NOAA/OAR/ESRL PSD, Boulder, Colorado, USA [27] were used for deriving the FPI. Monthly data from January 2004 to December 2012 were downloaded while the datasets corresponding to the missing datasets in GRACE TWSA were removed to create consistency in data comparison.

2.3.2.4 Dartmouth Flood Observatory (DFO)

Since ground flood monitoring data range from sparse to not available in the study area, the DFO data were used as validation of the performance of the DFO data beginning in 1985 and is based on flood reports from news and governmental sources and therefore mainly refers to large floods in densely populated regions. It also classifies a large flood event by the significant damage to structures, agricultural land, loss to human life and/or long duration [18]. The DFO data was downloaded as a GIS shapefile set providing catalog numbers and area affected map outlines, with much of the tabular attribute data (e.g., dates, duration and fatalities) also included. It is worthy of note that DFO data are mainly based on media reports which are expected to be biased towards the more densely populated regions and/or regions of interest [18].

2.3.3 Methods

2.3.3.1 GRACE-Derived Flood Potential Index

We followed the methodology proposed by Reager and Famiglietti [17] to compute monthly 2004–2012 FPI for the study area using the GRACE TWSA product. For each grid, we defined and computed the maximum water storage capacity (Smax) and storage deficit (Sdef). Smax is the historic maximum water storage capacity of the soil within a region [17] which for our study area we estimated to be the maximum of GRACE TWSA for LNRB from 2004 to 2012. The Sdef, which represents the available water on land before obtaining Smax, was calculated for each grid and month:

$$Sdef(t) = Smax - TWSA(t - 1) \quad (2.3)$$

where TWSA(t–1) is the saturation condition of the soil from the previous month [18]. The storage deficit shows how much more water the soil within an area can store before achieving the maximum capacity and was computed using the data from the previous month thus establishing a potential for forecasting. It is, however, expected that Sdef is low during wetter parts of the year and high during the drier part of the year. For visualization, Sdef for the study area was normalized to display the hydrological state of the basin in terms of available water.

GPCC monthly precipitation anomalies (P) were multiplied by the length of each month to estimate the amount of rainfall (in cm) that fell in the averaging interval:

$$Pmon(t) = P(t)dt. \tag{2.4}$$

Example of GRACE TWSC, Sdef and Pmon are shown in Figure 2.7 for 9.5°N, 12.5°E. The flood potential (F) for the month (t) was computed by:

$$F(t) = Pmon(t) - Sdef(t) \tag{2.5}$$

where Pmon is monthly precipitation. Flood potential, F (t) is the quantity of incoming water that cannot be stored based on the basin exceeding its maximum storage capacity. A high probability of flooding in the current month would mean a low storage deficit and high precipitation for the previous month [17]. The flood potential was further normalized to derive the Reager's flood potential index (FPI):

$$FPI(t) = F\frac{t}{\max[F(t)]}. \tag{2.6}$$

The values of FPI vary from $-\infty$ to 1 with positive values indicating that water input from precipitation is above the mean water storage and should be interpreted as a potential risk for flooding [17]. When normalized FPI nears 1, it indicates an abnormally high difference between precipitation and regional storage ability and therefore high flood likelihood [17]. The derived FPI was qualitatively validated against the DFO observational flood datasets.

2.3.3.2 Water Budget-Derived Flood Potential Index

The methodology in Section 2.3.3.1 was used in estimating the water budget FPI. The water budget Smax was estimated from the time series of the water budget TWSC. Then we calculated the water budget-based Sdef using Equation (2.3) and flood potential using Equation (2.5). For consistency,

we used the GPCC precipitation in the equation for calculating the water budget flood potential. Using Equation (2.6), we derived the water budget-based flood potential index.

2.4 Results

2.4.1 Analysis of GRACE TWSA and Validation

We compared the three official GRACE TWSA data to each other and generated the time series for the three solutions which gave a correlation coefficient of approximately 0.99 (Figure 2.4) showing similar accuracy although processed using different solutions. As a result, we used the ensemble mean [28,29] from the three solutions in our analysis.

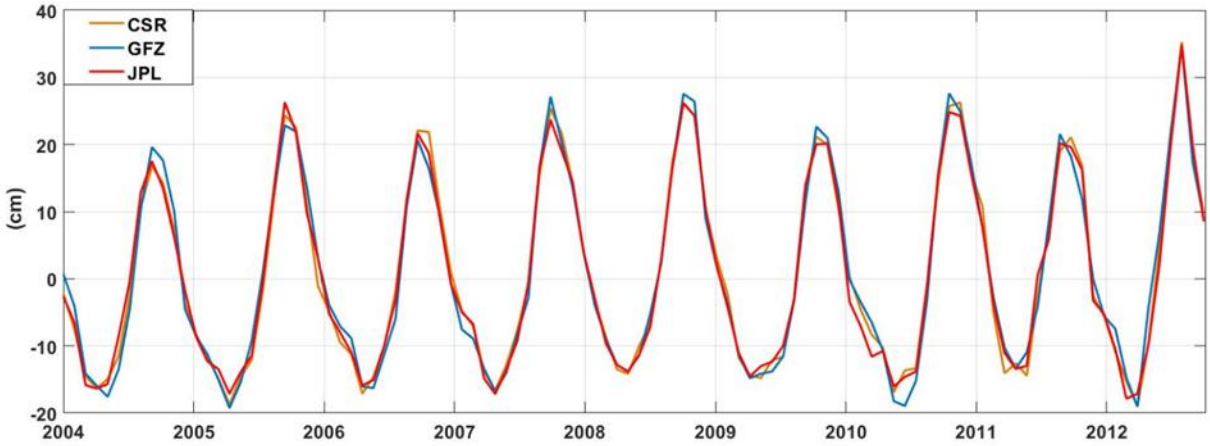

Figure 2.4: GRACE terrestrial water storage anomaly (TWSA) time series for the three solutions: CSR, GFZ and JPL for 9.5°N, 12.5°E from 2004 to 2012.

Furthermore, the time series of the GRACE-based TWSC and the derived water budget-based TWSC estimates show a considerable consistency with a correlation coefficient of 0.8. Additionally, they both are generally negative during the dry months (November to March) and positive during the wet months (April to October). Figures 2.5 and 2.6 display the graphical relationship between GRACE TWSC and water budget TWSC in the LNRB.

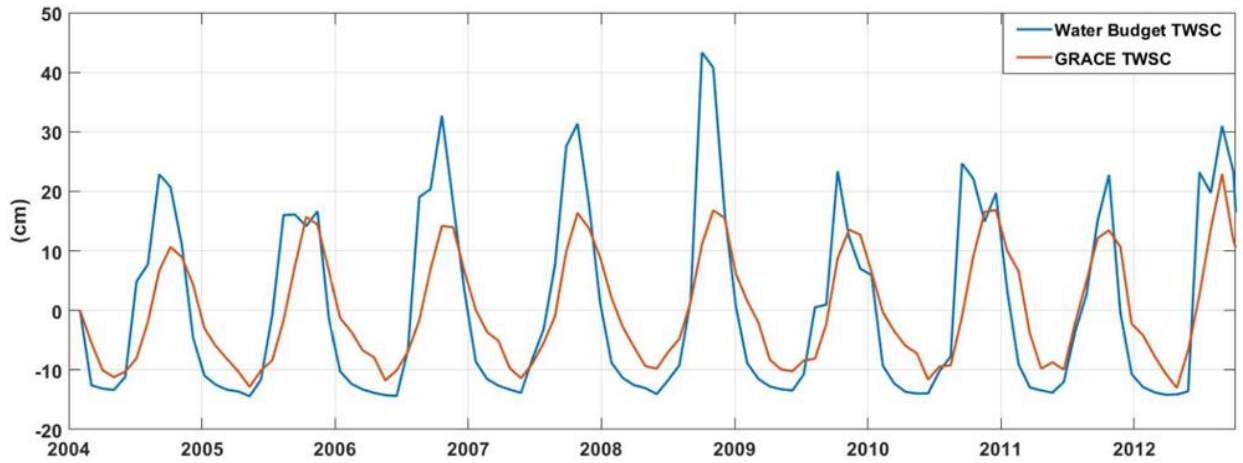

Figure 2.5: Comparison between GRACE terrestrial water storage capacity (TWSC) and derived water balance TWSC from 2004 to 2012 at the location of longitude 12.5 and latitude 9.5.

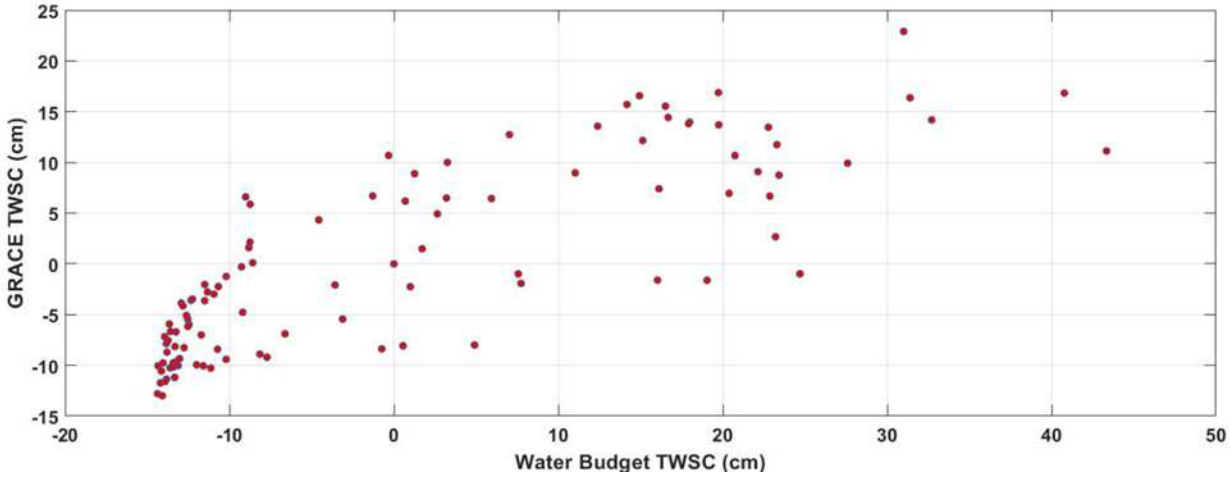

Figure 2.6: Scatterplot for GRACE TWSC and water budget-derived TWSC.

2.4.2 Hydrological State of the LNRB

Figures 2.7 and 2.8 graphically explain the relationship among the variables; GRACE-based TWSC, water budget-based TWSC and their respective Sdef and Pmon. It also shows how an increasing GRACE and water budget TWSC increases with precipitation, while there is a decrease in available storage relative to the other variables. The months during which these three variables intersect implies a potential for flooding to occur. In the LNRB, 2005, 2007, 2008, 2009, 2010,

2011 and 2012 were flooding years [22, 30, 31] which is consistent with Figures 2.7 and 2.8. Figure 2.7 also reveals that the 2012 flood was the worst event among all.

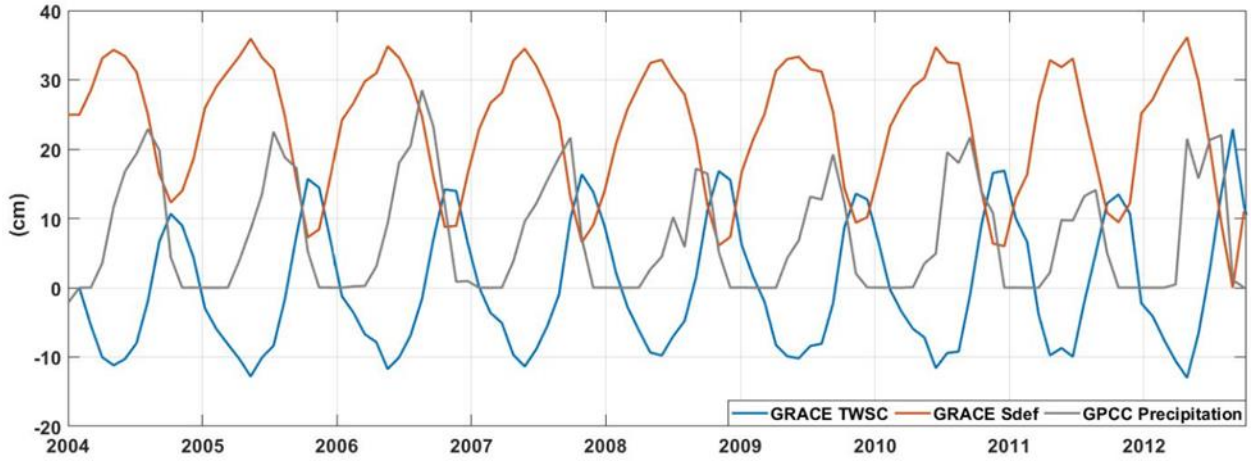

Figure 2.7: Variations in time series of monthly GRACE TWSC, storage deficit and precipitation for longitude 12.5 and latitude 9.5 from 2004 to 2012.

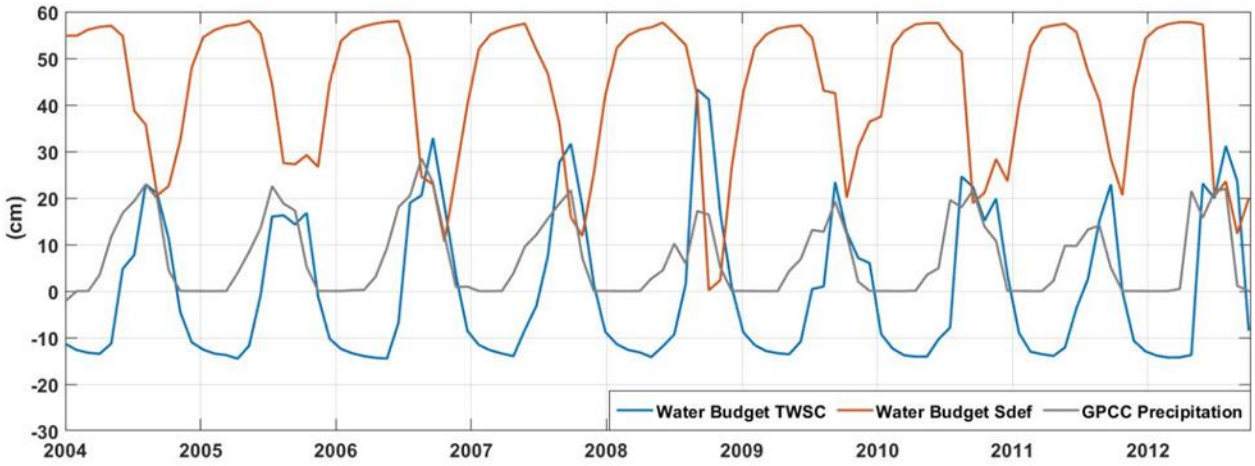

Figure 2.8: Variations in time series of monthly water budget TWSC, storage deficit and precipitation at the location of longitude 12.5 and latitude 9.5 from 2004 to 2012.

2.4.2.1 Precipitation within the LNRB

Rainy season varies for different geopolitical zones in Nigeria, which by extension is applicable to the LNRB. The GPCC precipitation data corresponds to the wet season within the basin (Figure

2.8). The rainy season is between April and October. The driest months are January and December which implies 0 precipitation in both January and December. The peak month in the north is August and September in the south, which agrees well with our results as shown in Figure 2.9.

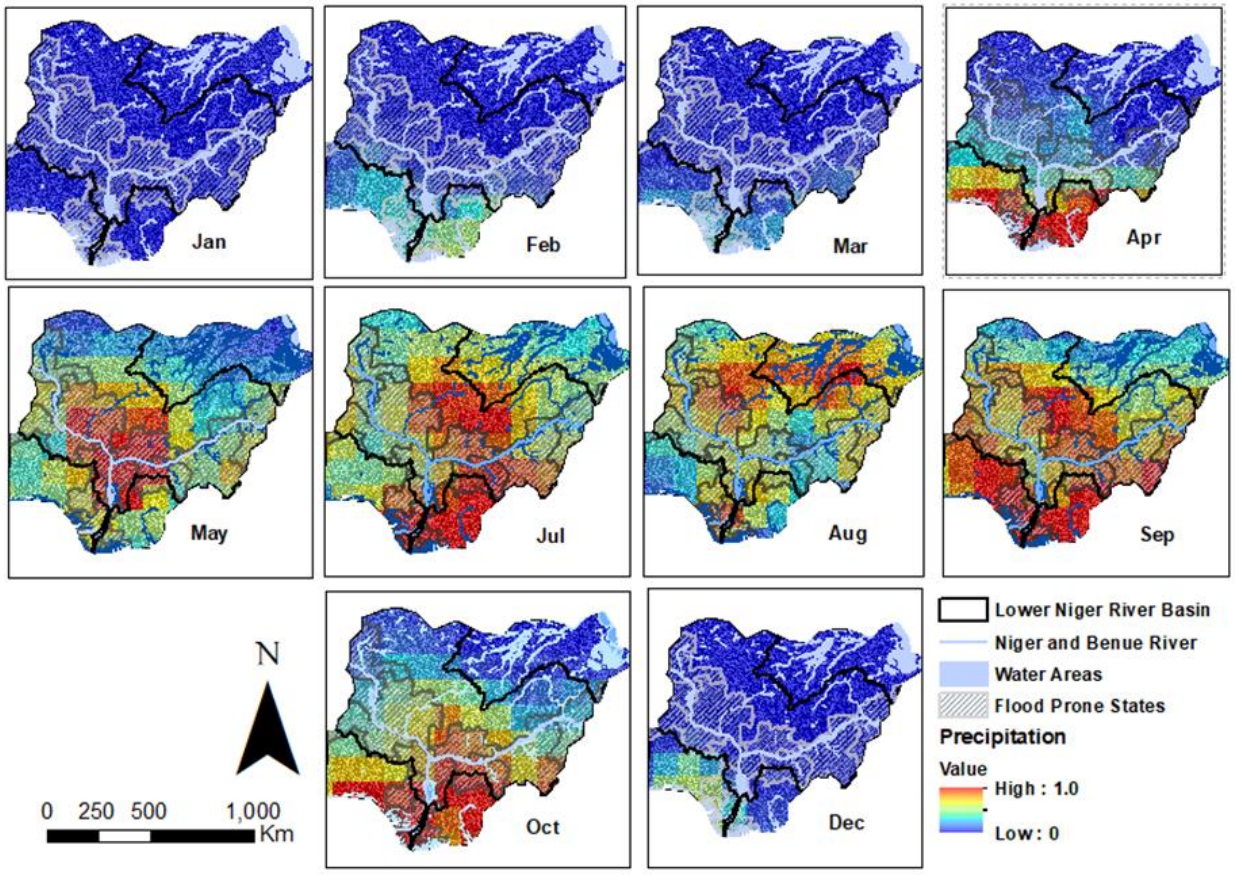

Figure 2.9: Spatiotemporal distribution of precipitation in the Lower Niger River Basin (LNRB) in 2012 from January to December. June and November were not displayed so as to show consistency when compared to GRACE data.

2.4.2.2 GRACE-Based Storage Deficit within the LNRB

Zooming in to the 2012 flood year in the LNRB, Figure 2.10 visually depicts how the available storage changes from surplus to deficit; because the storage deficit was derived using GRACE TWSA from the previous month, the amount of available storage for the coming month was approximated. For example, as shown in Figure 2.10, available storage for the month of September 2012 was derived using the GRACE TWSA from August and the result shows a low Sdef for

September 2012. With this, we estimate the amount of hydrological input necessary to cause the system to flood, hence, establishing the potential for flood prediction. Comparing Figures 2.9 and 2.10, we can infer that the available storage began to decline from the rainfall peak months, August and September.

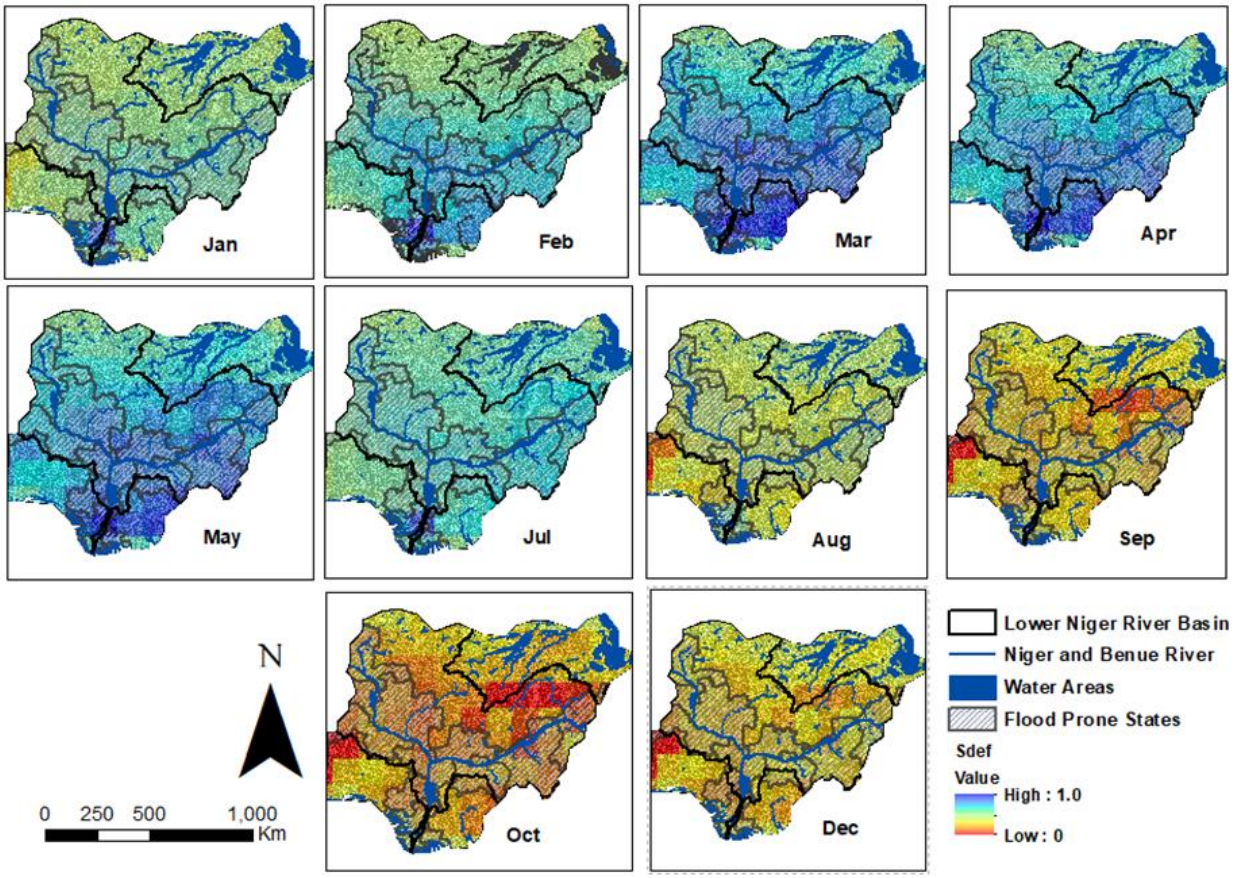

Figure 2.10: Spatiotemporal display of storage deficit (Sdef) (normalized) in the LNRB from January to December 2012. May and October 2012 are missing months in the GRACE TWSA time series due to battery management. Hence, no Sdef and flood potential index (FPI) for June and November. The red color shows areas with low Sdef while the blue areas represent areas with high Sdef.

2.4.2.3 GRACE Flood Potential Index (FPI)

The FPI for 2012 in the LNRB is shown in Figure 2.10. When compared to Figure 2.8, one could see how sensitive the index is to precipitation. Different areas within the basin experiences flooding at different rainfall peak times as shown in Figure 2.10. However, according to the

Nigerian NEMA, in September 2012, 30 out of 36 states in Nigeria was affected by flooding which corresponds to the prediction by the FPI.

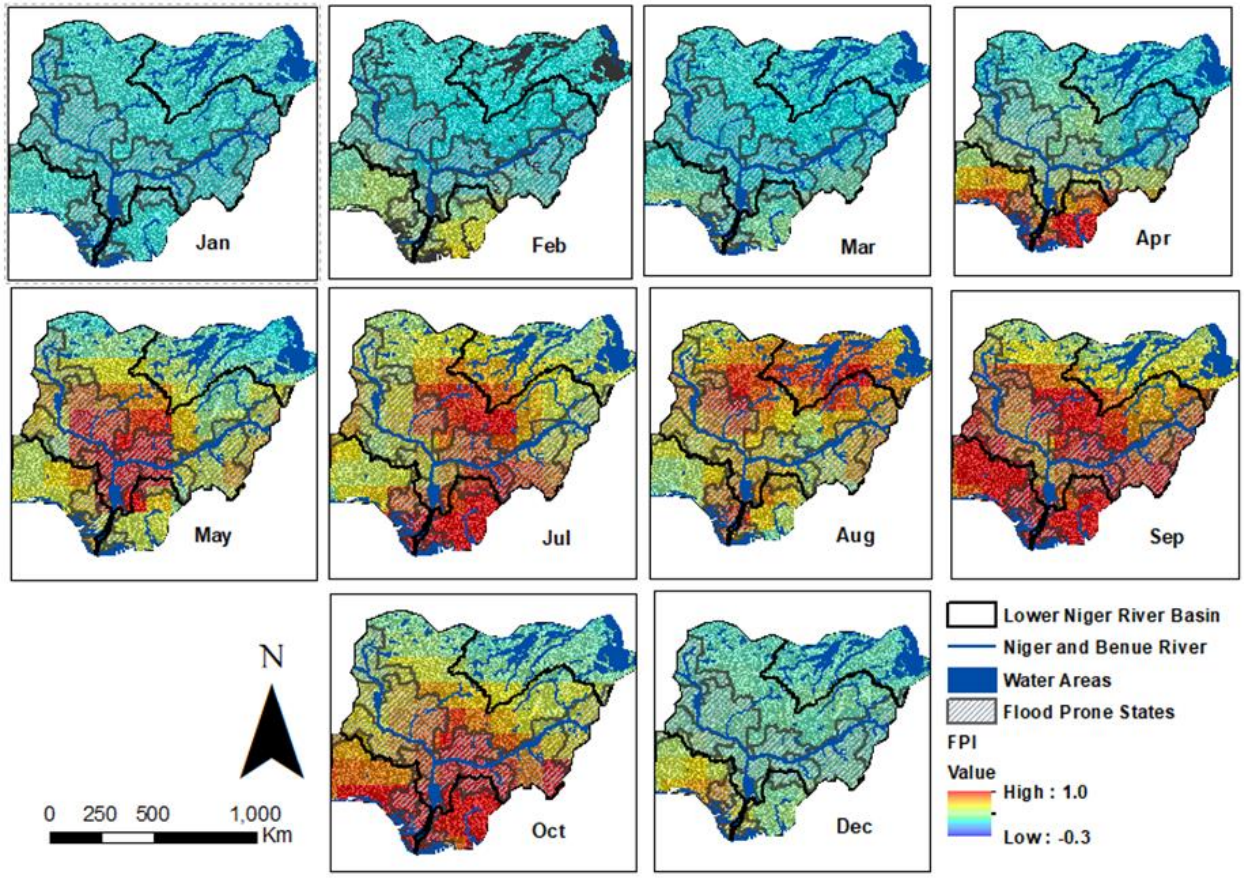

Figure 2.11: Spatiotemporal distribution of the flood potential index for 2012 in the LNRB. The red and blue areas indicate high and low probability or likelihood of flooding. According to the Nigerian National Emergency Management Agency (NEMA), 30 out of 36 states experienced flooding.

2.4.2.4 GRACE-Based RFPI Validation

We validated the GRACE-based FPI both quantitatively and qualitatively. The derived GRACE-based FPI was quantitatively compared to the water budget-derived FPI from 2004 to 2012 (Figure 2.12) and qualitatively validated against the DFO flood data for September 2005, 2007, 2009 and 2012 (Figure 2.13). We found a good agreement between the FPI derived from GRACE and water budget estimates as shown in Table 2.2, Figures 2.12–2.14. Figure 2.14 shows that both GRACE-

based FPI and water budget-based FPI trend in the same direction. Table 2.2 further shows the similarities between the FPI from GRACE and water budget.

Statistical Test for GRACE and Water Budget Flood Potential Index

For statistical significance, we posed a question of whether there is a significant difference in the flood potential derived using GRACE TWSC and water budget TWSC. We used a Wilcoxon rank-sum test to test the null hypothesis that there is no difference between the FPI estimates. We also tested an alternative hypothesis, that there is a difference between the FPI estimates. Using an Alpha level of 0.05, our result showed that we can accept the null hypothesis, and at $P > 0.05$, we have no reason to reject the null hypothesis that there is no difference in the flood potential estimates.

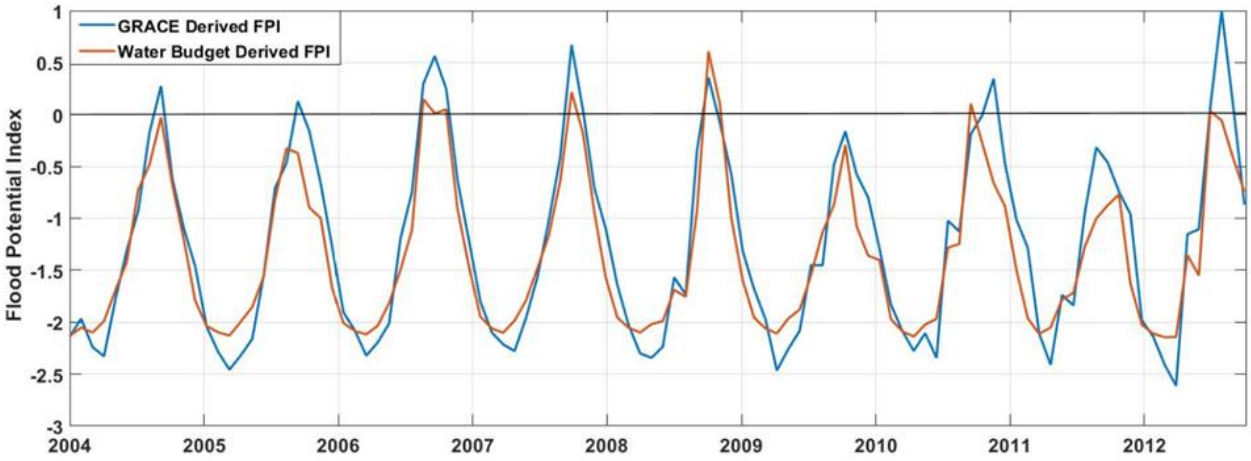

Figure 2.12: Graphical comparison and validation of FPI from GRACE using the FPI from water budget estimates.

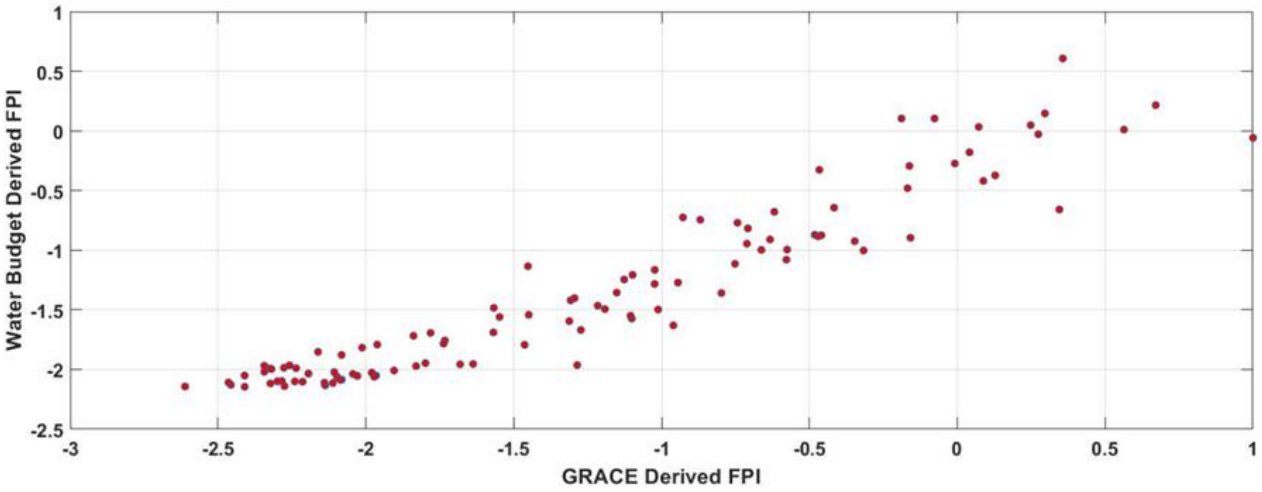

Figure 2.13: Scatterplot for GRACE-derived FPI and water budget-derived FPI.

Table 2.2: Tabular representation of the comparison between FPI from GRACE and water budget estimates.

Years	**Flood Potential Index**	
September	**GRACE-Based FPI**	**Water Budget-Based FPI**
2005	0.2	−0.3
2006	0.6	0.2
2007	0.7	0.3
2009	−0.3	−0.2
2010	0.4	0.2
2012	0.9	0.1

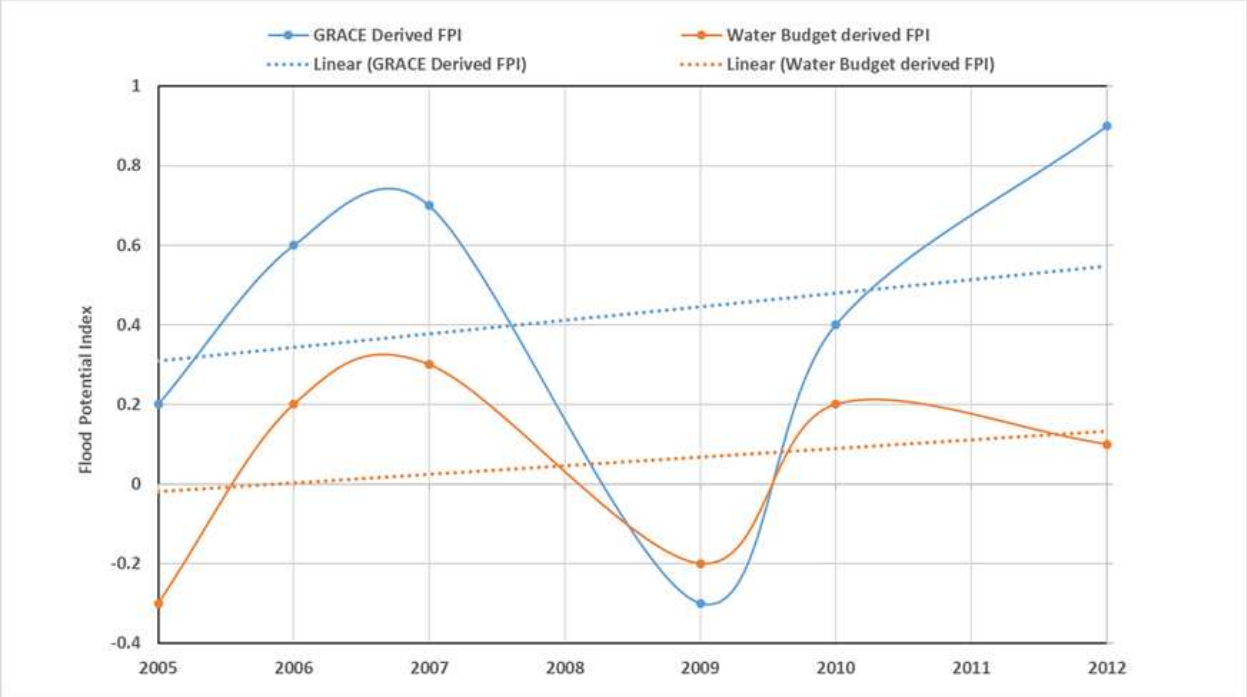

Figure 2.14: Trend plots for GRACE-derived and water budget-derived FPIs.

We chose big flood events that got publicity within our period of study to see how well the GRACE-based FPI compares to the DFO reported floods. However, because the DFO flood report is based on news, it is more biased towards urban flood events. These flood events reported in our study area in September 2005, 2007, 2009 and 2012 were also predicted by the GRACE-based FPI (Figure 2.15). Also, the FPI values from GRACE (Table 2.3) predicted flooding for the flood-prone/worst-hit state in September 2012 as reported by the Nigerian NEMA.

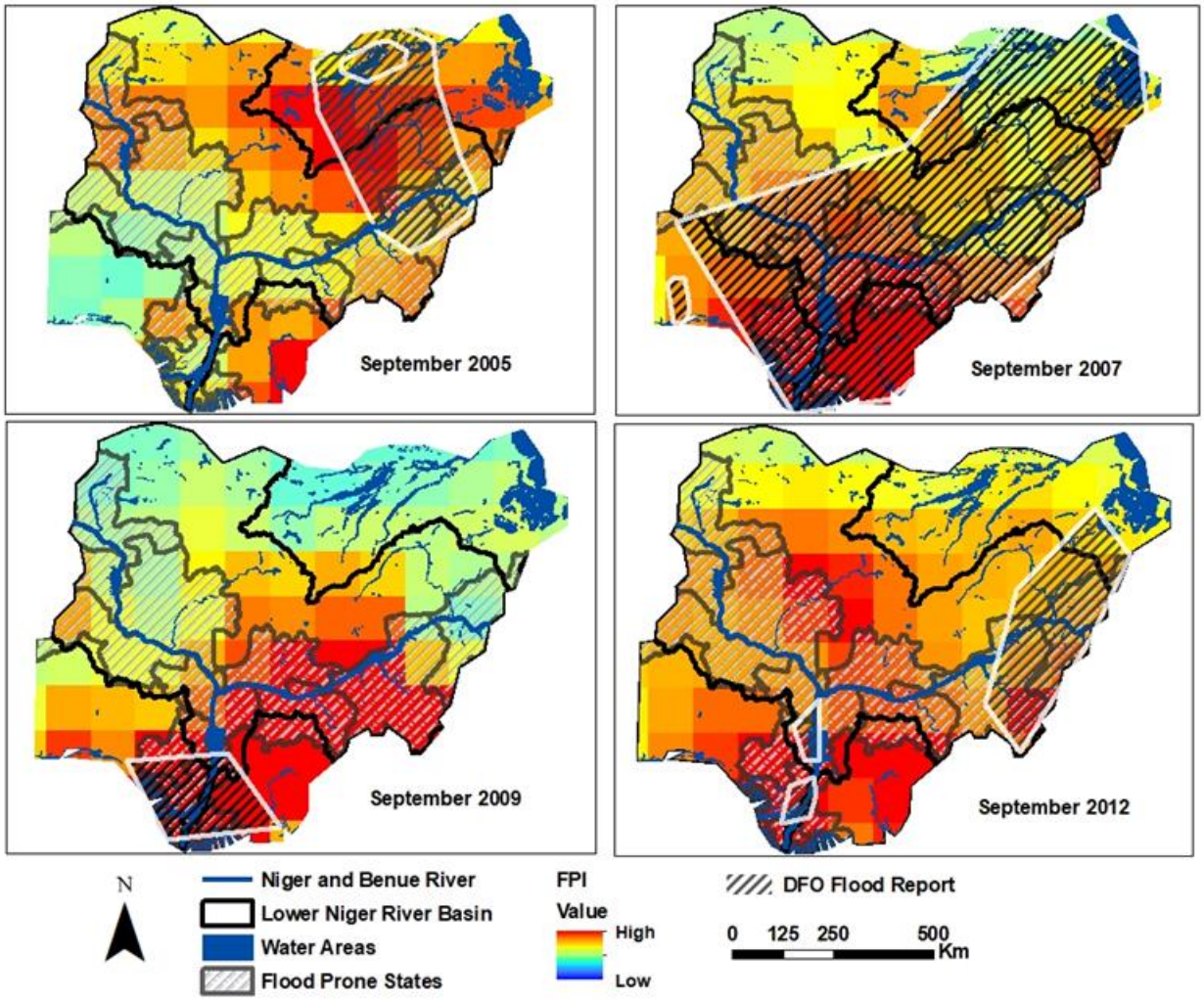

Figure 2.15: Comparison between GRACE-based FPI predicted floods and DFO reported floods.

Table 2.3: GRACE-based FPI values for the flood-prone/worst-hit states in September 2012.

Year	Flood Prone States	FPI
2012	Adamawa	1
	Anambra	0.5
	Bayelsa	0.4
	Benue	0.8
	Delta	0.5
	Edo	0.4
	Kebbi	0.5
	Kogi	0.7
	Kwara	0.5
	Nassarawa	0.4
	Niger	0.8
	Rivers	0.7
	Taraba	0.6

2.5 Discussion

Reager and Famiglietti [17] demonstrated that GRACE TWSA data can reveal when river basins have been filling with water over several months, when it rains, and the basin becomes full, and floods. The available storage or Sdef for LNRB (Figure 2.10) began to decrease August to October 2012 which represents the peak rainy season in the study area. Further, since soil moisture is critical in the accurate prediction of floods and general runoff [17], the storage deficit serves as an indicator in flood studies. The correlation coefficients of –0.7 for storage deficit and precipitation shows the inverse relationship that exists between the two variables which further supports the conclusion made by Reager and Famiglietti [17] that the storage deficit can be used with traditional methods of precipitation forecasting to determine the likelihood for flooding during the coming weeks. We also analyzed the relationship between storage deficit and FPI and found that storage decrease with an increase in the potential for flooding had a correlation coefficient of -0.8.

The FPI seems to perform well where flooding is mainly caused by heavy rainfall events [18] which was the case in Nigeria and by extension, LNRB. Heavy rainfall that occurred in August and September 2012 caused the major rivers, especially the Benue River, to overflow its banks, which led to authorities releasing water from the dams located within the basin (Cameroon). For our analysis, the FPI captured and predicted the flood events in LNRB in 2012 (Figures 2.11 and 2.12) which was also reported by the Nigerian NEMA and DFO (Figure 2.15) [30,31]. For validation of the GRACE-based FPI using the water budget-derived FPI, we tested the hypothesis that there is no difference between the indices using the alpha value of 0.05. With a correlation coefficient of 0.9 and $P > 0.05$ we have no reason to reject the null hypothesis.

The GRACE-based FPI and storage deficit, though invaluable, have limitations. The coarse spatial (>200 km^2) and temporal (monthly) resolutions of the GRACE data also makes it limited and unsuitable for forecasting local scale and flash floods [15,18], which may, therefore, make the FPI less effective. It has, however, an unequaled capability to monitor available water storage when combined with precipitation forecasting data and could increase warning lead time from one month to two months [17].

However, the relationship between the GRACE and water budget-based FPI shows promise when finer spatial and temporal resolutions data are used in deriving water budget TWSC (Equation (2.

1)), thus making it a supplement to the GRACE-based FPI and possibly reducing the limitation of the GRACE TWSA.

2.6 Conclusion

We estimated the hydrological conditions of the study area in terms of available storage and precipitation prior to the 2012 catastrophic flood using GRACE TWSA and GPCC data respectively. We also validated the GRACE TWSC using the water budget estimates TWSC, calculated the GRACE-based FPI for the basin, quantitatively and qualitatively compared the result to the water budget-based FPI and DFO flood report respectively. Based on our findings, we can make the following conclusions.

The GRACE TWSA and the derived FPI are both sensitive to precipitation by showing peaks and troughs in their time series which corresponds to wet season (peak) and dry season (trough). Based on the hydrological conditions of the study area in terms of precipitation and antecedent water storage state prior to flooding, the basin had a high amount of rainfall in August 2012 and could not balance the amount of incoming precipitation for September 2012 which then led to flooding.

The GRACE TWSA limitations could be managed assuming the GRACE-based FPI is supplemented with the water budget-derived FPI and using the water budget TWSC calculated from lower spatial and temporal data.

Therefore, the GRACE-based TWSA, Sdef and FPI in combination with other precipitation forecasting data and water budget-based TWSC/FPI could be utilized for operational flood monitoring in developing countries like Nigeria, where the unavailability of technical manpower, security and the cost of implementing and installing sophisticated flood monitoring/predicting measures could be prohibitive. In terms of cost, most satellite data are relatively cheap and readily available. Additionally, the current issue of security in some of the northern parts of the country prone to flooding might hinder the installation of flood monitoring devices, thus making remote-sensing products a viable option and an invaluable resource in flood studies in regions with little or no flood monitoring data.

2.7 References

1. Folorunsho, R.; Awosika, L.F. *Flood Mitigation in Lagos*, *Nigeria through Wise Management of Solid Waste: A Case of Ikoyi and Victoria Islands*, *Nigeria*; Paper presented at the UNESCO—CSI Workshop Maputo: Maputo, Mozambique, 19–23 November 2001.
2. Olajuyigbe, A.; Rotowa, O.; Durojaye, E. An assessment of flood hazard in Nigeria: The case of mile 12, Lagos. *Mediterr. J. Soc. Sci.* 2012, *3*, 367–375.
3. Bartholmes, J.C.; Thielen, J.; Ramos, M.H.; Gentilini, S. The European flood alert system EFAS – Part 2: Statistical skill assessment of probabilistic and deterministic operational forecasts. *Hydrol. Earth Syst. Sci.* 2009, *13*, 141–153.
4. Scawthorn, C. Modeling flood events in the US. In Proceedings of the Euro Conference on Global Change and Catastrophe Risk Management, HASA, Laxenburg, Austria, 6–9 June 1999.
5. Tariq, M.A.U.R. Risk-based planning and optimization of flood management measures in developing countries: Case Pakistan. PhD's Thesis, VSSD, Delft University of Technology, Delft, the Netherlands, 2012.
6. Victor, K. Remote Sensing of Floods and Flood-Prone Areas: An Overview. *J. Coast. Res.* 2015, *31*, 1005–1013.
7. Nasreddine, B.; Feng, Z.; Luca, B.; Yanbo, H.; Yumin, T. Near-Real-Time Flood Forecasting Based on Satellite Precipitation Products. *Remote Sens.* 2019, *11*, 252; doi:10.3390/rs11030252.
8. Sheffield, J.E.F.; Wood, N.; Chaney, K.; Guan, S.; Sadri, X.; Yuan, L.; Olang, A.; Amani, A.; Ali, S.; Demuth, L. A Drought Monitoring and Forecasting System for Sub-Sahara African Water Resources and Food Security. *Bull. Amer. Meteor. Soc.* 2014, *95*, 861–882, doi:10.1175/BAMS-D- 12-00124.1.
9. Zhang, X.; Tang, Q.; Liu, X.; Leng, G.; Li, Z. Soil Moisture Drought Monitoring and Forecasting Using Satellite and Climate Model Data over Southwestern China. *J. Hydrometeor* 2017, *18*, 23, doi:10.1175/JHM-D-16-0045.1.
10. Hossain, F.; Anagnostou, E.N. Assessment of current passive-microwave- and infrared-based satellite rainfall remote sensing for flood prediction. *J. Geophys. Res. Atmos.* 2005, *110*, D07102.

11. Brakenridge, R.; Anderson, E. Modis-Based Flood Detection, Mapping and Measurement: The Potential for Operational Hydrological Applications. In *Transboundary Floods: Reducing Risks Through Flood Management*; Marsalek J., Stancalie G., Balint G., Eds.; Nato Science Series: IV: Earth and Environmental Sciences, Springer: Dordrecht, The Netherland, 2006; pp. 1–12.
12. Zhan, X.; Ryu, D.; Crow, W. *Improving Flood Prediction Through the Assimilation of AMSR-E Soil Moisture Retrievals into a Hydrologic Model*; American Geophysical Union, Fall Meeting: Moscone Center, CA, USA, 2006; abstract ID: H23E-1545.
13. Adam, D. Gravity measurement: Amazing GRACE, *Nature* 2002, *416*, 10–11.
14. Chen, J.L.; Wilson, C.R.; Tapley, B.D.; Ries, J.C. Low degree gravitational changes from GRACE: Validation and interpretation. *Geophys. Res. Lett.* 2004, *31*, L22607.
15. Longuevergne, L.; Scanlon, B.R.; Wilson, C.R. GRACE Hydrological estimates for small basins: Evaluating processing approaches on the High Plains Aquifer, USA. *Water Resour. Res.* 2010, *46*, W11517, doi:10.1029/2009WR008564.
16. Reager, J.T.; Thomas, B.F.; Famiglietti, J.S. River basin flood potential inferred using GRACE gravity observations at several months lead-time. *Nat. Geosci.* 2014, *7*, 588–592.
17. Reager J.T.; Famiglietti, J.S. Global terrestrial water storage capacity and flood potential using GRACE. *Geophys. Res. Lett*. 2009, *36*, L23402.
18. Molodtsova, T.; Molodtsov, S.; Kirilenko, A.; Zhang, X.; VanLooy, J. Evaluating flood potential with GRACE in the United States. *Nat. Hazards Earth Syst. Sci*. 2016, *16*, 1011–1018.
19. Sun, Z.; Zhu, X.; Pan, Y.; Zhang, J. Assessing Terrestrial Water Storage and Flood Potential Using GRACE Data in the Yangtze River Basin, China. *Remote Sens*. 2017, *9*, 1011.
20. IFRCS — International Federation of Red Cross and Red Crescent Emergency Appeal; Nigeria: Floods. Available online: http://reliefweb.int/sites/reliefweb.int/files (accessed on 10 January 2019)
21. Kwari, J.W.; Paul, M.K.; Shekarau, L.B. The Impacts of Flooding on Socio-Economic Development and Agriculture in Northern Nigeria: A Case Study of 2012 Flooding in Yola and Numan Areas of Adamawa State Nigeria. *Int. J. Sci. Eng. Res.* 2015, *6*, 1433–1442.

22. Mazawaje, D.F.; Tsenbeya I.T.; Ismaila A.B. Analysis of the determinants of floods in Numan Town, Nigeria. Journal of Environmental Science and Engineering B 3 (2014) 264–273. Molodtsova, T.; Molodtsov, S.; Kirilenko, A.; Zhang, X.D.; VanLooy, J. Evaluating flood potential with grace in the United States. *Nat. Hazards Earth Syst. Sci.* 2016, *16*, 1011–1018.
23. NASA Earth Observatory – Flooding in Nigeria. Available online: (accessed on 20 August 2019). https://earthobservatory.nasa.gov/images/79404/flooding-in-nigeria.
24. Swenson, S.C. GRACE monthly land water mass grids NETCDF RELEASE 5.0. Ver. 5.0. PO. DAAC, CA, USA, 2012. Available online: http://dx.doi.org/10.5067/TELND-NC005 (accessed on 20 September 2018).
25. Velicogna, I.; Wahr, J. Measurements of time-variable gravity show mass loss in Antarctica. *Science* 2016, *311*, 1754–1756.
26. EartH2Observe project, Plymouth Marine Laboratory Remote Sensing Group, European Union's Seventh Programme for research, technological development and demonstration under grant agreement No. 603608. Available online: https://wci.earth2observe.eu/ (accessed on 10 October 2018).
27. Schneider, U.; Becker, A.; Finger, P.; Meyer-Christoffer, A.; Rudolf, B; Ziese, M. GPCC Full Data Reanalysis Version 6.0 at 1.0°: Monthly Land-Surface Precipitation from Rain-Gauges built on GTS-based and Historic Data, 2011, Available online: https://opendata.dwd.de/climate_environment/GPCC (accessed on 23 September 2018).
28. Sakumura, C.; Bettadpur, S.; Bruinsma, S. Ensemble prediction and intercomparison analysis of GRACE time-variable gravity field models. *Geophys. Res. Lett.* 2014, *41*, 1389–1397, doi:10.1002/2013GL058632.
29. NASA-JPL. *GRACE D-103133 Gravity Recovery and Climate Experiment Level-3 Data Product User Handbook*; NASA-JPL: Pasadena, CA, USA, 2019.
30. DFO (Dartmouth Flood Observatory), Global Active Archive of Large Flood Events. Available online: http://www.dartmouth.edu/~floods/Archives/ (Accessed on 14 December, 2018).
31. Climate-Data.Org. Climate Adamawa. Available online: https://en.climate-data.org/africa/niger/zinder/adamawa-349376/ (accessed on 22 February 2019).

CHAPTER 3

SPATIOTEMPORAL EVALUATION OF FLOOD POTENTIAL INDICES FOR WATERSHED FLOOD PREDICTION IN MISSISSIPPI RIVER BASIN, USA

Reproduced with permission from the *Environmental and Engineering Geoscience* [1]

Dorcas Idowu[2], *Wendy Zhou*[3]

3.1 Abstract

Gravity Recovery and Climate Experiment (GRACE) and GRACE Follow-on (GRACE-FO) twin satellites have revealed mass variation over time by measuring Earth's gravity field anomalies since 2002. These variations can be interpreted as changes in water storage on and beneath the Earth's surface. The water storage anomaly, also known as the Terrestrial Water Storage Anomaly (TWSA), has been successfully utilized to estimate a Flood Potential Index (FPI). The GRACE-based FPI is a good indicator of when a region is at risk of flooding. However, the GRACE data are limited by low spatial resolution, which has limited applicability to study areas smaller than 200,000 km2. Since the change in storage derived from the traditional water budget equation has the same physical meaning as GRACE TWSA, we hypothesize similarities in their derived FPIs. Here, we propose another index, known as Water Budget-based Flood Potential Index (WB-FPI), derived using higher spatial resolution hydrological datasets, which could produce similar but higher-resolution results to the GRACE-FPI. When combined with the GRACE-FPI, the index could be valuable in providing estimates on flood prediction on a catchment scale. Additionally, a combination of both indices could significantly reveal hydrological details for small basins. Both the GRACE-FPI and WB-FPI are applied to a case study of the flood potential of the Mississippi River Basin, USA. Our study reveals a good correlation between the resampled GRACE-FPI and WB-FPI using Nash-Sutcliffe Efficiency (NSE) index to compare application efficacy.

[1] See Appendix A for permissions.

[2]Graduate student, department of Geology and Geological Engineering, Colorado School of Mines. Leading author
[3]Department of Geology and Geological Engineering, Colorado School of Mines. Thesis advisor and corresponsding author

3.2 Introduction

Of all weather-related natural disasters, floods are the most common and widespread. Flooding is a natural hazard experienced in all regions of the world that receives one form of precipitation or the other and every state of the United States (U.S.) territory. In the U.S, fatalities resulting from flooding average 95 yearly during the last ten years, which are more than any other natural weather-related disasters such as tornadoes, hurricanes, or lightning. The most common cause of the flooding is heavy rain and/or snowmelt that accumulates water faster than the ground can absorb or rivers can contain.

The Midwestern United States was the wettest (Figure 3.1) on record between January to May of 2019 due to widespread extreme weather and heavy rainfalls. "The Great Flood of 2019", named by the New York Times, affected nearly 14 million people in the midwestern and southern states [1] and at least three fatalities were reported. Damages were also done to agricultural land, and at least 4,047 km2 of U.S agricultural land in nine major grain-producing states were flooded.

Longer lead-time flood prediction could remarkably reduce flood-related losses but requires accurate information on the hydrologic state of a whole river catchment, that is, its total water storage. Unfortunately, such detailed data are arduous to acquire with existing hydrological networks. However, data from GRACE twin satellites have exhibited some usefulness at monitoring the total/terrestrial water storage (TWS) and ultimately predicting floods [5, 10, 15]. It provides means to detect monthly variations in TWS within large river basins (>200,000 km2) based on measurements of changes in Earth's gravity field. The TWS indicates the land's temporal ability to process and account for all water on and beneath the Earth's surface.

A satellite and storage-based "flood potential" method using GRACE measurements has also proven invaluable at identifying major flood occurrences globally [14]. Over the GRACE twin satellite mission length, each region tends to exhibit an effective storage capacity, beyond which marked increases in runoff or evaporation must balance additional precipitation. These saturation periods indicate the possible transition to flooding [15].

TWS is a major element in the global and continental water cycle [7, 21]. "GRACE has provided a highly valuable dataset, which allows the study of TWS over larger river basins worldwide." [21]. However, the GRACE effective spatial resolution of 200,000 km2 makes it only possible to observe monthly variations in TWS at a continental or regional scale.

Reager and Famiglietti (2009) introduced a quantitative, effective terrestrial storage capacity and defined a flood potential index to emphasize the information contained within the GRACE data pertinent to regional flooding. Idowu and Zhou (2019), in their study using 1° by 1° grid datasets, showed that some correlation exists between the GRACE-derived TWS and the water storage derived from hydrological water budget.

The effective spatial resolution of GRACE data for resolving the localized hydrologic-related problem has been a debate. Several researchers [9, 19, 20, 22] proposed a series of methods to improve its spatial resolution. Since the minimum effective signal-to-noise ratio dictates the effective GRACE spatial resolution, the WB-FPI could complement the GRACE-based FPI. Combining these two indices could reduce the limitation of the GRACE-FPI for studying small areas or local scale hydrologic events. Therefore, our study evaluated the use of model-based data with finer spatial resolution in deriving a water budget-based TWS and produced water budget-based Flood Potential Index (WB-FPI), which could serve as an auxiliary for the GRACE-based TWS and FPI. The efficacy of the derived water budget-based TWS and WB-FPI were assessed on the continental US by evaluating how well the predictions compare to streamflow datasets.

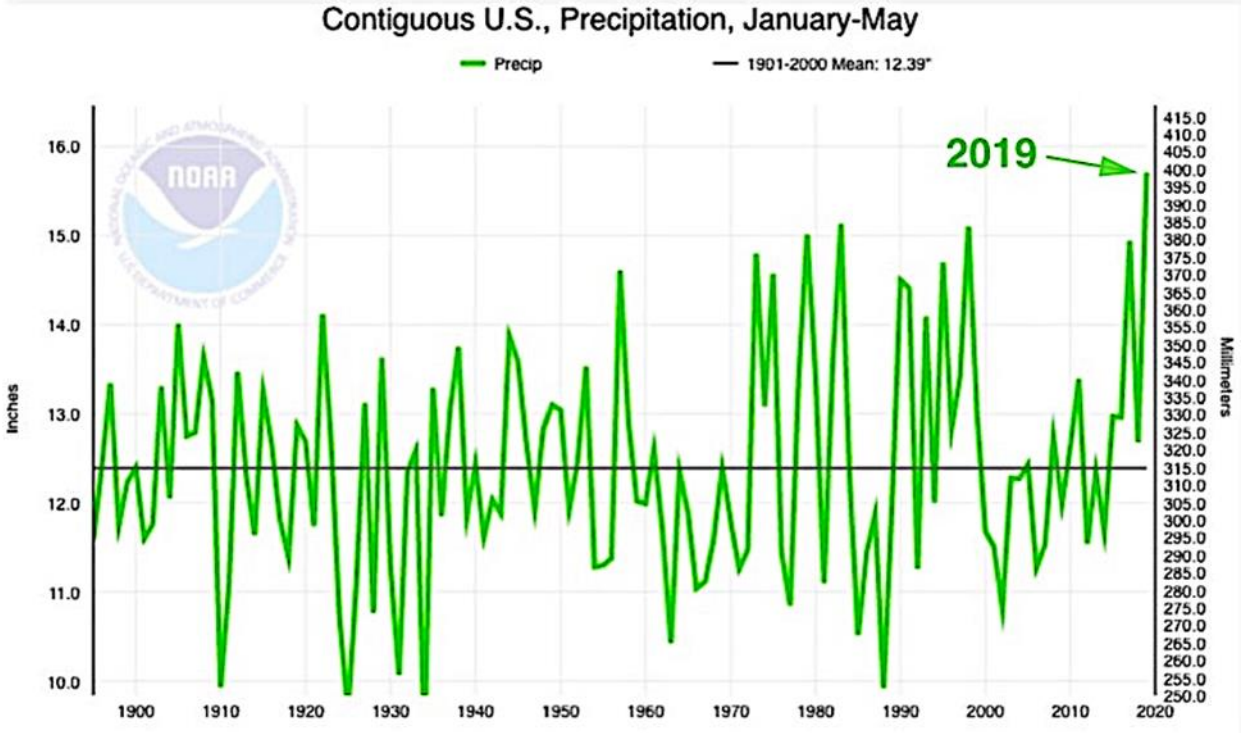

Figure 3.1: Precipitation averaged across the contiguous U.S. for the period Jan.-May for all years going back to 1895, with 2019 standing head and shoulders above all prior years to date. Image credit: NOAA (National Oceanic and Atmospheric Administration).

3.3 Study Area

The Mississippi River is the second longest river on the North American continent. Its drainage basin is the world's second largest, drains an approximate area of 4,800,000 km2, which includes tributaries from 32 U.S. states and two Canadian provinces. The Mississippi River watershed encompasses 40% of the contiguous United States, and the major tributaries include the Missouri, Ohio, Arkansas-Red-White, and Tennessee Rivers. It consists of five major sub-basins, including the Upper Mississippi, Lower Mississippi, Missouri, Arkansas Red-White, Ohio, and Tennessee River Basins (Figure 3.2).

The Mississippi River and its tributaries have flooded on many occasions. Historically, heavy rainfall and snowmelt events that cause a slow rise in the rivers and extend for days or weeks seem to be the major culprit responsible for flooding along the river. Floods and flood damages significant enough to merit regional or national attention have occurred in the Mississippi River Basin between the 19th and 21st centuries. In 2019, flooding along the Mississippi River was not

the result of a single weather event. Instead, the Mississippi River flooding of record duration consisted of a series of flood events in tributary basins. Different measures, including structural and non-structural flood control measures [2, 6, 16-18] have been taken to mitigate the devastating effects of floods along the river, yet it is persistent. Longer flood warning lead time could give stakeholders enough time to take measures that may reduce the economic impact and damages resulting from floods along the river.

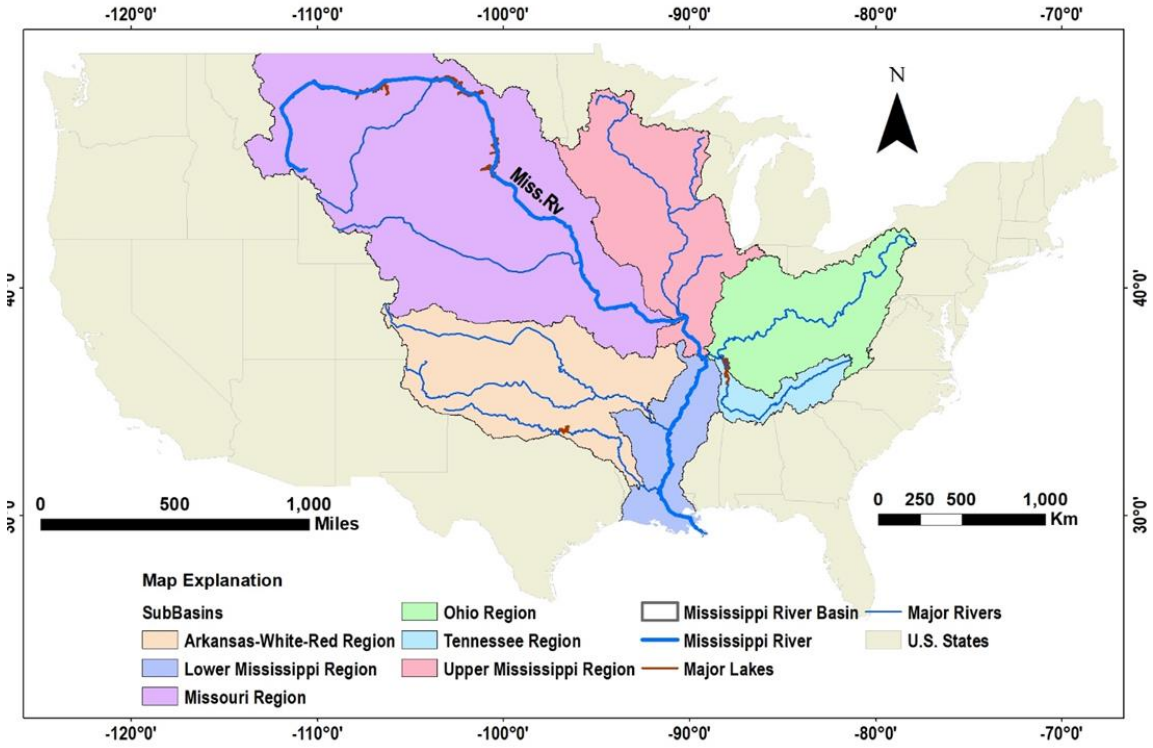

Figure 3.2: Map of the United States of America showing the Mississippi River and its major drainage basins.

Reager et al. (2014) showed that GRACE-based TWS information could increase regional warning lead times to as long as five months. However, the GRACE spatial resolution could be a limiting factor for its application to the study of flood potential on a basin-scale or to pinpoint approximate locations within a basin that require emergency flood mitigation measures. Here, we tested the accuracy and performance of a 0.125° X 0.125° water budget-based TWS at predicting flood

within the Mississippi River Basin and compared the accuracy to the predictions from GRACE-based TWS.

3.4 Datasets

3.4.1 GRACE Terrestrial Water Storage (TWS)

The GRACE satellite and its Follow-On twin measure the changes in the Earth's gravity field on a monthly temporal scale at a spatial resolution of 1° X 1°. These observed changes are related to changes in surface mass resulting from movement of water on and/or within the surface of the Earth or mass redistribution from earthquakes. The GRACE-based TWS on land represents the combination or sum of all water stored on the land surface. Data acquired by the satellites, which are spherical harmonics, are officially processed by three centers: Jet Propulsion Laboratory (JPL), GeoforschungsZentrum Potsdam (GFZ), and Center for Space Research (CSR) at the University of Texas. Despite the centers applying different processing methods and techniques on the GRACE spherical harmonics, the resulting products were similar, referred to as solutions. For our study, we used the 1° X 1° spherical harmonics solution from the Center for Space Research (CSR) at the University of Texas, Austin. The GRACE RL05 TWSA products were downloaded online at http://grace.jpl.nasa.gov/. The spatial resolution is approximately 111km X 111km. We downloaded data for May 2011 in the Mississippi River basin. We also obtained the Jet Propulsion Laboratory (JPL) TELLUS GRACE Follow-On (GRACE-FO) Level-3 data from January to May 2019 available at the Physical Oceanography Distributed Active Archive Center of the National Aeronautics and Space Administration, JPL, California Institute of Technology (http://podaac.jpl.nasa.gov/dataset/TELLUS_GRFO_L#_JPL_RL06_LND).

3.4.2 North American Land Data Assimilation System (NLDAS) Data

The NDLAS land-surface model (LSM) datasets, derived from a collaborative project among several groups, are spatially and temporally consistent from the best available observations and reanalyzed to support modeling activities. This effort is a core project with support from the National Oceanic and Atmospheric Administration (NOAA) climate program office's Modelling, Analysis, Prediction and Projections (MAPP) program. Monthly 0.125° X 0.125° mosaiced and secondary forcing NDLAS data for some hydrological variables were retrieved from the National

Aeronautics and Space Administration (NASA) Land Data Assimilation System website. The spatial resolution is approximately 11km by 11km.

3.4.3 Precipitation Data

The 1° X 1° Global Precipitation Climatology Centre (GPCC) data provided by the NOAA/OAR/ESRL PSD, Boulder, Colorado, USA were used for deriving the GRACE-based FPI. The 0.125° X 0.125° NDLAS Secondary Forcing precipitation data downloaded from the NASA NLDAS were used for deriving the water budget-based FPI.

3.4.4 Dartmouth Flood Observatory (DFO) Data

The DFO is an active global archive of large flood events. Information in the archive is derived from news, governmental, instrumental, and remote sensing sources. We used the zip-compressed GIS shape format, which displays a polygon of the total area affected by flooding for different dates. Polygons of dates corresponding to our study baseline were used for our validation. It is worthy of mention that the DFO source of validation is the news media and government sources and may thus be biased towards large flood events.

3.4.5 United States Geological Survey (USGS) Streamflow Data

Maps of monthly-averaged streamflow from the USGS water watch data services were also used to validate our analysis. The map displays river discharge in percentile classes on a scale of one hundred. For instance, "above normal" is for streamflow greater than the 75th percentile, while "normal" is between 25th and 75th percentiles, and "below normal" is for streamflow less than the 25 percentiles. These maps were georeferenced in the ArcGIS suite.

3.4.6 Sentinel-2 data

The Copernicus Sentinel-2 satellite mission monitors variability in land surface conditions while its swath width (290 km) and revisit-time support monitoring of Earth's surface changes. The satellite also provides systematic global acquisitions of high spatial and temporal resolution multispectral images or observations for land-cover maps, land-change detection maps, and

geophysical variables. The European Space Agency's Sentinel-2 satellite mission monitors the variability of land surface conditions. The Sentinel-2 optical satellite imageries were used for validation of our results. The satellite data can be obtained via the Copernicus Open Access Hub (https://scihub.copernicus.eu).

3.5 Methodology

In deriving the GRACE-based and WB-based FPIs, we applied the methodology proposed by Reager and Famiglietti (2009) and Idowu and Zhou (2019). To compare the index performance, we present two case studies for the Mississippi River basin (Figure 3.2), i.e., the 2011 and 2019 flood events. Furthermore, for consistency in our analysis, we used the GRACE TWSA baseline because it has a shorter record length (2004 - 2017) in comparison to the NLDAS datasets (1979 – recent). To further test the WB-based FPI derived using the 0.125° X 0.125° NLDAS datasets, we studied the recent 2019 flood event (Figure 3.1) within the basin and validated the predictions using the streamflow datasets and satellite imageries from the Sentinel-2 satellite.

3.5.1 GRACE Flood Potential Index

Throughout the GRACE TWSA record length, there are persistent annual maxima that correspond to hydrological extremes. As a result, we defined our maximum water storage capacity (Smax) as the historical maximum water storage capacity within the Mississippi drainage basin, our area of interest. The storage deficit (Sdef), which is the available water on land before attaining the Smax was derived using equation (3.1):

$$Sdef\ (t) = Smax - TWSA\ (t-1) \qquad (3.1)$$

where TWSA(t-1) is the total water storage from the previous month [5], and Sdef implies a shortage or deficit in water storage within a basin or an area on the land. The deficit, Sdef, is expected to increase or decrease during the drier or wetter part of the year.

The flood potential, which is the quantity of incoming water above available storage, was calculated using:

$$F\ (t) = Pmon\ (t) - Sdef\ (t) \qquad (3.2)$$

where F (t) is the flood potential, and P(mon) is monthly precipitation from the GPCC. The flood potential was further normalized [14] to derive the GRACE-based FPI:

$$FPI\ (t) = F\ (t)\ /max[F\ (t)] \qquad (3.3)$$

The GRACE-based FPI values range from -∞ to 1, with positive values implying the hydrological inputs are above the normal water storage and should be interpreted as a potential flood risk.

3.5.2 Water Budget Flood Potential Index (WB-FPI)

First, we derived the TWSA, which is also ds/dt, by using the traditional water balance equation:

$$ds/dt = P - ET - R - SM \qquad (3.4)$$

where ds/dt is TWSA, P is precipitation, which includes rainfall and snow, ET is evapotranspiration, R is the runoff, and SM is soil moisture. Here, we assumed there was no net groundwater flow. Next, we applied the methodology for deriving the GRACE-FPI in calculating the water budget-based FPI.

3.5.3 GRACE-based FPI and WB-FPI Comparison

As validation of the WB-FPI, we tested its skill of prediction against the GRACE-based FPI for May 2011 (Figure 3.3) in the Mississippi River basin and the six United States regions (Missouri, Upper Mississippi, Ohio, Lower Mississippi, Arkansas-White-Red, and Tennessee) using the Nash-Sutcliffe Efficiency (NSE) index, Pearson's correlation coefficient (r) and coefficient of determination (R2). The NSE is an efficiency index that is potentially reliable and commonly used for assessing the goodness of fit of hydrological models [8, 12]. It is commonly referred to as the efficiency index (Ef) and defined as:

$$Ef \ = \ 1 \ - \frac{\Sigma n\ (X - Y)2}{\Sigma\ (Y - Z)2} \qquad (3.5)$$

where n is the sample size, X is the observation value, Y is the simulated value, and Z is the mean of observed data [11]. Generally, NSE ranges from -∞ to 1. Moriasi et al. (2007) suggested that NSE values generally between 0 and 1 are viewed as acceptable levels of performance while NSE values less or equal to 0 are interpreted where the mean observed value is a better predictor than the simulated value. The R2 and r are used to describe the level of collinearity between simulated and measured data. R2 indicates how much variance in the measured data s explained by the model and ranges from 0 to 1 with higher values suggesting less error variance. Commonly, values higher than 0.5 are considered acceptable [11]. Pearson's correlation coefficient is an index that explains

the level of the linear relationship between observed and simulated data [11]. It ranges from -1 to 1. When r is 1 or -1, there exists a perfect positive or negative linear relationship, and when r is 0, no linear relationship exists.

In continuing towards the index comparison, we resampled the GRACE-based FPI resolution of 1° X 1° to that of the WB-FPI, which is 0.125° X 0.125°. With this, we computed and compared the statistics for both indices.

3.5.4 Georeferencing USGS Streamflow Condition Datasets

The USGS streamflow condition maps were obtained in raster format (Graphics Interchange Format) without having prior spatial reference information. To view, query, analyze, and accurately compare them to the predictions by the WB-FPI for our study period, we georeferenced them. Georeferencing is associating a physical map or raster image with spatial locations or map coordinates. In other to achieve this, we built an attribute table for each of the maps by using their unique values. The values in the USGS maps that are of interest to us were those having a percentile value of above normal to high streamflow readings. We isolated these pixels by reclassifying the maps and setting irrelevant pixels to NoData, leaving us with pixels of interest that were georeferenced.

3.5.5 Predictive Performance Test

Our classification utilized only two classes. Formally, each instance (e.g., the USGS streamflow condition) is mapped to one element of the set {p (flood), n (no flood)} of positive and negative class (flood or no flood) labels. A classification model (or classifier, which in this case is WB-FPI) is a mapping from instances to predicted classes [23]. Some models produce discrete class labels indicating only the predicted class of an instance. To differentiate between the actual class and the predicted class (Table 1), we used the labels {Y, N} for the class predictions produced by our model. Given a classifier (WB-FPI) and an instance (USGS streamflow condition), there are four possible outcomes (Table 3.1). A positive instance classified as positive is counted as a True Positive (TP). If classified as negative, it is counted as False Negative (FN). However, if the instance is negative and classified as negative, it is counted as True Negative (TN), and if classified as positive, is counted as False Positive (FP).

Table 3.1: The contingency table and some performance metrics

	USGS Streamflow Condition	
WB-FPI	Actual Yes	Actual No
Predicted Yes	True Positive (TP) or hit	False Positives (FP)
Predicted No	False Negatives (FN)	True Negatives (TN)
	True Positive Rate (TPR) = TP/Actual Yes	False Positive Rate (FPR) = FP/Actual No

The Receiver Operative Characteristics (ROC) is a technique for visualizing, organizing, and selecting classifiers based on their performance and are generally useful performance graphing methods [23]. ROC graphs that show the relative tradeoffs between TP and FP are two-dimensional graphs in which the True Positive Rate (TPR) is plotted on the Y-axis, and the False Positive Rate (FPR) is plotted on the X-axis. It is also commonly used as a method for testing the performance of a continuous index (such as the FPI) as a discrete classifier against the USGS streamflow datasets. A discrete classifier is one that outputs only a class label. Each discrete classifier produces a pair of TPR and FPR corresponding to a single point in the ROC space. Here, we compared the performance of the WB-FPI against the USGS streamflow data from January 2019 to May 2019 within the Mississippi River watershed and each month represents a point on the ROC space. Several points in the ROC space are important to note, and informally, one point in the ROC space is better than another [23]. The 1:1 diagonal line in a ROC plot represents a random guess, which is no predictive skill, while areas below the line assume predictive skill worse than a random guess. The closer the points are to the upper left corner of the graph, the better the predictive skill.

3.6 Results

Figure 3.3 is the visual comparison of both indices at their inherent spatial resolution, which displays a similar spatial pattern. Qualitatively, both indices predicted flood in areas where the DFO reported flood for May 2011 in the Mississippi River basin. The WB-FPI, when statistically compared to the GRACE-based-FPI after resampling to 0.125° X 0.125°, shows some agreement with the index (Table 3.2).

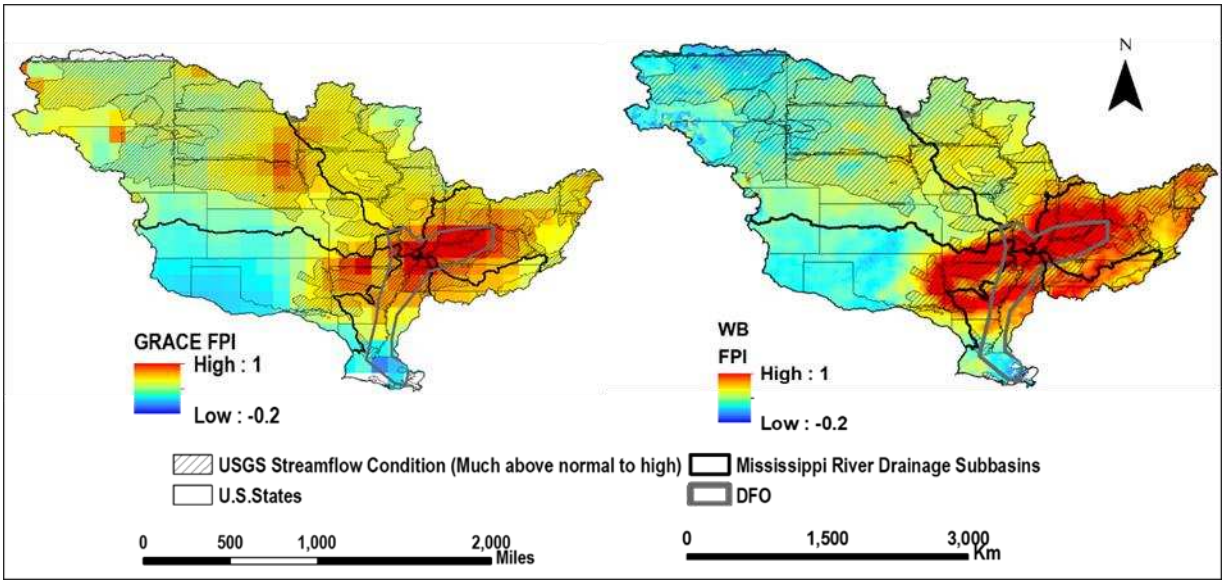

Figure 3.3: (a) GRACE-based FPI and (b) WB-based FPI for May 2011 showing areas of high (red) FPI and low (Blue) FPI in the Mississippi River Basin.

Table 3.2: Statistical Comparison of GRACE-Based and WB FPI for May 2011

Statistics of individual layers	**GRACE-BASED FPI**	**WB-FPI**
Min	-0.2	-0.3
Max	1.0	1.0
Mean	0.2	0.2
Standard Deviation	0.2	0.2
Correlation Coefficient	**0.8**	

Figure 3.4 shows the computed GRACE-based FPI and WB-based FPI at their inherent spatial resolution for the Tennessee region within the Mississippi River Basin. Visually, there exist some similarities in the spatial variation of indices despite having a different spatial resolution. Relatively speaking, the GRACE-based FPI tends to underestimate the flood potential, especially in the central portion of the Tennessee Region.

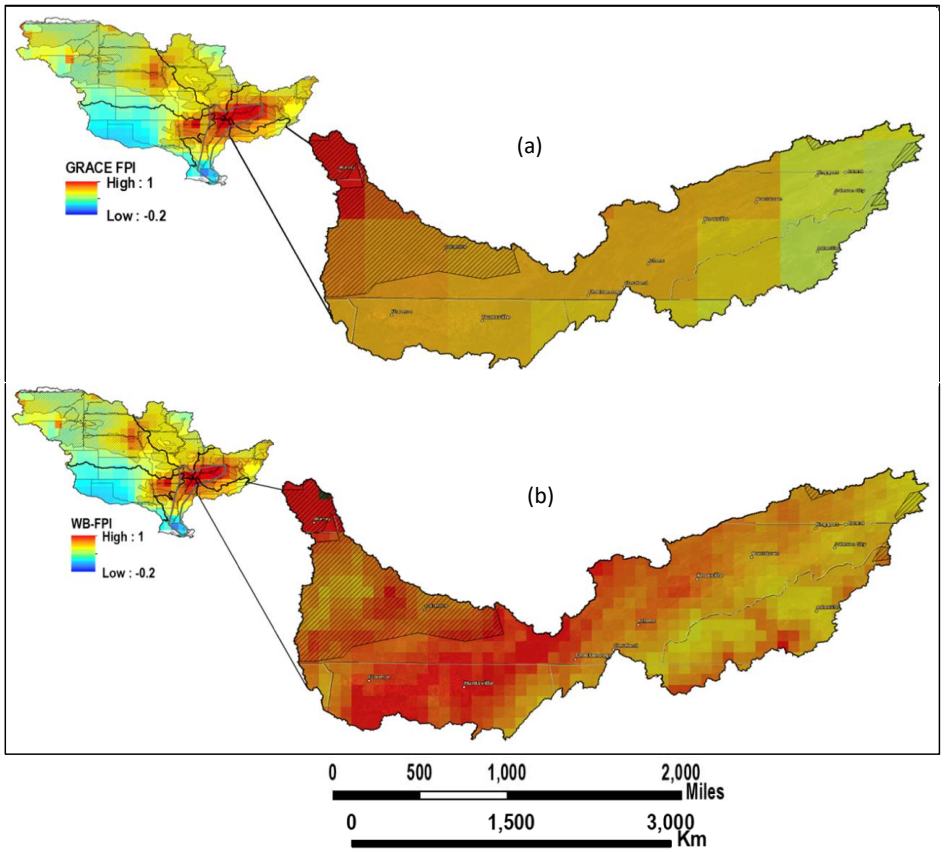

Figure 3.4: (a) GRACE-based FPI at a spatial resolution of 1° X 1° and (b) WB-based FPI at a spatial resolution of 0.125° X 0.125° in May 2011 for the Tennessee Region within the Mississippi River basin.

Furthermore, we computed the GRACE-based FPI and WB-FPI for each region within the Mississippi River basin from January to May 2019. These months were named the wettest on record. We compared the indices qualitatively and quantitatively (Figure 3.5). For each month, Table 3.3 shows that the NSE values for the regions suggest an acceptable level of the WB-FPI

performance for flood prediction using the data from January to May 2019. The r and R2 values also indicate some agreement between both indices.

Table 3.3: Statistical Comparison of GRACE-Based and WB FPI using NSE, r and R^2 methods from January to May 2019

United States Regions	**NSE**	**r**	**R2**
Missouri Region	0.1	0.6	0.4
Upper Mississippi Region	0.3	0.9	0.8
Ohio Region	0.9	0.8	0.7
Lower Mississippi Region	0.8	0.8	0.7
Arkansas-White-Red Region	0.6	0.8	0.7
Tennessee Region	0.9	0.9	0.8
Average	**0.6**	**0.8**	**0.7**

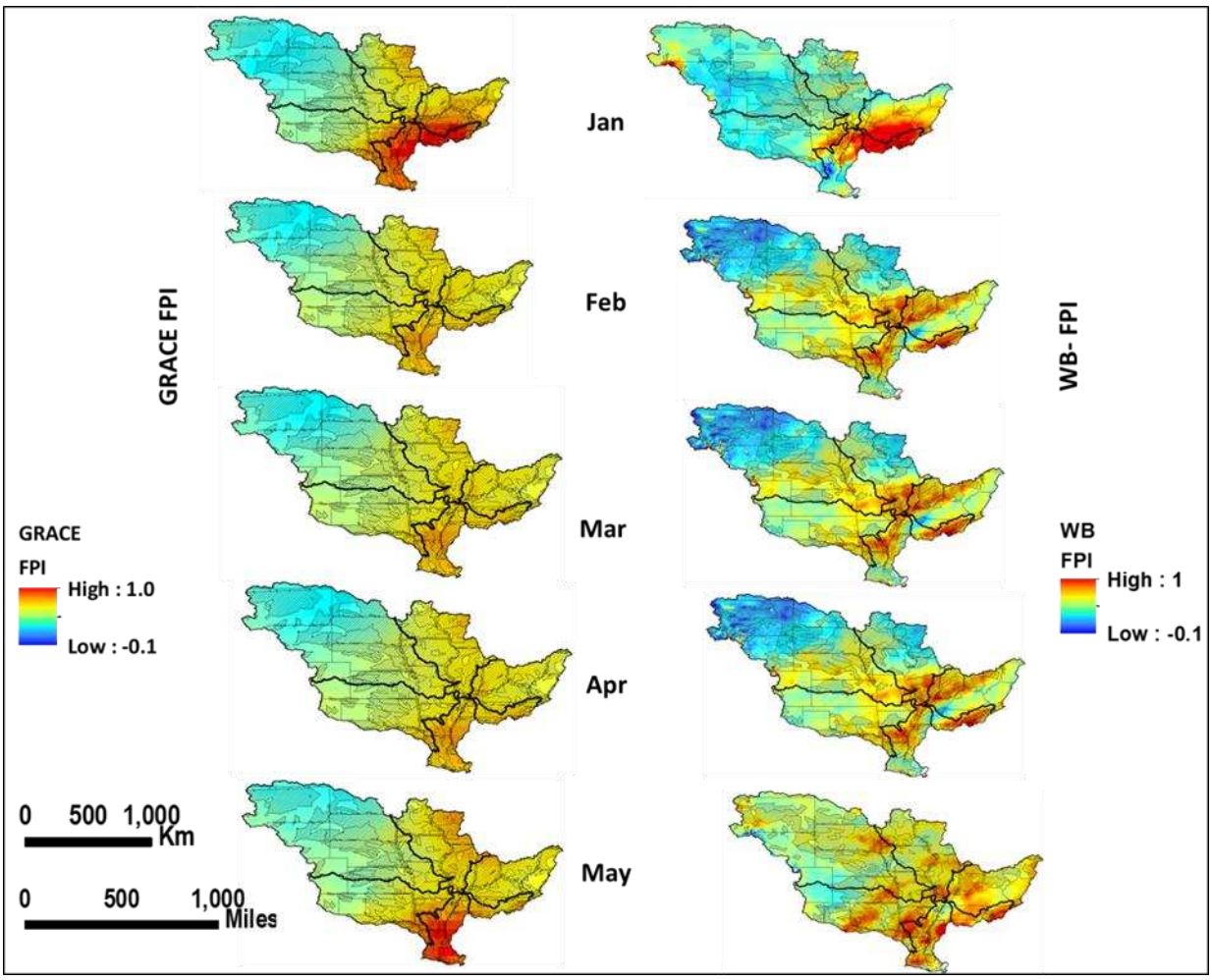

Figure 3.5: Visualization and comparison of the spatial distribution of the (a) GRACE-based FPI and (b) WB-based FPI for the Mississippi River basin from January to May 2019.

The predictive skills of the WB-FPI were tested against the USGS streamflow polygons using the contingency table and ROC space graph. The polygons resulted from georeferencing the USGS streamflow maps and converting them from raster to polygon. We then computed a contingency table (confusion matrix) using a discrete classifier where we have two classes (Yes (flood) or No (no flood). We assigned the class "Yes (flood)" to all areas within the USGS streamflow polygon and a class "No (no flood)" for areas outside the USGS streamflow polygon. Each contingency table produces a TPR, FPR, accuracy, and precision for a discrete classifier (Table 3.4). We plotted the TPR for each month against the FPR on a ROC space graph to test

how the WB-FPI predicted floods compared to the USGS streamflow data from January to May. Figure 3.6 shows that each point and averaged point plotted on the graph fell on the better half of the graph above the random guess line and suggests that WB-FPI is a better classifier [23].

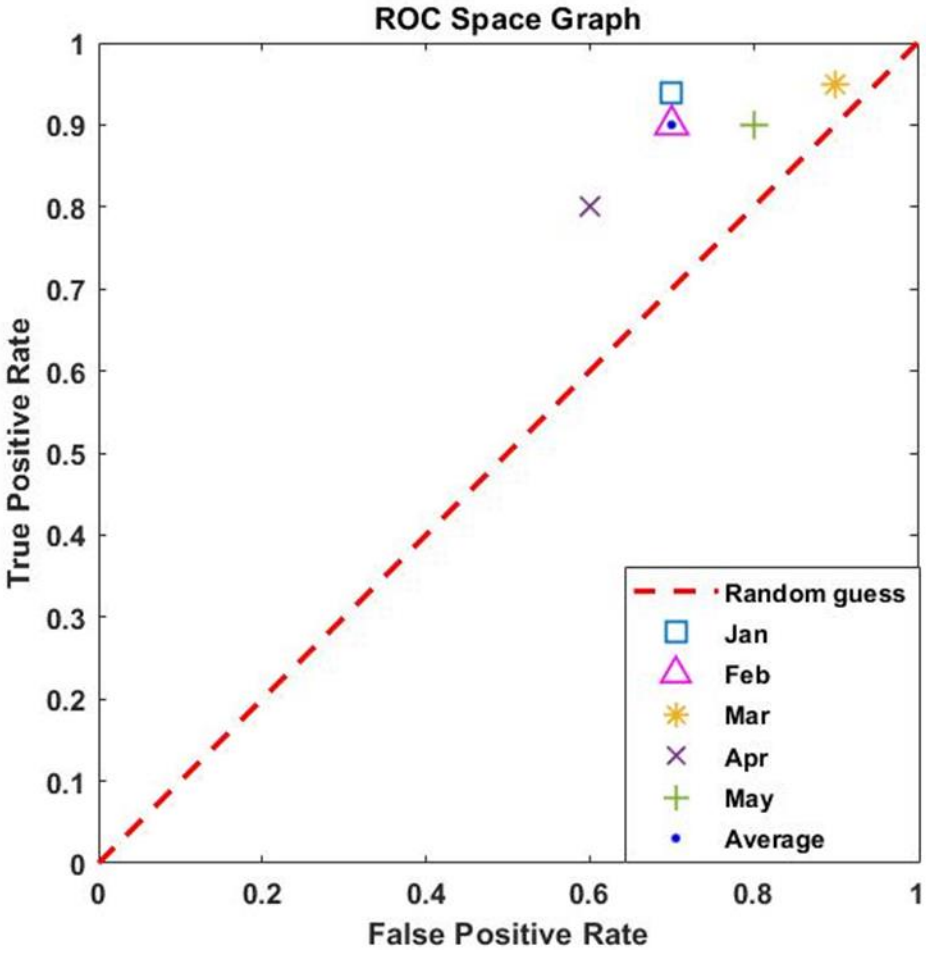

Figure 3.6: ROC space graph showing a flood classification of the WB-based FPI and the USGS streamflow condition from January to May 2019 and their average point.

Table 3.4: ROC space graph performance metrics from January to May 2019.

	Accuracy	**TPR**	**FPR**	**Precision**
January	0.8	0.9	0.7	0.9
February	0.7	0.9	0.7	0.7
March	0.7	0.9	0.0	0.7
April	0.7	0.8	0.6	0.8
May	0.9	0.9	0.8	0.9
Average	**0.8**	**0.9**	**0.7**	**0.8**

We qualitatively compared pre-and post-flood scenes from Sentinel-2 to areas with positive WB-FPI from January to May 2019. The WB-FPI predicted flood in areas in the Sentinel-2 scenes. All WB-FPI values compared to the Sentinel-2 scenes have FPI values greater than zero (Figures 3.7 - 3.9), which is indicative of a flood situation. The WB-based FPI shows areas of high (red) and low (blue) FPI, and areas of high FPI are shown on the during-flood Sentinel-2 scenes for January and May 2019. The spatial variations in the FPI values from as seen in Figures 3.7, 3.8, and 3.9, are a result of the changes in water storage within the basin, which can be associated with heavy rainfall and/or snowmelt. These variations are also reflected in Figure 3.6.

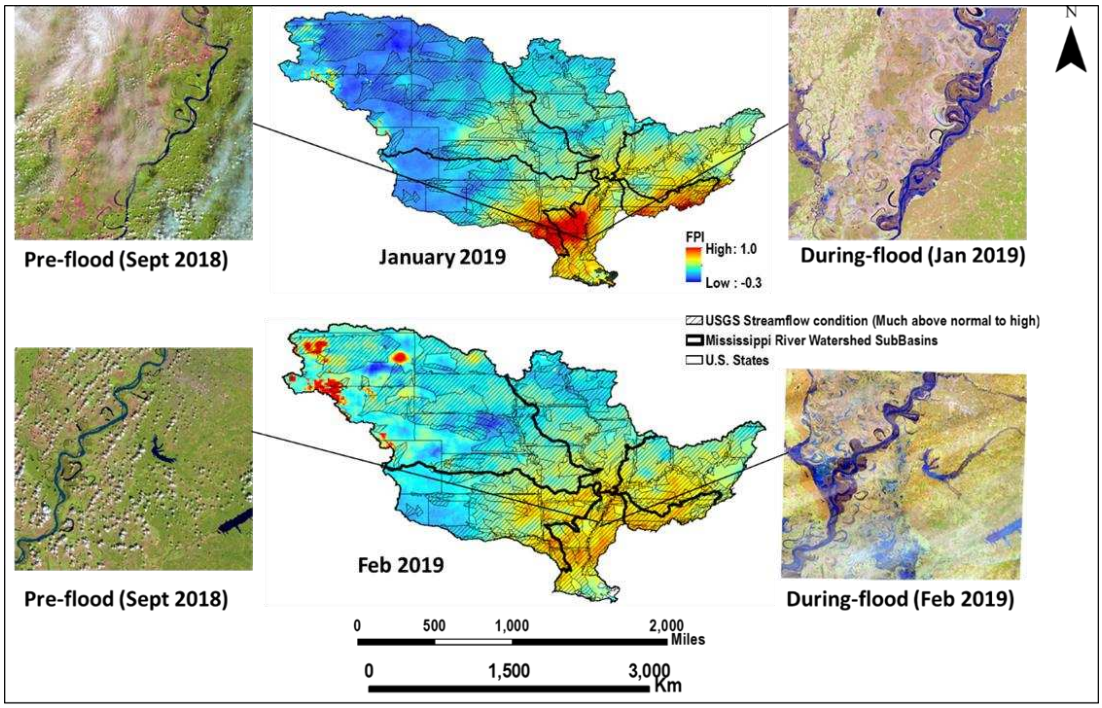

Figure 3.7: Pre- and During-flood Sentinel-2 scenes with WB-based FPI for January and February 2019 for an example section of the Mississippi River.

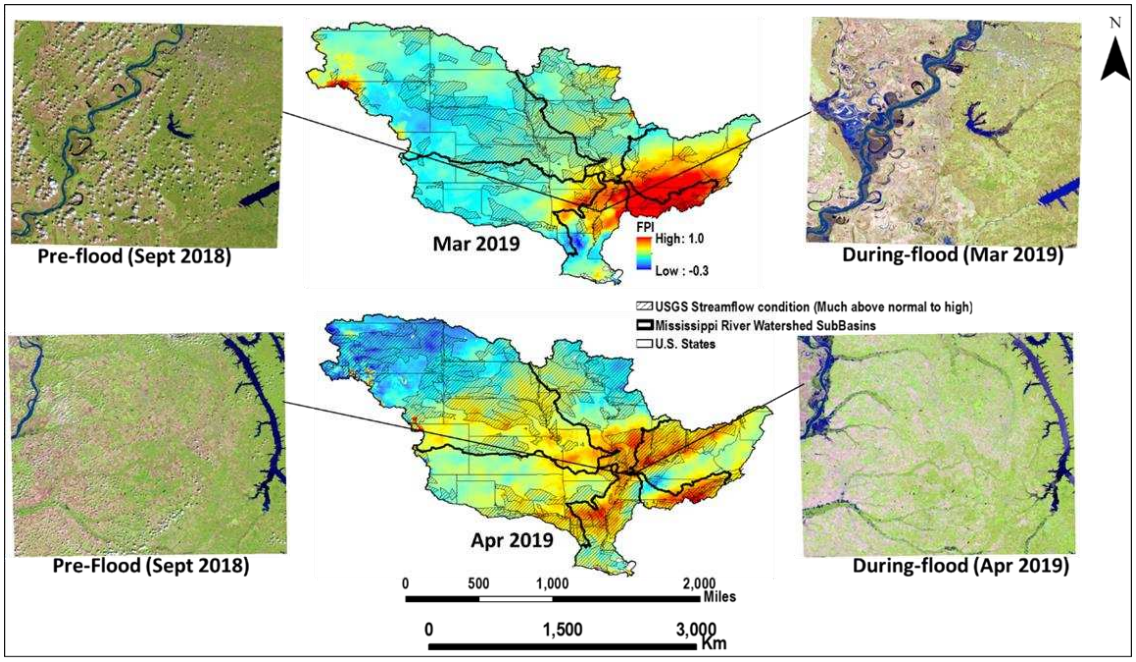

Figure 3.8: Pre- and During-flood Sentinel-2 scenes with WB-based FPI for March and April 2019 for an example section of the Mississippi River.

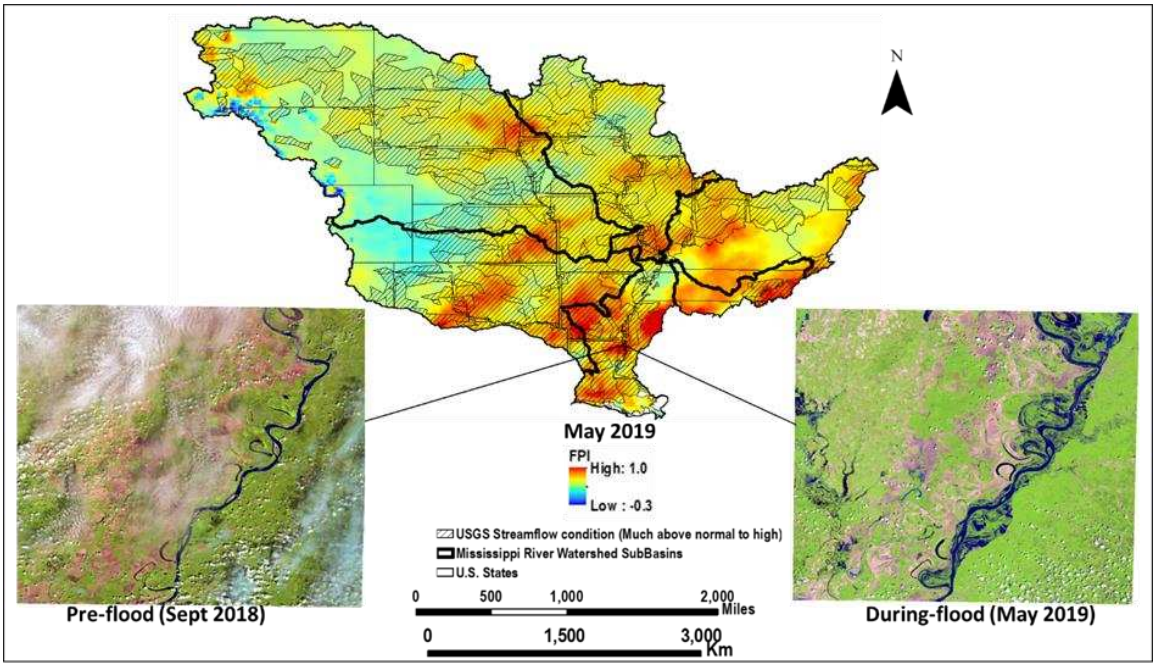

Figure 3.9: Pre- and During-flood Sentinel-2 scenes with WB-based FPI for May 2019 for an example section of the Mississippi River.

3.7 Discussion and Conclusion

Our study suggests a good correlation between the comparison of the resampled GRACE-based FPI and WB-FPI (Figure 3.3) for the Mississippi River basin. The ROC space graph plotted for WB-FPI was to determine how well it predicted flood at different times when compared to the USGS streamflow data. The points plotting above the diagonal line (random guess line) imply a better classification (Figure 3.6). The location of the points (upper left above the random guess line) implies the WB-FPI could predict every flood event correctly (high TPR) but also have the tendency to over-predict floods (hence the high FPR). The GRACE-based FPI has a similar down-side [5]. A machine learning method could be applied to the data to reduce the FPR. Furthermore, the differences between the indices possibly resulting in high FPR could be attributed to measurement errors and uncertainties inherent in the data [4].

The statistical similarities between the GRACE-based FPI with a spatial resolution of 1° X 1° and WB-FPI having a spatial resolution of 0.125° X 0.125° further suggest that the WB-FPI derived using a satellite-based high-resolution data could predict flooding on a local scale. The ability to predict effectively floods for smaller areas could further improve flood prediction, especially in developing countries where ground flood monitoring systems are sparse or not available.

Data continuity presented by the GRACE-FO and that by the NLDAS shows the potential for future flood potential or prediction studies using the methodologies presented in this research or a combination with other flood prediction or forecasting models.

3.8 References

1. Almukhtar, S.; Migliozzi, B.; Schwartz, J.; AND Williams, J., 2019, The Great Flood of 2019: A Complete Picture of a Slow-Motion Disaster. New York Times. Retrieved November 22, 2019.
2. DeHaan H.; Stamper J.; AND Walter B., 2012, Mississippi River and Tributaries System 2011 post-flood report: Documenting the 2011 Flood, the Corps' response, and the performance of the MR&T System. USACE, Mississippi Valley Division, https://hdl.handle.net/11681/19106.
3. DFO (Dartmouth Flood Observatory), n.d., Global Active Archive of Large Flood Events. Available online: http://www.dartmouth.edu/~{}floods/Archives/ (accessed on 14 December 2018).
4. Güntner, A., 2008, Improvement of Global Hydrological Models Using GRACE Data. Surv Geophys **29,** 375–397. https://doi.org/10.1007/s10712-008-9038-y

5. Idowu, D.; AND Zhou, W., 2019, Performance Evaluation of a Potential Component of an Early Flood Warning System—A Case Study of the 2012 Flood, Lower Niger River Basin, Nigeria. Remote Sensing, 11(17), 1970. https://doi.org/10.3390/rs11171970
6. Isaacson E.; Stoker J.; AND Troesch A, 1956, Numerical solution of flood prediction and river regulation problems. New York University Institute of Mathematical Sciences. Contract DA-33-017.ENG.267 prepared under the sponsorship of U.S. Army Corps of Engineers, Ohio River division.
7. Landerer F. W.; AND Swenson S. C., 2012, Accuracy of scaled GRACE terrestrial water storage estimates. Water Resources Research, Vol 48, W04531, 11 PP, doi:10.1029/2011WR011453.
8. McCuen, R. H.; Knight, Z.; AND Cutter, A. G., 2006, Evaluation of the Nash-Sutcliffe efficiency index. J. Hydrol. Eng., 11(6), 597–602.10.1061/(ASCE)1084-0699(2006)11:6(597)
9. Miro, E. M.; AND Famiglietti, S. J., 2018, Downscaling GRACE remote sensing datasets to high-resolution groundwater storage change maps of California's Central Valley. Remote Sens. 10, 143
10. Molodtsova, T.; Molodtsov, S.; Kirilenko, A.; Zhang, X.; AND VanLooy, J., 2016, Evaluating flood potential with GRACE in the United States. Nat. Hazards Earth Syst. Sci. 16, 1011–1018.
11. Moriasi,D.N.,Arnold,J.G.,VanLiew,M.W.,Bingner,R.L.,Harmel,R.D.,&Veith,T.L.(2007). Model evaluation guidelines for systematic quantification of accuracy in watershed simulations. Transactions of the ASABE, 50(3), 885e900.

12. Nash, J. E., and Sutcliffe, J. V. (1970). River flow forecasting through conceptual models. 1: Discussion of principles. J. Hydrol., 10(3), 282–290.10.1016/0022-1694(70)90255-6
13. Polansek, T., 2019, U.S. disaster aid won't cover crops drowned by Midwest floods. Reuters, via Climate Signals. Retrieved November 22, 2019.
14. Reager, J. T.; AND Famiglietti, J.S., 2009, Global terrestrial water storage capacity and flood potential using GRACE. Geophys. Res. Lett. 36, L23402.
15. Reager, J. T.; Thomas, B. F.; AND Famiglietti, J. S., 2014, River basin flood potential inferred using GRACE gravity observations at several months lead time. Nature Geoscience, 7(8), 588-592.
16. Semmens, S. N.; Zhou, W.; AND Robbins, B., 2021, Empirical Assessment of Blanket Thickness as an Indicator of Backward Erosion Piping, Lower Mississippi Valley, USA, Natural Hazards Review 22(2), 1-9. https://doi.org/10.1061/(ASCE)NH.1527-6996.0000445
17. Semmens, S. N.; AND Zhou, W., 2020, Predicting Backward Erosion Piping Hazard, Lower Mississippi Valley, USA, Quarterly Journal of Engineering Geology and Hydrogeology, 54(1). https://doi.org/10.1144/qjegh2020-035
18. Semmens, S. N.; Zhou, W.; van Wesenbeeck, B. K.; and Santi, P. M., 2017, Application of Multiple Criteria Decision Making Model for Evaluation of Levee Sustainability, Environmental & Engineering Geoscience, 23(2), 65-78.
19. Seyoum, W. M.; AND Milewski, A. M., 2017, Improved methods for estimating local terrestrial water dynamics from grace in the northern high plains. Adv. Water Resour. 110, 279–290.

20. Sun, A.Y., 2013, Predicting groundwater level changes using GRACE data. Water Resour. Res. 49, 5900–5912.

21. Wenjie Y.; Litang H.; Shin-Chan H.; Menglin Z.; AND Yanguo T., 2019, "Reconstructing Terrestrial Water Storage Variations from 1980 to 2015 in the Beishan Area of China," Geofluids, vol. 2019, Article ID 3874742, 13 pages.

22. Zaitchik, B. F.; Rodell, M.; AND Reichle, R. H., 2008 Assimilation of GRACE terrestrial water storage data into a land surface model: Results for the Mississippi River Basin. J. Hydrometeorol. 9, 535–54

23. Fawcett T. An introduction to ROC analysis Pattern Recognition. Letters 27 (8) (2006), pp. 861-874.

CHAPTER 4

LAND USE AND LAND COVER CHANGE ASSESSMENT IN THE CONTEXT OF FLOOD HAZARD IN LAGOS STATE, NIGERIA

Reproduced from a publication in the Water[1]

Dorcas Idowu[2]*, Wendy Zhou*[3]

4.1 Abstract

Incessant flooding is a major hazard in Lagos State, Nigeria, occurring concurrently with increased urbanization and urban expansion rate. Consequently, there is a need for an assessment of Land Use and Land Cover (LULC) changes over time in the context of flood hazard mapping to evaluate the possible causes of flood increment in the State. Four major land cover types (water, wetland, vegetation, and developed) were mapped and analyzed over 35 years in the study area. We introduced a map-matrix-based, post-classification LULC change detection method to estimate multi-year land cover changes between 1986 and 2000, 2000 and 2016, 2016 and 2020, and 1986 and 2020. Seven criteria were identified as potential causative factors responsible for the increasing flood hazards in the study area. Their weights were estimated using a combined (hybrid) Analytical Hierarchy Process (AHP) and Shannon Entropy weighting method. The resulting flood hazard categories were very high, high, moderate, low, and very low hazard levels. Analysis of the LULC change in the context of flood hazard suggests that most changes in LULC result in the conversion of wetland areas into developed areas and unplanned development in very high to moderate flood hazard zones. There was a 69% decrease in wetland and 94% increase in the developed area during the 35 years. While wetland was a primary land cover type in 1986, it became the least land cover type in 2020. These LULC changes could be responsible for the rise in flooding in the State.

[2]Graduate student, department of Geology and Geological Engineering, Colorado School of Mines. Leading author
[3]Department of Geology and Geological Engineering, Colorado School of Mines. Thesis advisor and corresponding author

4.2 Introduction

Located in Nigeria's southwestern zone, Lagos State is regarded as a hotspot in terms of urban expansion. Among all the 36 states in Nigeria, it is the smallest in area, comprising 19 local government areas, including the City of Lagos, the nation's largest metropolitan area (Figure 1). The United Nations predicted there would be a megacity in Africa by 2015 [1], the City of Lagos made that mark by 2020 [2]. The city currently ranks number seven in the fastest growing cities and urban areas globally, with an average annual growth of 4.4% in population from 2006 to 2020. It continues to grow in population density and urbanization, with a current population of over 21 million and over 6000 residents per square kilometer. A rise in population in urban areas is known to directly affect the demand for housing, which in turn leads to an increase in developed land. Urban development in Lagos State is taking place by land reclamation [3] through dredging from lagoons and converting coastal wetlands into urbanized communities, which is a direct result of urban sprawl. Urban sprawl means the loss of wetland, forest, and agricultural land to houses, roads, and industries, leading to environmental challenges and changing demographics [4]. Environmental challenges, such as flooding, are the major natural disaster that plagues Lagos State, which is assumed to be stimulated by urban sprawl. The expansion of developed land is taking place in many flood-prone areas and has also led to a change in the coastline geometry (Figure 1). Monitoring urban sprawl and identifying the pace of the spread and spatial pattern is a primary concern for urban planners and policymakers, primarily due to insufficient data availability and lack of technical knowledge and tools. Additionally, there are no data from "standard" hydrology and climatology for most developing counties, such as Nigeria. It should be noticed that the accuracy of the presented study cannot be compared with modern techniques based on well-sampled water bodies. Still, in this case, those data are practically inaccessible.

Changes in Land Use and Land Cover (LULC) associated with urban sprawl can be measured and analyzed [5] using remote sensing and Geographic Information Systems (GIS) [6–13] but have not been done yet for the entire Lagos State due to the is-sues mentioned above. Commonly, LULC analysis aims to identify changes in the same geographical area between the two timeframes considered [14]. Remotely sensed satellite imageries enable us to look at LULC retrospectively and could be used to monitor urban sprawl over time [15,16]. Images from different timeframes

can be compared after using satellite image-based land cover classification techniques to illuminate the developed and undeveloped land changes.

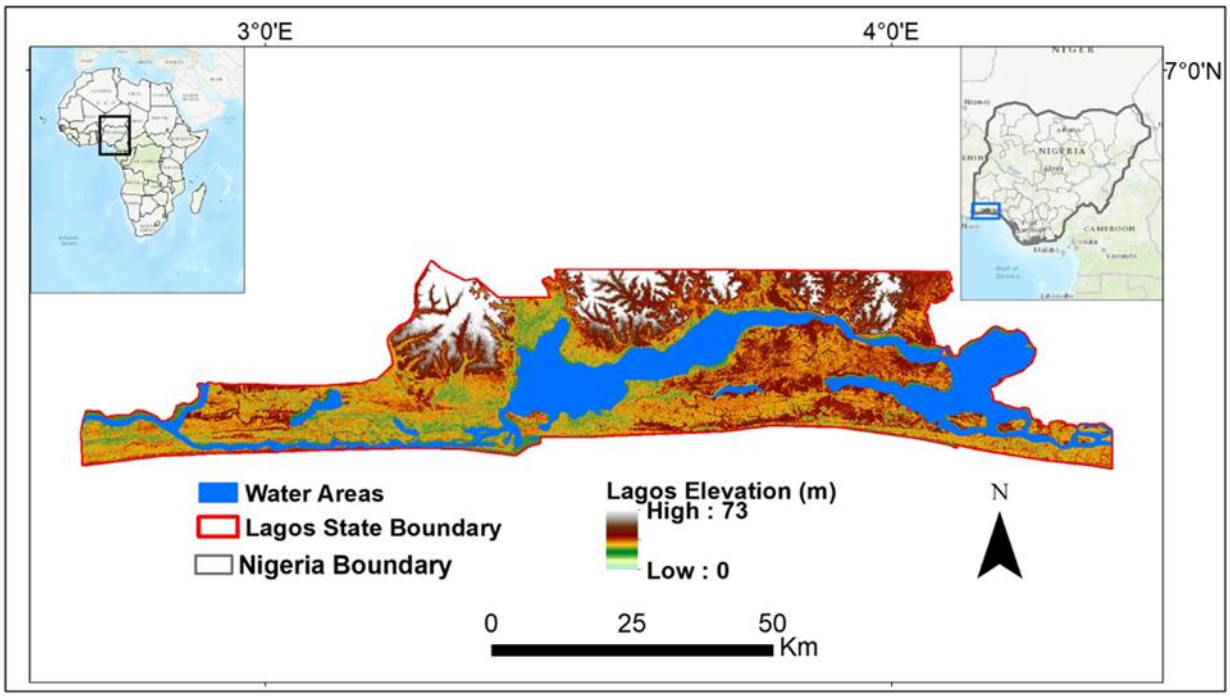

Figure 4.1: Location map of Lagos State.

Several studies have linked urban expansion in Lagos, Nigeria, to flooding [17–19]. The area comprises islands of different water bodies, ranging from lagoons and beaches to creeks, making it naturally susceptible to flooding. Urban flooding in Lagos State is expected, and the socioeconomic impact keeps increasing over the years. Urbanization is a common phenomenon in different parts of the world [20]. However, intensive unplanned urban growth has negative consequences on many environmental aspects [21]. For instance, urbanization resulting in a decrease in wetland, vegetation [22,23], and soil cover leading to an increase in impermeable surfaces can reduce rain-fall infiltration and increase runoff to streams and rivers, and eventually cause flooding [24,25]. Vegetation can significantly affect hydrological fluxes due to variations in the physical characteristics of the land surface, soil, and vegetation [22,23]. The ad-verse effects of flooding could be reduced with proper urban planning, starting with the identification of flood-

prone areas through flood hazard mapping and assessment of LULC changes causing flooding in those areas [26].

Flood hazard mapping requires specific hydrologic measurements [27,28] from flood monitoring systems such as river and stream gauges, which are valuable but can be time-consuming, and expensive [29]. More so, in most developing countries, such hydrologic records are insufficient or absent, and the cost of installing these systems could be limiting [30]. Consequently, flood hazard studies based on direct measurements may be impossible in most developing countries because there are no historical data available to determine certain flood levels and recurrence intervals for a particular flood event [30]. Flood hazard evaluation based on satellite data and damage re-ports could substitute for unavailable quantitative data [31–33]. Here, we created a remote sensing and GIS-based flood hazard map using seven criteria combined in a weighted overlay analysis. Each criterion's weight was estimated using the Multiple-Criteria Decision-Making (MCDM) methods which suggest the different influence each criterion has on the hazard delineation process.

Multiple-Criteria Decision-Making (MCDM) and Geographic Information System (GIS) methods have been considered by several researchers [34–41] to be very versatile in terms of providing the techniques and strategies for analyzing complex decision-making problems comprising incomparable criteria. The MCDM methods are broadly categorized into objective and subjective methods [42], with each category based on the role of the decision-maker in the context of determining the importance of a criterion. Of all the different MCDM methods for determining the weights of each criterion in GIS applications, the Analytic Hierarchy Process (AHP) [42–54] is commonly used, while the Shannon Entropy weighting method is less widely used [55–58]. A combined AHP and GIS approach was used in Kenya and Greece for urban flood vulnerability and risk mapping [59,60]. This study applied a combined (hybrid) AHP and entropy MCDM method for flood hazard mapping in Lagos State, an approach suggested to be efficient for determining criteria weights for GIS-based applications [56,59].

Therefore, this work aims to detect the link between LULC dynamics and flooding in Lagos State over 35 years through a multi-year (1986, 2000, 2016, and 2020) study. A map-matrix-based post-classification method was used to investigate LULC changes to identify the losses or increase in the specified land cover types. Additionally, a flood hazard map was created to evaluate LULC

morphology and impacts to the continuous rise of flooding in the State using a hybrid weighting MCDM approach. This study could ultimately bring awareness to the public, urban planners, and land-use managers on increasing flood hazard areas due to the loss of wetland and the expansion of the developed area, hence, promoting a better practice of land use in Lagos State.

4.3 Data and Methods

This section presents the data acquisition and data processing methods for LULC analysis and flood hazard mapping. Approaches used to analyze the accuracy of the studies are also included in this section.

4.3.1 Land Use and Land Cover (LULC) Analysis

The purpose of the LULC analysis was to quantify the changes in the land cover types over time in Lagos State, Nigeria, and ascertain how these changes influence flooding. Certain land cover losses, such as loss of wetland and vegetation, when replaced with an impervious surface such as pavements, could decrease rainfall infiltration and increase the surface runoff.

4.3.2 Data Acquisition and Preprocessing

The Landsat 5, Landsat 7 Enhanced Thematic Mapper Plus (ETM+), and Landsat 8 Operational Land Imager (OLI) scenes were downloaded via the United States Geological Survey (USGS) Global Visualization Viewer (Glovis—https://glovis.usgs.gov/app?fullscreen=1 (accessed on 12/11/2020)) for this study. The satellite images were used as they provide data dating back to 1986, which is the start of our time step. The spatial resolution of the Landsat images is 30 m. Table 1 shows the Landsat data types and their corresponding acquisition date for the multispectral scenes.

Table 4.1: Summary of the acquired multispectral Landsat scenes

Data	Date (Dd/Mm/Yyyy)	Source
Landsat 5	24 December 1986	Unites States Geological Survey (USGS)
Landsat 7 ETM +	6 February 2000	
Landsat 8 OLI	10 February 2016 20 January 2020	

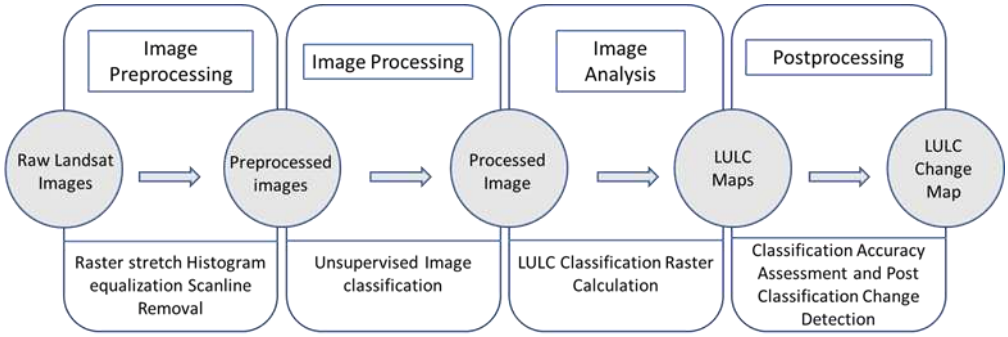

Figure 4.2: Work flowchart for creating the LULC and LULC change maps.

The Landsat scenes were mosaiced and clipped to the study area. Scan lines and black backgrounds were then removed from the images (Figure 2). The images were further enhanced by applying the standard deviation stretch to improve the images' appearance and interpretability (Figure 2).

4.3.3 Scenes Classification and Post-classification Change Detection Analysis

Once the data were downloaded, an Iso Cluster unsupervised classification technique was applied to LULC assessment images. The LULC classification was restricted to areas where satellite imagery has minimal cloud cover. Since we are interested in changes associated with wetland, vegetation, and developed areas, we classified the images into four classes, i.e., water, wetland, vegetation, and developed. Table 2 shows the land cover types and the explanations used in this study. The recoding values in Table 2 were used for the analysis of land cover change detection as described next [60].

Table 4.2: Land cover types, descriptions, and their recoded values.

Land Cover	Description	Recoding Values
Water	Streams, Canals, Lakes, Bays, and Estuaries	1
Wetland	Swamps, Marshes, and Mudflats	5
Vegetation	Agricultural land, Rangeland, and Forestland	7
Developed	Urban or Built-up land such as residential, industrial and commercial	11

Several change detection methods have been proposed, including image differencing, principal component analysis [55–58], and post-classification comparison [59–64]. The post-classification change detection method we used here involves LULC changes estimated by performing map matrix (in ArcMap) calculations categorized into two steps. The first step was LULC map recoding, followed by raster calculation comprising map multiplication and addition. We reclassified the LULC maps for all the years (1986, 2000, 2016, and 2020) using the recoding values listed in Table 2. Furthermore, we paired the years from past to recent such that the resulting intervals were 1986–2000, 2000–2016, and 2016–2020. Raster multiplication was performed on each pair of LULC maps. Finally, we performed a raster addition between the raster multiplication output and the most recent years in each interval. The resulting maps from the above calculations quantitatively depict the changes for the different land covers over time. Equations (1) and (2) explain the above process mathematically.

$$Y_t = Y_{t1} * Y_{t2} \quad (1)$$

$$CD = Y_t + Y_{t2} \quad (2)$$

where: Yt1 is the LUL map from a previous year, Yt2 is the LULC map for a recent year, Yt denotes LULC map product from previous and recent years, CD is the detected change, which is the addition of the LULC map product (Yt) and the LULC map for a recent year (Yt2).

4.3.4 LULC Map Accuracy Assessment

An assessment of the LULC map accuracy was made to evaluate the reliability of the classified images. This accuracy assessment is based on ground referencing, also known as ground-truthing. Ground referencing includes comparing data collected in the field or data from higher spatial resolution imagery to a classified map. As a result of the field data unavailability, we compared our classified images to images from Google Earth. The imageries from our analysis and Google Earth were used to calculate an error matrix, which is a table comparing the land cover classes found on the Google Earth imagery to those in the classified images at the same location. To ascertain the classified images' accuracy, we sampled 100 points on the derived landcover maps to Google Earth imageries by constructing a confusion matrix and estimated the producer's accuracy, user's accuracy, and kappa.

4.3.5 Flood Hazard Analysis

This analysis was essential to delineate the different levels of hazard and exposure of various areas of Lagos State to flooding categorically. Additionally, apart from get-ting an insight into the most dominant criteria responsible for flooding in the study area, the spatial distribution of the changes in the wetland, vegetation, and developed land covers in relation to the identified flood hazard zones could be assessed.

4.3.6 Criteria for Flood Mapping

A combination of criteria has been suggested by several researchers [65–70] to be factors at play in flood-prone areas. Seven criteria were identified and defined to be critical for delineating flood hazard areas in Lagos State, Nigeria. These factors include elevation, rainfall intensity, Flood Potential Index (FPI), Storage Deficit (Sdef), flow accumulation, proximity to water areas, and stream network. For these data, we created a rainfall intensity map from the downloaded Global Precipitation Climatology Center (GPCC) at the NASA GES DISC Earth Data website. A 30 m Shuttle Radar Topography Mission (SRTM) Digital Elevation Model (DEM) was downloaded from the USGS Earth Explorer website. The slope and stream polyline map for our area of interest were generated using the DEM data, while the water area map was downloaded from the ArcGIS online map service in ArcMap. The FPI and Sdef were calculated following the methodology by [71]. Based on the workflow displayed in Figure 3, we produced a flood hazard map for the entire area of Lagos State.

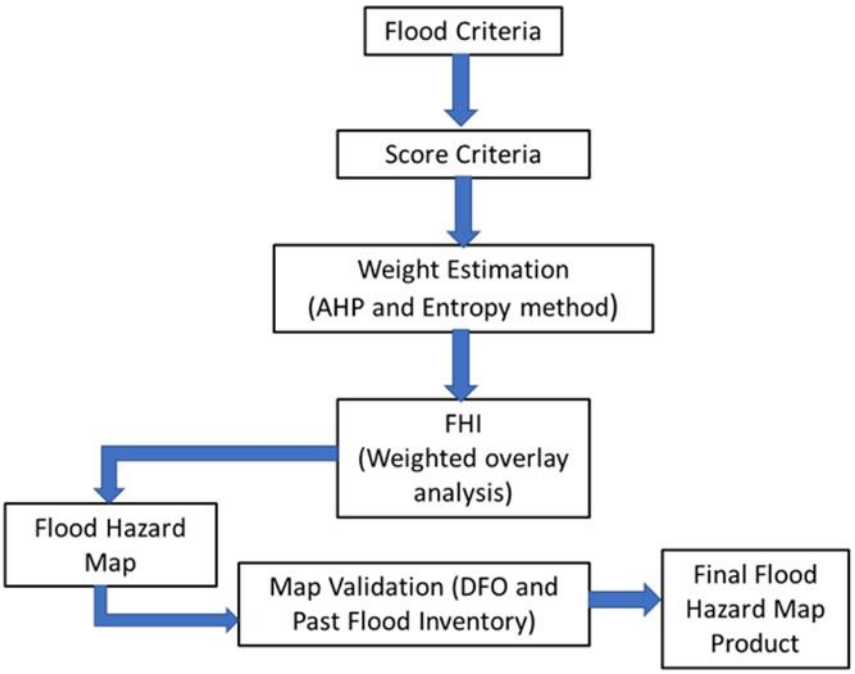

Figure 4.3: Flood Hazard Mapping Workflow.

4.3.7 Determining the Weighs of Each Criterion

A combined (hybrid) AHP and Shannon Entropy weighting method was applied to determine each criterion's weight for the flood hazard assessment analysis. Initially, we computed the criteria weights using the individual MCDM (AHP and Shannon Entropy) method and subsequently applying Equation (3) to combine the weights estimated from both methods. Hence, a hybrid approach combined the MCDM methods from AHP and Shannon Entropy weighing estimation methods. We used the methods proposed by [72,73] for computing the AHP and Entropy weights, respectively.

$$W_j = (X_j + Y_j)/2 \qquad (3)$$

where Wj, Xj, and Yj are the hybrid, AHP, and Entropy weights and j = 1… n) to generate the hybrid weights.

4.3.8 Weighted Overlay Analysis

The weighted overlay analysis is one of the approaches applied to multi-criteria problems. Flood hazard mapping requires the determination of contributing factors to flooding in an area. Based on

data availability, for our analysis, we hypothesized that areas with a high amount of rainfall, low elevation, high FPI, low Sdef, high flow ac-cumulation, close to water bodies are more susceptible to flooding. In order to carry out the weighted overlay analysis, thematic map layers were created for each criterion and normalized to the same scale. The map formats were unified into raster format since the datasets were a mixture of vector and raster formats. The weighted overlay analysis could only be performed on raster datasets in ArcGIS. The streamlines and water area map layers were rasterized from shapefiles to distance raster using the Euclidean distance tool, which calculates the Euclidean distance from the source for each cell in a raster. The final model was produced by applying Equation (4).

$$FHI = \sum C_i * w_i \qquad (4)$$

where FHI is the Flood Hazard Index resulting from the weighted overlay analysis, Ci is the ith criterion, wi represents the ith criterion's corresponding weight, i=1….n, and n is the total number of criteria.

4.3.9 Model Validation

The flood hazard map produced was qualitatively validated using the flood inventory map created by compiling past flood events in the study area from 1968 to 2020. Table 3 summarizes the flood events in 26 locations within Lagos State throughout the years. We also compared the flood hazard map generated from our study to the flood reports by the Dartmouth Flood Observatory (DFO) in Lagos State over the years. The DFO reports flood events worldwide based on news, governmental, instrumental, and remote sensing sources and might be biased towards more significant flood events [71].

Table 4.3: List of recorded flood events in various locations within Lagos State from 1968 to 2020 compiled based on literature [19] and online news sources (e.g., Aljazeera, Arise News, GistNigeria by Channels, and Floodlist)

Location	Dates	Number of Flood Events	Longitude	Latitude
Lagos Island	June 1968, July 1970, July 1971, July 1972, July 1990, July 2002, June 2004, July 2005, October 2008, July 2009, October 2010, July 2011, October 2012, and June 2020	14	3°22′51.695″ E	6°27′23.17″ N
Lekki Phase 1	June 2015, July 2017, October 2019, and June 2020	4	3°28′35.334″ E	6°26′37.688″ N
Victoria Island	June 2000, July 2000, September 2000, June 2015, July 2017, and October 2019	6	3°24′52.979″ E	6°25′57.26″ N
Ijora	June 1968	1	3°21′35.892″ E	6°27′53.491″ N
Surulere	June 1969, July 1974, October 2010, and June 2020	4	3°20′50.41″ E	6°29′34.561″ N
Yaba	June 1969 and July 1974	2	3°22′41.588″ E	6°29′49.722″ N
Idiaraba Mushin	June 1974, May 1999, June 1999, July 1999, July 2011, and June 2020	6	3°21′5.571″ E	6°31′15.631″ N
Ikorodu	August 1974, June 2015, and June 2020	3	3°29′51.137″ E	6°37′39.699″ N
Ikoyi	August 2007, June 2000, July 2000, September 2000, and June 2015	5	3°26′44.157″ E	6°27′23.17″ N
Kosofe	August 2007 and July 2017	2	3°25′13.193″ E	6°36′3.682″ N
Apapa	October 2010 and June 2015	2	3°21′51.053″ E	6°26′37.688″ N
Lagos Mainland	June 2015	1	3°22′16.32″ E	6°30′45.31″ N
Ikeja	July 2011, June 2015, and October 2019	3	3°20′45.357″ E	6°36′34.003″ N
Oshodi	October 2019	1	3°20′20.089″ E	6°33′37.13″ N
Badagry	June 2015	1	2°53′43.177″ E	6°25′52.206″ N
Ketu	June 2015	1	3°23′1.802″ E	6°35′13.147″ N
Ojota	May 2018 and June 2020	2	3°22′41.588″ E	6°34′17.558″ N
Bariga	May 2018	1	3°22′51.695″ E	6°32′21.327″ N
Maryland	May 2018 and October 2019	2	3°21′30.839″ E	6°34′17.558″ N
Ogba	July 2011, June 2015, and October 2019	4	3°20′30.196″ E	6°38′4.967″ N

Oworonshoki	May 2018	1	3°24′32.765″ E	6°32′46.595″ N
Shomolu	May 2018	1	3°23′32.123″ E	6°32′31.434″ N
Ebute Ero	October 2010, July 2011, October 2012, and June 2020	4	3°24′32.765″ E	6°26′57.902″ N
Agege	July 2011, June 2015, and October 2019	3	3°19′9.34″ E	6°38′4.967″ N
Agbede	June 2015 and June 2020	2	3°30′36.619″ E	6°36′23.896″ N

4.4 Results

This section describes the results from landcover classifications for the images acquired in 1986, 2000, 2016, and 2020, as well as the LULC change detection in the context of flood mapping. Assessment of the accuracies of the classification and change detection analysis were also presented.

4.4.1 Land Cover Classification

Using the Iso Cluster unsupervised classification, four major land cover types were classified. These include water, wetland, vegetation, and the developed areas. Figures 4 visually depict the land cover changes for 1986, 2000, 2016, and 2020. Figure 5a,b explain each land cover type's area relative to the total area of the study area be-tween 1986 and 2020. In 1986, water, wetland, vegetation and developed were 14%, 33%, 27% and 26%, respectively, and by 2020, they were 13.3%, 10.3%, 26.4% and 50%, respectively. Table 4 further explains a pair-wise evaluation of the change across the 35 years included in the study. There is a dramatic increment in the developed areas and a significant loss of wetland. The negative and positive signs associated with the table's values depict an increase (positive values) or decrease (negative values) in a particular land cover type in each paired time category. While the water, wetland, and vegetation land cover fluctuate between increasing and decreasing, the developed land cover increased in all the paired timeframes.

We compared 100 points sampled on the derived land cover maps from this anal-ysis to higher resolution Google Earth imageries by constructing a confusion matrix to ascertain the accuracy of the classified images. We found that the producer's accuracy, user's accuracy, and kappa are 0.96, 0.98, and 0.87, respectively.

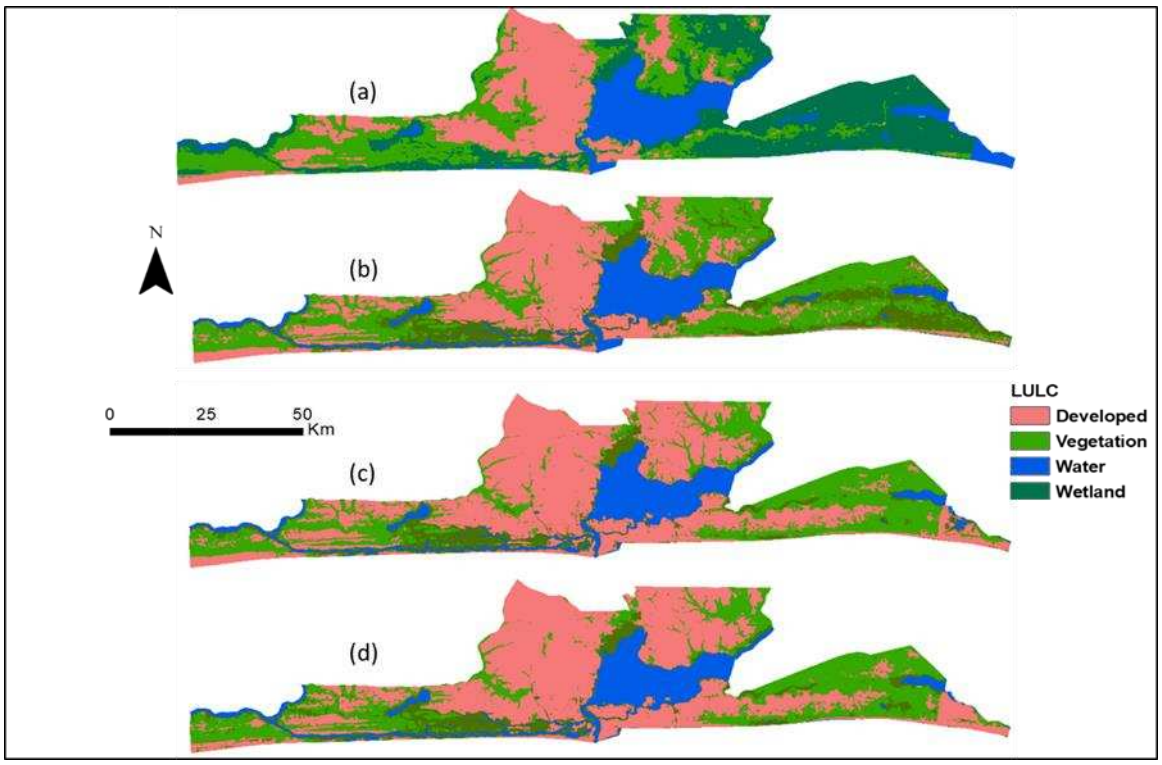

Figure 4.4: LULC classification maps for (a) 1986, (b) 2000, (c) 2016, and (d) 2020 for the State of Lagos, Nigeria.

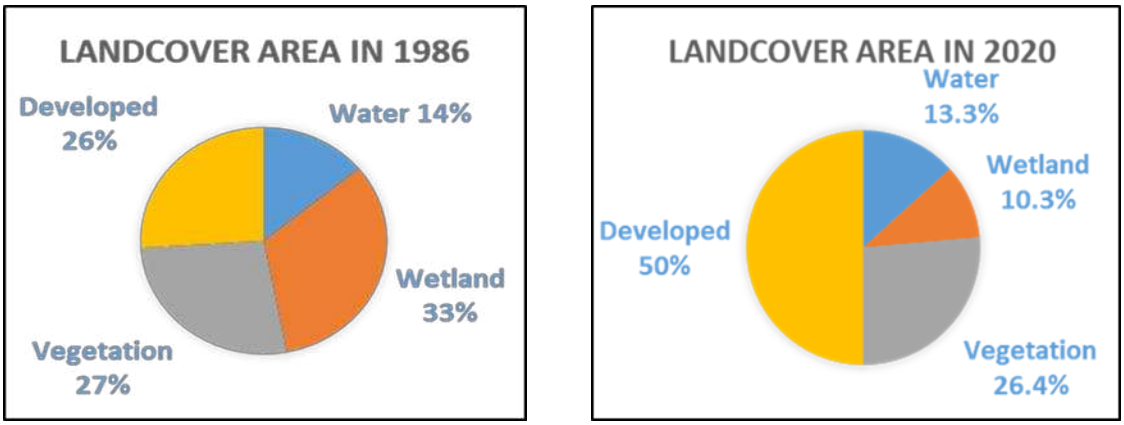

(a) (b)

Figure 4.5. Graphical representation of a 34-year LULC change in the study area between (a) 1986 and (b) 2020.

Table 4.4: Pair-wise percentage change for the year of study

Land-Cover Types	Percentage Change (%)			
	1986 - 2000	2000 - 2016	2016 - 2020	1986 -2020
Water	5	-6	-3	-4
Wetland	-50	-43	8	-69
Vegetation	24	-18	-3	-2
Developed	37	40	1	94

4.4.2 Change Detection

The post-classification change detection analysis resulted in a map showing the transformation of one land cover type to another. The change detection process was estimated for the paired timeframes of 1986–2000, 2000–2016, 2016–2020, and 1986–2020, respectively. Figure 6 visually displays the LULC changes from 1986 to 2020. For the purpose of visual illustration of all changes, especially those related to developed areas, we grouped all changes from water-developed, wetland-developed, and vegetation-developed together as developed areas for 2020 (developed area 2020) in Figure 6a. We kept these land cover changes separate in Figure 6b. In contrast, developed areas in 1986 were classified as developed to developed in Figure 6b and within the cross-hatched area in the landcover change map of Figure 6a. Overall, half (52%) of the total study area changed between 1986 and 2020.

Assessment of the post-classification change detection accuracy was carried out by comparing the changed areas to Google Earth imagery and identifying areas of known changes in Lagos State. Figure 7 is the visual comparison of three areas of known changes to our change detection map. In Figure 7, the Google Earth image on the left is the Eko Atlantic in Lagos State; the middle image represents two reclaimed islands through dredging. The image on the right is the Dangote refineries still under construction.

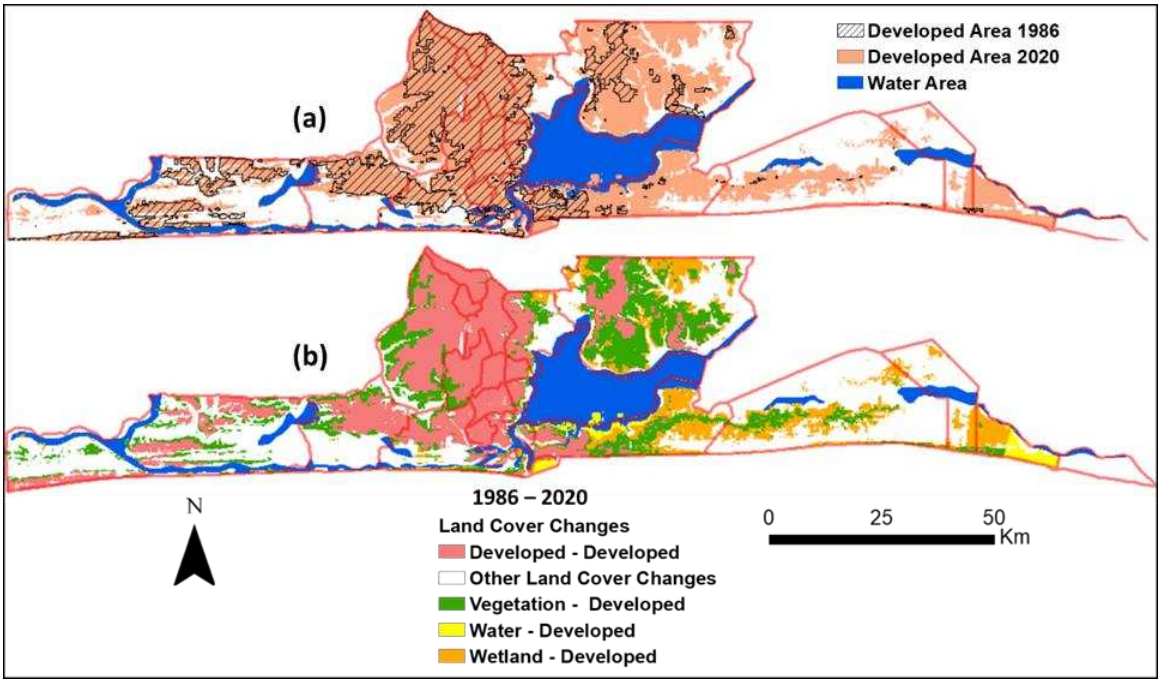

Figure 4.6: (a) the spatial distribution of developed and undeveloped areas in 1986 (hatched areas) and 2020 (solid color). (b) the distribution of landcover changes in one land cover type with reference to another land cover type from 1986 to 2020.

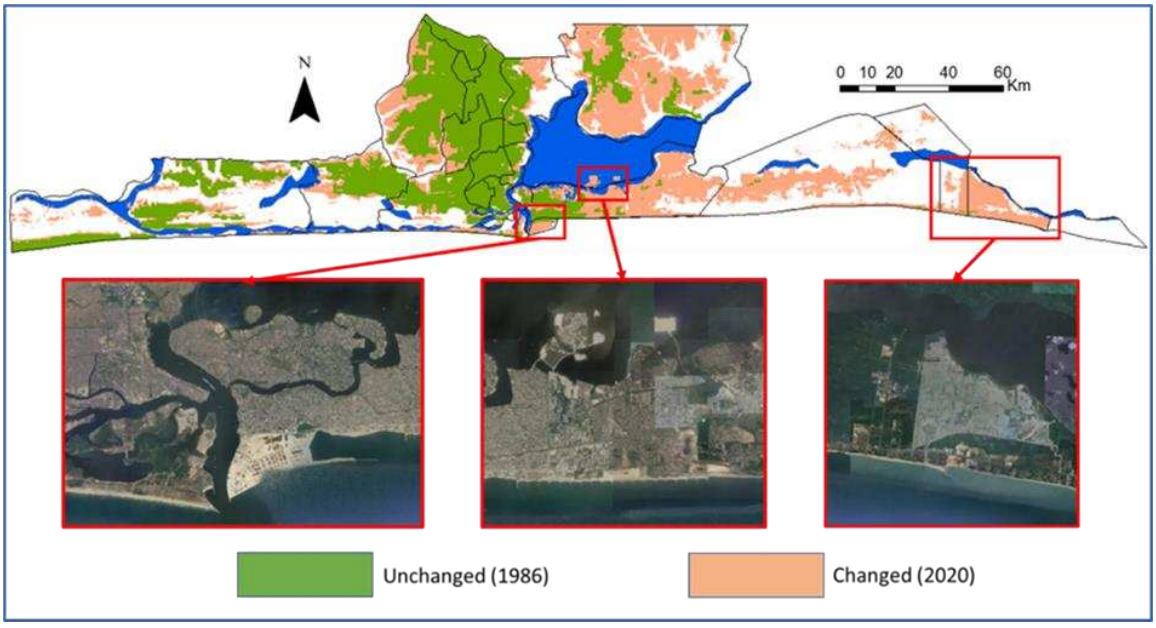

Figure 4.7: Land cover changes in comparison to Google Earth Images acquired 2019 showing changes on the ground for the Eko Atlantic (left), two reclaimed islands through dredging (middle), and the Dangote refineries (right).

4.4.3 Flood Hazard mapping

We applied the weighted overlay method in creating the flood hazard map. In or-der to perform this analysis, we estimated the weights of the seven criteria identified as contributing factors to flooding in Lagos State. The AHP and Shannon Entropy weighting methods were used for the weight estimation, and eventually, a combined (Hybrid) weight was adopted in our hazard map production. Table 5 summarizes the result of the AHP weighting method, which is considered a subjective method of criteria weight estimation. The method weighted rainfall intensity (31.9%) more than the other criteria and suggests the criterion to be the most important criteria for flood hazard in the study area. However, the entropy weighting method is considered an objective method of generating criteria weights. The method weighted elevation (34.0%) more than the other criteria. A combination (hybrid) of both methods' values by simply averaging them gave elevation (30.3%) more weights than the other criteria.

Table 4.5: Criteria weights from the AHP, Entropy, and Hybrid weighting methods

Criteria	**AHP Weights (%)**	**Entropy Weights (%)**	**Hybrid Weight (%)**
Elevation	26.5	34.0	30.3
Rain	31.9	20.4	26.2
FPI	14.2	15.4	14.8
Sdef	14.2	15.4	14.8
Flow Accumulation	5.4	5.2	5.3
Stream	3.9	4.5	4.2
Water	3.9	5.1	4.5

The weighted overlay calculations gave a range of values from zero to one where values close to one would be very high flood hazard zones, and values close to zero would be low flood hazard zones. We reclassified the flood hazard map using the Jenks natural breaks classification into five categories: very high, high, moderate, low, and very low.

For validation, the resulting flood hazard map produced from the weighted over-lay method was compared to past flood inventory in Lagos State (Figure 8 and Table 6). The past flood events were represented with points proportional to the number of repeated flood events for that particular area (Figure 8). We extracted the flood hazard zones' values to the flood inventory points (Table 6) and found that 92% of the points fell within the very high to moderate flood hazard zones, while 8% was within the low flood hazard zone. In general, the flood inventory points show good agreement with our flood mapping and flood hazard classification.

In addition to comparing the flood hazard map to past flood events, we also compared the flood hazard map to the DFO-reported flood in Lagos State. Each entry in Table 7 represents a discrete flood event displayed in polygons with the center point coordinates. For our study area, large flood events archived by the DFO are for the years 1990, 2002, 2004, and 2007, respectively (Table 7). The areas where the DFO re-ported flooding were within the flood hazard zone of the map we produced.

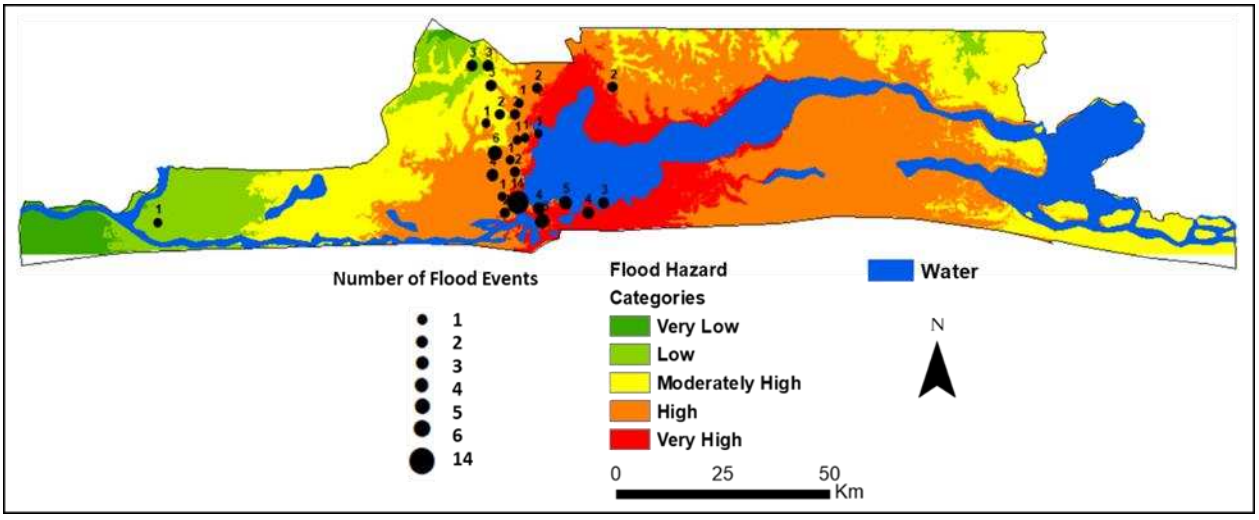

Figure 4.8: Flood hazard map with past flood inventory points.

Table 4.6: Percentages of the flood inventory points within the flood hazard categories

Flood Hazard Category	Percentage of Inventory Points (%)
Very High	19
High	54
Moderate	19
Low	8
Very Low	0

Table 4.7: Dartmouth Flood Observatory reported flood events in the study area

Longitude	Latitude	Began	Ended	Validation	Dead	Displaced	Main Cause	Severity
3°31'2.59 "E	6°30'43.165 "N	7/3/1990	7/4/1990	News	5	3000	Heavy rain	1
3°16'51.805 "E	6°34'50.3509 "N	7/24/2002	7/26/2002	News	2	0	Heavy rain	1
3°29'11.065 "E	6°34'54.5939 "N	6/17/2004	6/17/2004	News	0	0	Heavy rain	1
3°17'54.902 "E	6°29'59.0489 "N	8/1/2007	8/15/2007	News	6	5000	Heavy rain	1

Since part of our analysis is seeking the impact of urbanization on the incessant flooding in Lagos State, we superimposed the LULC map of developed areas from 1986 to 2020 on the flood hazard map to aid visual interpretation. We also converted the developed area raster layer to points and extracted the flood hazard map values to each of the points. The result (Table 8 and Figure 9) revealed that approximately 91% of the points correspond to very high to moderate flood hazard zones. This outcome indicates a strong correlation between developed areas and flood events, which could imply that urbanization is responsible for increasing flood hazards in Lagos State. With over 90% of the centroids of developed areas inside the very high to moderate flood zones, we infer that Lagos State is in exceedingly flood-prone areas.

Table 4.8: Analysis of Changes in Flood Hazard Areas

Flood Hazard Category	Percentages of developed Areas (1986-2020) %
Very High	26.5
High	46.4
Moderate	18.2
Low	6.5
Very Low	1.8

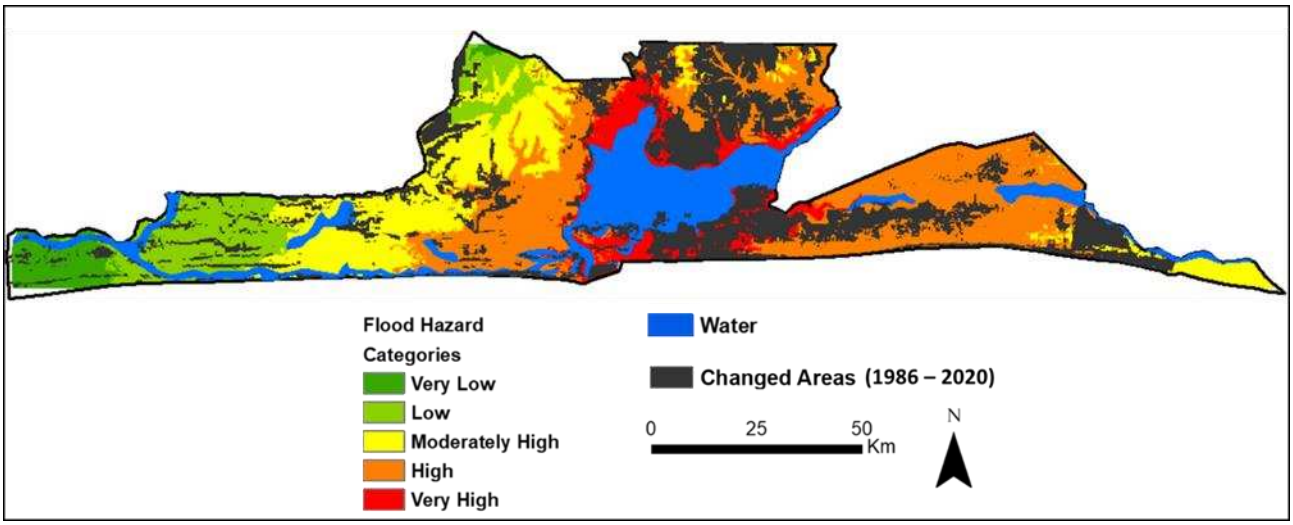

Figure 4.9: An overlay of developed areas on the flood hazard map.

4.5 Discussion

We classified the study area into four major land cover types, including water, wetland, vegetation, and the developed areas, based on satellite images acquired in 1986, 2000, 2016, and 2020. Rapid growth in population results in urban sprawl into wetland and lagoons areas. The creation of impervious surfaces and ultimately more runoff could be the major reason for flooding in Lagos State.

The post-classification change detection analysis resulted in a map showing the transformation of one land cover type to another. The change detection process was estimated for the paired timeframes of 1986–2000, 2000–2016, 2016–2020, and 1986–2020, respectively. Figure 6 visually displays the LULC changes from 1986 to 2020. Our study revealed that of all the land cover types identified in Lagos State, decrement in wetland and increment in developed areas

consist of the most land cover changes from 1986 to 2020. Our study further revealed that urban development encroachment into wetland areas is supported by estimating the wetland areas and developed land areas in 1986 and 2020, respectively. With 33% of the study area's total area, the wetland was the primary land cover in 1986, and it became the least with 10.3% of the total area by 2020. The developed area also increased from 26% to 50% of the total area, al-most doubling in the study area over 35 years. The areas of vegetation and water bodies remained approximately the same over the same period.

Seven causative criteria or contributing factors were used for flood hazard mapping. We used the weighted overlay MCDC method in combining these criteria and creating the flood hazard map. The weights of the seven criteria were estimated by a combined (hybrid) AHP and Shannon Entropy methods. We reclassified the resulting flood hazard map using the Jenks natural breaks classification into five categories: very high, high, moderate, low, and very low. Our results have also shown that over the years, urbanization has been happening in areas susceptible to very high to moderately high flood hazard zones, which is evident by the recent increase in flood occurrence in these areas.

We could not perform an accuracy assessment based on ground referencing or ground-truthing due to the lack of field data. Instead, we compared our classified maps to higher resolution images from Google Earth. An assessment of its accuracy was made to evaluate the reliability of the classified images. The outcome of the accuracy assessment of the LULC classification against the Google Earth imagery showed that 93 of 100 points were correctly classified. Evaluation of the accuracy of the post-classification change detection was also carried out by comparing the changed areas to higher resolution Google Earth imagery due to the unavailability of in situ da-ta. Three areas within known LULC changes in Lagos State were used for the comparisons. These comparisons show good agreement. For validation of flooding analysis, the flood hazard map produced from this study was compared to flood inventory in Lagos State. The comparison showed that 92% of the flooding events fell within the very high to moderate flood hazard zones, while 8% was within the low flood hazard zone. In general, the flood inventory points show good agreement with our flood mapping and flood hazard classification. In addition, we also compared the flood hazard map to the DFO reported flood in Lagos State. The large flood events archived by the DFO were within the flood hazard areas of the map produced in this study. The high-lights of our study include (1) introduced a map-matrix-based, post-classification LULC change

detection method to estimate multi-year land cover changes over a few decades; (2) used a combined (hybrid) Analytical Hierarchy Process (AHP) and Shannon Entropy weighting method to carry out a weighted overlay MCDM flooding mapping; (3) put the LULC changes in the context of flood hazards and identify the possible causes of continuous rise in flooding in Lagos State, Nigeria.

4.6. Conclusions

Lagos State is bounded on the south by the Atlantic Ocean, which makes it flood-prone geographically. Our study reveals the extent to which different regions of the State are vulnerable to flooding and provides insights for urban planning, urban regulation, hazard awareness, insurance of property, and mitigation actions to alleviate flood hazards. Lagos is currently a megacity with a population of over 21 million people, and at the present rate of population rise, 2.5 billion people will live in urban areas by 2050. More so, our study revealed that there is a significant loss of wetland, and this has doubled in developed areas during the past few decades. Most developed areas are already in flood hazard zones.

Consequently, more attention should be given to flood mitigation measures for existing and proposed developed areas. Existing developed land cover, such as buildings already situated in flood hazard zones, could be flood-proof to minimize flood damages to properties. New developed areas could make provisions for flooding during the initial design and construction of structures by avoiding floodplains and/or incorporating necessary drainage measures to construct flood-proof facilities.

The assessment of the LULC changes in the context of flooding hazards in Lagos State brings insights into how these changes are worsening the already flood-prone areas. The situation can be mitigated by practicing adequate urban planning and regulation. Inadequate urban planning and lacking regulations have direct consequences of incessant flooding in the State. Additionally, our study emphasized the importance of remote sensing and GIS for LULC assessment and flood studies in developing countries, where there are no data from “standard” hydrology and climatology, and there is an increased rate of urban expansion in high flood hazard zones. Here, we present a low to no cost method to estimate LULC changes and identify flood hazard levels where ground-based data unavailability or security prohibits installing such systems. It should be

emphasized that the accuracy of the presented method cannot be com-pared with modern techniques based on well-sampled water bodies. Still, in this case, those data are practically inaccessible. Our study tackled a complex problem with the help of publicly available data and their detailed analysis.

4.7 References

1. United Nations: World Urbanization Prospects: The 2014 revision. United Nations Department of Economic and Social Affairs Rep., 517 pp., https://population.un.org/wup/Publications/Files/WUP2014-Report.pdf.
2. Idowu, T. E.; Home, P. G. Probable Effects of Sea Level Rise and Land Reclamation Activities on Coastlines and Wetlands. In The 2015 JKUAT Scientific Conference (pp. 207–220).
3. Eko Atlantic - The new gateway to Africa. Retrieved September 6, 2015, from http://www.ekoatlantic.com/wpcontent/uploads/2012/12/EKOATLANTIC_Broch_2012.pdf
4. Barrington-Leigh, C.; Millard-Ball, A. A century of sprawl in the United States. Proceedings of the National Academy of Sciences. 2015;112(27):8244–8249.
5. Idowu, D.; Zhou W. Land Use/Land Cover Measurements and Flood Hazard Mapping in Lagos State, Nigeria. 3rd Conference of the Arabian Journal of Geosciences (CAJG), (in press).
6. Mahesh, K. J.; Garg, P. K.; Deepak, K. Monitoring and modelling of urban sprawl using remote sensing and GIS techniques, International Journal of Applied Earth Observation and Geoinformation, 2008; Volume 10, Issue 1, pp. 26-43, ISSN 0303-2434, https://doi.org/10.1016/j.jag.2007.04.002.
7. Sudhira, H. S.; Ramachandra, T. V.; Jagadish, K. S. Urban sprawl: metrics, dynamics and modelling using GIS Int. J. Appl. Earth Observ. Geoinform., 2004; 5, pp. 29-39.
8. Yang, X., Liu, Z. Use of satellite derived landscape imperviousness index to characterize urban spatial growth. Comput. Environ. Urban Syst., 2005; 29, pp. 524-540.
9. Haack, B. N.; Rafter, A. Urban growth analysis and modelling in the Kathmandu valley, Nepal Habitat International, 2006; 30 (4), pp. 1056-1065.

10. Gomarasca, M.A.; Brivio, P.A.; Pagnoni, F.; Galli, A. One century of land use changes in the metropolitan area of Milan (Italy). Int. J. Remote Sens., 1993; 14 (2), pp. 211-223.
11. Green, K.; Kempka, D.; Lackey, L. Using remote sensing to detect and monitor land-cover and land-use change. Photogr. Eng. Remote Sens., 1994; 60, pp. 331-337.
12. Yeh, A.G.O.; Li, X. Measurement and monitoring of urban sprawl in a rapidly growing region using entropy. Photogr. Eng. Remote Sens., 2001; 67 (1), p. 83.
13. Yang, X.; Lo, C. P. Modelling urban growth and landscape changes in the Atlanta metropolitan area. Int. J. Geogr. Inform. Sci., 2003; 17 (5), pp. 463-488
14. Radke J.; Andra S.; Al-Kofani O.; Roysan B. Image change detection algorithms: a systematic survey. IEEE Trans Image Process, 2005; 14 (3) pp. 291-307.
15. Tewolde, M.G.; Cabral, P. Urban Sprawl Analysis and Modeling in Asmara, Eritrea. Remote Sens. 2011; 3, 2148-2165. https://doi.org/10.3390/rs3102148
16. Magidi J.; Ahmed F. Assessing urban sprawl using remote sensing and landscape metrics: A case study of City of Tshwane, South Africa (1984–2015). The Egyptian Journal of Remote Sensing and Space Science 2019; Volume 22, Issue 3, pp. 335-346, https://doi.org/10.1016/j.ejrs.2018.07.003.
17. Adeloye, A.; Rustum, R. Lagos (Nigeria) flooding and influence of urban planning. Proceedings of the Institution of Civil Engineers- Urban Design and Planning, 2011; 164(3), pp. 175 - 187. https://doi.org/10.1680/udap.1000014
18. Adelekan, I. O. Vulnerability of poor urban coastal communities to flooding in Lagos, Nigeria. Environment and Urbanization. SAGE 2010; 22, pp. 433-450 https://doi.org/10.1177/0956247810380141
19. Nkwunonwo, U. C.; Whitworth, M.; Baily, B. Review article: A review and critical analysis of the efforts towards urban flood risk management in the Lagos region of Nigeria, Nat. Hazards Earth Syst. Sci., 2016; 16, pp. 349–369, https://doi.org/10.5194/nhess-16-349-2016.
20. Ritchie, H; Roser, M. "Urbanization". Published online at OurWorldInData.org. 2018, Retrieved from: 'https://ou worldindata.org/urbanization' (accessed Apr 2, 2021).
21. Miller, J. D.; Hutchins, M. The impacts of urbanisation and climate change on urban flooding and urban water quality: A review of the evidence concerning the United

Kingdom, Journal of Hydrology: Regional Studies, 2017; Volume 12, pp. 345-362, ISSN 2214-5818, https://doi.org/10.1016/j.ejrh.2017.06.006.

22. Srivastava, A.; Kumari, N.; Maza, M. Hydrological Response to Agricultural Land Use Heterogeneity Using Variable Infiltration Capacity Model, Water Resour Manage, 2020; 34, pp. 3779–3794. https://doi.org/10.1007/s11269-020-02630-4.
23. Maza, M.; Srivastava, A.; Bisht, D. S.; Raghuwanshi, N. S.; Bandyopadhyay, A.; Chatterjee, C.; Bhadra, A. Simulating the hydrological response of a monsoon dominated reservoir catchment and command with heterogeneous cropping pattern using VIC model. Journal of Earth System Science, 2020; 129(1), pp. 1-16. https://doi.org/10.1007/s12040-020-01468-z.
24. Konrad, C.P. Effects of Urban Development on Floods; Fact Sheet 076-03; U.S. Geological Survey: Tacoma, WA, USA, 2016. Available online: https://pubs.usgs.gov/fs/fs07603/ (accessed Feb 25, 2021).
25. Konrad, C.P.; Booth, D.B. Hydrologic trends associated with urban development for selected streams in western Washington: U.S. Geological Survey Water-Resources Investigations Report 2002; 02-4040, 40 p., accessed (25/2/2021), Available online: ohttp://water.usgs.gov/pubs/ wri/wri024040.
26. Rahmati, O.; Pourghasemi, H.R. Identification of Critical Flood Prone Areas in Data-Scarce and Ungauged Regions: A Comparison of Three Data Mining Models. Water Resour Manage 2017; 31, pp. 1473–1487. https://doi.org/10.1007/s11269-017-1589-6
27. Spachinger K.; Dorner W.; Metzka R.; Serrhini K.; Fuchs S. Flood risk and flood hazard maps – visualization of hydrological risks. IOP Conf Series: Earth Environ Sci 2008; 4, 012043. doi: 10.1088/1755-1307/4/1/012043
28. Brunner, G.W. HEC-RAS, River Analysis System Hydraulic Reference Manual; US Army Corps of Engineers Hydrologic Engineering Center: Davis, CA, USA, 2016; pp. 1–547
29. Thiemig, V.; Bisselink, B.; Pappenberger, F.; Thielen, J. A pan-African flood forecasting system Hydrol. Earth Syst. Sci. Discuss., 2014; 11, pp. 5559-5597.
30. Kossi, K.; Jeffrey, N.; Mark A. T.; Bernd D.; Modelling of flood hazard extent in data sparse areas: a case study of the Oti River basin, West Africa, Journal of Hydrology:

Regional Studies, Volume 10, 2017; pp. 122-132, ISSN 2214-5818, https://doi.org/10.1016/j.ejrh.2017.03.001.

31. Brakenridge, G.R. Flood Risk Mapping From Orbital Remote Sensing. In Global Flood Hazard (eds G.J.-P. Schumann, P.D. Bates, H. Apel and G.T. Aronica) 2018; https://doi.org/10.1002/9781119217886.ch3
32. Argaz, A.; Ouahman, B.; Darkaoui, A.; Bikhtar, H.; Ayouch, E.; Lazaar, R. Flood Hazard Mapping Using remote sensing and GIS Tools: A case study of Souss Watershed. Journal of Materials and Environmental Sciences Environ. Sci., 2019; 10 (2), pp. 170-181
33. Gashaw, W.; Legesse D. Flood Hazard and Risk Assessment Using GIS and Remote Sensing in Fogera Woreda, Northwest Ethiopia. In: Melesse A.M. (eds) Nile River Basin. Springer 2011; Dordrecht. https://doi.org/10.1007/978-94-007-0689-7_9
34. Rincon, D.; Khan, U.; Armenakis, C. Flood risk mapping using gis and multi-criteria analysis: A greater Toronto area case study. Geosciences 2018; 8(8), 275 (21)
35. Fernández, D. S.; Lutz M. A. Urban flood hazard zoning in Tucumán Province, Argentina, using GIS and mul-ticriteria decision analysis. Eng Geol 2010; 111: pp. 90–98. doi:10.1016/j.enggeo.2009.12.006
36. Gamper, C.; Thöni, M.; Weck-Hannemann, H. A conceptual approach to the use of cost benefit and multi criteria analysis in natural hazard management. Natural Hazards and Earth System Sciences 2006; 6 (2), pp. 293-302
37. Omid, R.; Hossein, Z., Mosa, B. Flood hazard zoning in Yasooj region, Iran, using GIS and multi-criteria decision analysis, Geomatics, Natural Hazards and Risk 2016; 7:3, pp. 1000-1017, DOI: 10.1080/19475705.2015.1045043
38. Elsheikh, R.; Ouerghi, S.; Elhag, A. Flood Risk Map Based on GIS, and Multi Criteria Techniques (Case Study Terengganu Malaysia). Journal of Geographic Information System 2015; 7, pp. 348-357. doi: 10.4236/jgis.2015.74027.
39. 26. Odu, G. Weighting methods for multicriteria decision making technique. J. Appl. Sci. Environ. Manag. 2019; 23, pp. 1449–1457.
40. Semmens, S.N.; Zhou, W.; van Wesenbeeck, B.K.; Santi, P.M. Application of Multiple Criteria Decision Making Model for Evaluation of Levee Sustainability. Environ. Eng. Geosci. 2017; 23(2), pp. 65-78 https://doi.org/10.2113/gseegeosci.23.2.65

41. Seejata, K.; Yodying, A.; Wongthadam, T.; Mahavik, N.; Tantanee, S. Assessment of flood hazard areas using Analytical Hierarchy Process over the Lower Yom Basin, Sukhothai. Province Procedia Eng 2018; 212, pp. 340–347
42. Gigović, L.; Pamučar, D.; Bajić, Z.; Drobnjak, S. Application of GIS-Interval Rough AHP Methodology for Flood Hazard Mapping in Urban Areas. Water 2017; 9, 360. https://doi.org/10.3390/w9060360
43. Yagoub, M.M.; Alsereidi, A.A.; Mohamed, E.A.. Newspapers as a validation proxy for GIS modeling in Fujairah, United Arab Emirates: identifying flood-prone areas. Nat Hazards 2020; 104, pp. 111–141. https://doi.org/10.1007/s11069-020-04161-y
44. Radwan, F.; Alazba, A.A.; Mossad, A. Flood risk assessment and mapping using AHP in arid and semiarid regions. Acta Geophys 2019; 67, pp. 215–229 https://doi.org/10.1007/s11600-018-0233-z
45. Danumah, J.H.; Odai, S.N.; Saley, B.M. Flood risk assessment and mapping in Abidjan district using multi-criteria analysis (AHP) model and geoinformation techniques (cote d'ivoire). Geoenviron Disasters, 2016; 3, 10 https://doi.org/10.1186/s40677-016-0044-y
46. Chen J.; Li Y.; Zhou W.; Xu C.; Wu S.; Yue W. AHP-Based Susceptibility Assessment on Debris Flows in Semiarid Mountainous Region: A Case of Benzilan-Changbo Segment in the Upper Jinsha River, China. In: Yuan H., Geng J., Liu C., Bian F., Surapunt T. (eds) Geo-Spatial Knowledge and Intelligence. GSKI 2017. Communications in Computer and Information Science, Springer, Singapore 2018; vol 848, pp. 495-509
47. Zhou, W.; Minnick M.; Chen, J.; Garret, J.; Acikalin E. GIS-based Landslide Susceptibility Analysis Methods Suitable for Different Sizes of Study Area. Nat. Hazards Rev., Forthcoming, DOI: 10.1061/(ASCE)NH.1527-6996.0000485
48. Malczewski, J.; Rinner, C. Multicriteria Decision Analysis in Geographic Information Science; Springer 2015; New York, NY, USA, p. 335
49. Nyimbili, P.H.; Erden, T. A Hybrid Approach Integrating Entropy-AHP and GIS for Suitability Assessment of Urban Emergency Facilities. ISPRS Int. J. Geo Inf. 2020; 9(7):419.
50. Wu, S.; Chen, J.; Xu, C.; Zhou, W. Susceptibility Assessments and Validations of Debris-Flow Events in Meizoseismal Areas : Case Study in China's Longxi River Watershed. Nat.

Hazards Rev. 2020; 21(1), pp. 1–13. https://doi.org/10.1061/(ASCE)NH.1527-6996.0000347

51. Chen, J.; Li, Y.; Zhou, W.; Iqbal, J.; Cui, Z. Debris-Flow Susceptibility Assessment Model and Its Application in Semiarid Mountainous Areas of the Southeastern Tibetan Plateau. Nat. Hazards Rev. 2017; 18(2): 05016005 https://doi.org/10.1061/(ASCE)NH.1527-6996.0000229
52. Ouma, Y. O.; Tateishi, R. Urban flood vulnerability and risk mapping using integrated multi-parametric AHP and GIS: methodological overview and case study assessment. Water, 2014; 6(6), pp. 1515-1545.
53. Stefanidis, S.; Stathis, D. Assessment of flood hazard based on natural and anthropogenic factors using analytic hierarchy process (AHP). Natural hazards, 2013; 68(2), pp. 569-585.
54. Vanolya, N.M.; Jelokhani-Niaraki, M. The use of subjective–objective weights in GIS-based multi-criteria decision analysis for flood hazard assessment: A case study in Mazandaran, Iran. GeoJournal 2019; pp. 1–20
55. Mamdouh M. E. Applying post classification change detection technique to monitor an Egyptian coastal zone (Abu Qir Bay), The Egyptian Journal of Remote Sensing and Space Science, Volume 19, Issue 1, 2016; pp. 23-36, ISSN 1110-9823, https://doi.org/10.1016/j.ejrs.2016.02.002.
56. Hafez A. A. Evaluation of change detection techniques for monitoring land-cover changes: A case study in new Burg El-Arab area, Alexandria Engineering Journal, 2011; Volume 50, Issue 2, pp. 187-195, ISSN 1110-0168, https://doi.org/10.1016/j.aej.2011.06.001.
57. Al-doski, J.; Mansor, S.B.; Shafri, H.Z.M. Change detection process and techniques. Civ. Environ. Res. 2013; 3, pp. 37–45.
58. Lu, D.; Mausel, P.; Brondízio, E.; Moran, E. Change detection techniques, International Journal of Remote Sensing 2004; 25:12, pp. 2365-2401, DOI: 10.1080/0143116031000139863
59. Jensen, J.R.; Ramsat, E.W.; Mackey, H.E.; Christensen, E.J.; Sharitz, R.P. Inland wetland change detection using air-craft MSS data. Photogrammetric Engineering and Remote Sensing 1987; 53, pp. 521-529.

60. Anderson, J. R.; Hardy, E. E.; Roach, J. T.; Witmer R. E. A Land Use and Land Cover Classification System for Use with Remote Sensor Data, U.S. Geol. Survey Prof. Paper 1976; 964, p. 28.
61. Dimyati, M.; Mizuno, K.; Kobayashi, S.; Kitamura, T. An analysis of land use/ cover change using the combination of MSS Landsat and land use map-a case study in Yogyakarta, Indonesia. International Journal of Remote Sensing 1996; 17, pp. 931–944. http:// dx.doi.org/10.1080/01431169608949056.
62. Fichera, C.R.; Modica, G.; Pollino, M. Land cover classification and change-detection analysis using multi-temporal remote sensed imagery and landscape metrics. Eur. J. Remote Sens. 2012; 45, pp. 1–18.
63. Macleod R.D.; Congalton R.G. A quantitative comparison of change-detection algorithms for monitoring eel-grass from remotely sensed data. Photogrammetric Engineering and Remote Sensing 1998; 64, pp. 207–216.
64. Ward, D.; Phinn, S.R.; Murray, A.T. Monitoring growth in rapidly urbanizing areas using remotely sensed data. Professional Geographer 2000; 52, pp. 371-386. http://dx.doi.org/10.1111/0033-0124.00232.
65. Cirella, G.T.; Iyalomhe, F.O. Flooding Conceptual Review: Sustainability-Focalized Best Practices in Nigeria. Appl. Sci. 2018, 8, 1558. https://doi.org/10.3390/app8091558
66. Ozkan, S.P.; Tarhan, C. Detection of Flood Hazard in Urban Areas Using GIS: Izmir Case. Procedia Technol. 2016; 22, pp. 373–381.
67. Mukherjee, F.; Singh, D. Detecting flood prone areas in Harris County: a GIS based analysis. GeoJournal 2019; pp. 1, –17.
68. Boakye, K. O.; Isaac, A.; Anthony, E.; Etornam, B. F. Assessment of flood prone zones in the Tarkwa mining area of Ghana using a GIS-based approach, Environmental Challenges, 2021; Volume 3, 100028, ISSN 2667-0100, https://doi.org/10.1016/j.envc.2021.100028.
69. Jamal, M. S.; Ibne, A.; Imtiaz Saimon, M. N.; Afrin, S.; Islam, S.; Mila, S. A.; Sazzad, T. M. S. GIS Based Information System to Identify Flood Prone Area in Bangladesh, 2020 2nd International Conference on Sustainable Technologies for Industry 4.0 (STI), Dhaka, Bangladesh, 2020; pp. 1-4, doi: 10.1109/STI50764.2020.9350430.

70. Diakakis, M.; Deligiannakis, G.; Pallikarakis, A.; Skordoulis, M. Factors controlling the spatial distribution of flash flooding in the complex environment of a metropolitan urban area. The case of Athens 2013 flash flood event. International journal of disaster risk reduction, 2016; 18, pp. 171-180.
71. Idowu, D.; Zhou, W. Performance Evaluation of a Potential Component of an Early Flood Warning System—A Case Study of the 2012 Flood, Lower Niger River Basin, Nigeria. Remote Sens. 2019; 11(17):1970. https://doi.org/10.3390/rs11171970
72. Saaty, T.L. The Analytic Hierarchy Process: Planning, Priority Setting, Resources Allocation 1980; Mcgraw-Hill, New York.
73. Shannon, C.E.; Weaver, W. The Mathematical Theory of Communication. 1949; Univ. of Illinois Press, Urbana.

CHAPTER 5
GENERAL CONCLUSIONS

The ultimate goal of this research is to evaluate a remote sensing-based Flood Potential Index to predict floods in developing countries where ground monitoring for floods is lacking or inadequate due to expense and security concerns. Additionally, the research seeks to understand the land use changes responsible for incessant flooding in Lagos State, Nigeria, in the context of flood hazard mapping and how all the different components could function in a people-centered early flood warning system

5.1 Flood Potential Index

The flood potential amount is the amount of incoming water that cannot enter storage for a coming month based on the observed maximum storage capacity for the basin of interest. The normalized flood potential amount, which is the FPI when close to 1, indicates an abnormally high difference between precipitation and storage ability which is an indication of flooding.

5.1.1 GRACE-Based Flood Potential Index

The GRACE-based FPI, when evaluated over the Lower Niger River Basin (LNRB) to test its accuracy on the prediction of the 2012 catastrophic flooding in Nigeria, showed some promise on improving flood prediction in Nigeria. We also assessed the predisposition of the LNRB to flooding before the flooding months by observing the storage deficit (Sdef) variable derived from the GRACE data. The GRACE Sdef provides insight into the soil moisture condition before the 2012 flooding situation, suggesting when the LNRB has been filling up with water since July 2012, when the basin was full, and followed by floods in September 2012. This is as expected as soil moisture serves as a proxy in flood studies [1]. The index performance over the LNRB was compared to the Dartmouth Flood Observatory (DFO) reports for the basin in 2012, and there was a good agreement between the flood prediction by the GRACE-FPI and the DFO flood report suggesting the index could be used for flood prediction in Nigeria.

5.1.2 Water-Budget-based Flood Potential Index

The Terrestrial Water Storage Anomaly (TWSA), the signal the GRACE data present, represents the sum of all waters on and beneath the surface and is similar to the change in storage from the traditional water budget model. We went further to compare their similarities statistically, and the result was a strong correlation between them. Consequently, we developed another index using the traditional water budget equation at the same resolution as the GRACE data. Overall, the GRACE-FPI and Water-Budget-FPI predicted floods in the same area in the LNRB.

5.2 GRACE Limitation

The coarse spatial and temporal resolution of GRACE, which limits its use for hydrological studies in smaller basins, was assessed by proposing the use of water budget data with finer spatial and temporal resolution to derive the Water-Budget-based FPI. The performance of the derived Water-Budget-based FPI was tested in the Mississippi River basin in the US. The index predicted the May 2011 and 2019 flooding in the basin, comparing statistically well to the GRACE-FPI, thereby showing potential for predicting floods in smaller basins. We infer the Water-Budget-based FPI, when used with the GRACE-FPI, could improve flood prediction using remote sensing data.

5.3 Flooding in Lagos State Nigeria

The rise in population leads to an increased demand for housing, which gives rise to urban development with environmental consequences such as incessant flooding and is investigated in Lagos State to understand the link between this phenomenon.

5.3.1 Wetland Loss

Wetlands are areas of land that are flooded by water either permanently or seasonally. Part of their use is to provide flood and erosion control. There are different types of wetlands and several ways to divide them. NOAA classifies wetlands into five general types: marine (ocean), estuarine (estuary), riverine (river), lacustrine (lake), and palustrine (marsh). Typical names for wetlands include marshes, estuaries, mangroves, mudflats, mires, ponds, fens, swamps, deltas, coral reefs, billabongs, lagoons, shallow seas, bogs, lakes, and floodplains, to mention a few. The two types of wetlands prevalent in the Lagos area are swamps and mangroves [2]. Rapid urbanization and urban developments are known to create negative impacts on the environment [3] as they result in

changes in landscape patterns, ecosystem functions, and their ability to carry out functions in support of human populations. This is prevalent when rapid or unplanned urban expansion occurs in areas of highly vulnerable systems such as wetlands. The conversion of large areas of wetlands to built-up areas results in increased impervious surfaces, which result in flooding and altered aquifer recharge [4].

We explored the changes in land use resulting in flooding in Lagos state. Our Land Use Land Cover analysis for 1986, 2000, 2016, and 2020 suggests that Lagos State was mainly a wetland environment in 1986 (supporting the obvious geographic location that Lagos as a coastal city), which is now a megacity with a more developed land area in 2020. We found that, of all the four land cover types identified in Lagos State (water, wetland, vegetation, and developed), the wetland was the major land cover in 1986, and by 2020, it was the least while developed had an approximately 100% increase. We infer that the developed land cover in Lagos state increases at the expense of other land cover types, especially the wetland land cover.

5.3.2 Development in Flood Hazard Zones

The assessment of land use changes related to flood hazard zonation in Lagos State suggests the replacement of wetland areas with urban development in very high to moderately high flood hazard areas. As suggested by our studies, flood hazard criteria revealed that low elevation and heavy rainfall are important defining factors for flooding in the state. With this, we could categorize the causes of flooding in Lagos State into natural and anthropogenic causes. A combination of low elevation, heavy rainfall (natural causes), and encroachment of urban development in flood hazard areas (anthropogenic) could be the reason for the rise in incessant flooding in Lagos State.

5.4 Summary of Research Contribution

Addressing flooding in most developing countries comes down to identifying the causative factors and hydrologic variables that serve as a precursor to flooding. These would require having a standard system for data acquisition for hydrologic modeling. Many of these systems are absent in most developing countries, especially in the rural areas where most of the flooding events result in loss of lives. However, this research has shown that [5]

- Remote sensing data could make a difference in developing countries such as Nigeria, where sophisticated ground measurements are absent.
- The GRACE-FPI and WB-FPI could be used for flood prediction in Nigeria, provided there is continuous data available.
- Where satellite data for estimation of the water budget parameters are present, the WB-FPI could predict flooding on a basin scale, especially when flooding results from heavy precipitation.
- The flood hazard mapping presented in this study combined with the flood potential method could serve as components of an early warning system in Nigeria.

Furthermore, our research presents [6-8]

1. A low to no cost approach for flood prediction in developing countries (especially Nigeria) using publicly available satellite datasets
2. A new Flood Potential Index (WB-FPI) using the traditional water budget estimates method
3. An approach to handling the GRACE data limitation of coarse spatial and temporal resolution using water budget parameters with finer spatial and temporal resolutions for estimating the water budget TWSA
4. A map-matrix-based, post-classification LULC change detection method to estimate multi-year land cover changes over a few decades
5. A combined/hybrid Analytical Hierarchy Process (AHP) and Shannon Entropy weighting method to carry out a weighted overlay MCDM flooding mapping
6. An approach to put LULC changes in the context of flood hazards in other to identify the possible causes of continuous rise in flooding in Lagos State, Nigeria

5.5 Future Work

The development of an operational flood prediction system for Nigeria presents many aspects to explore because of the growing number of human populations living within flood hazard zones. The functionality of the FPI in an early warning system still needs to be assessed and evaluated because of the required need for accuracy in the estimation of flood magnitude, location, and timing to save lives and properties. Flooding is an annual occurrence in Nigeria, and the level of

the havoc caused is on the rise, especially in riverine and coastal areas. Hence, the need for an operational, low to no cost operational flood warning system cannot be over-emphasized. Our study showed that the FPIs could predict flooding in developing countries where flooding is mostly because of heavy rainfall. Also, we established that remote sensing data could be used for flood hazard mapping and LULC change analysis. Therefore, with further evaluation and data availability, the GRACE and Water Budget FPI coupled with other ancillary data could be used as an operational flood prediction tool in developing countries, especially Nigeria. It could be combined with other remote sensing methods to form the first component of an early warning system in flood-prone areas of the country. We suggest more work to be done on evaluating how all the parts of this research would fit into a people-centered early flood warning system, especially in developing countries whereby the flood hazard mapping and the FPIs methods could be the risk knowledge and monitoring/warning service component of the system.

5.6 References

[1] Beven, K. J., and Kirkby, M. J. (1979). A physically based, variable contributing area model of basin hydrology, Hydrol. Sci. Bull., 24, 43–69.

[2] Obiefuna, J.; Nwilo, P. C.; Atagbaza, A. O.; and Okolie, C. J. (2013). Spatial Changes in the Wetlands of Lagos/Lekki Lagoons of Lagos, Nigeria. Journal of Sustainable Development; Vol. 6, No. 7; https://doi.org/10.5539/jsd.v6n7p123.

[3] UN-Habitat. (2010). Urban Development, Biodiversity and Wetland Management: Expert Workshop Report. Expert Workshop, 16 - 17 November 2009. Kenya Wildlife Training Institute, Naivasha, Kenya.

[4] Odunuga, S., and Oyebande, L. (2007). Change Detection and Hydrological Implications in the Lower Ogun Flood Plain, SW Nigeria. In Owe, M., & Neale, C. (Eds). Proceedings of Symposium on Remote Sensing for Environmental Change Detection. International Association of Hydrological Sciences (IAHS) Publication, 316, 91-99.

[5] Idowu, D. and Zhou, W. (2019) Performance Evaluation of a Potential Component of an Early Flood Warning System—A Case Study of the 2012 Flood, Lower Niger River Basin, Nigeria. Remote Sens. 11(17), 1970; https://www.mdpi.com/2072-4292/11/17/1970.

[6] Idowu, D.; Zhou, W. (2021). Land Use and Land Cover Change Assessment in the Context of Flood Hazard in Lagos State, Nigeria. Water 2021, 13(8), 1105; https://doi.org/10.3390/w13081105.

[7] Idowu, D., and Zhou W., (in press), Land use land cover assessment and flood hazard mapping in Lagos State (Nigeria) using optical remote sensing data, 3rd Conference of the Arabian Journal of Geosciences (CAJG), 2-5 November 2020, Sousse Tunisia.

[8] Idowu, D., and Zhou W., (accepted, Paper no - EEG-D-20-00056), Spatio-temporal Evaluation of Flood Potential Indices for Watershed Flood Prediction in Mississippi River Basin, USA, Environmental and Engineering Geoscience.

APPENDIX A

COPYRIGHT PERMISSION

Figures 1.2 – 1.4: These are open access images distributed under the Creative Commons Attribution License which permits unrestricted use, distribution, and reproduction in any medium, provided the original work is properly cited.

This is a screenshot of the copyright permission received from the Engineering and Environmental Geosciences journal.

From: **Shakoor, Abdul** <ashakoor@kent.edu>
Date: Thu, Apr 29, 2021, 10:17 AM
Subject: Re: EXT: Copyright Permission Request for Accepted Journal (Paper no - EEG-D-20-00056)
To: Dorcas Idowu <doidowu@mymail.mines.edu>
Cc: kesmith6@kent.edu <kesmith6@kent.edu>

Dear Dorcas,
You have Journal's permission to include your accepted paper, "Spatiotemporal Evaluation of Flood Potential Indices for Watershed Flood Prediction in Mississippi River Basin, USA" (EEG-D-20-00056), as a chapter in your dissertation.. Thank you for your contribution to the journal and good luck with your dissertation.
Abdul Shakoor, Co-Editor
Environmental and Engineering Geoscience journal

From: Dorcas Idowu <doidowu@mymail.mines.edu>
Sent: Wednesday, April 28, 2021 12:51 PM
To: em@editorialmanager.com <em@editorialmanager.com>; Shakoor, Abdul <ashakoor@kent.edu>; kesmith6@kent.edu <kesmith6@kent.edu>
Subject: EXT: Copyright Permission Request for Accepted Journal (Paper no - EEG-D-20-00056)

Dear all,

I hope this email finds you all well and safe at this time.

I am a co-author for the paper "Spatiotemporal Evaluation of Flood Potential Indices for Watershed Flood Prediction in Mississippi River Basin, USA" with paper no - EEG-D-20-00056.

Colorado School of Mines allows me to include published or accepted papers into my dissertation chapters provided I get an approval or permission from the journal. I want to include the accepted manuscript by the EEG journal in my thesis and would like to know how I can obtain the permission of EEG.

Hoping to hear from you soon. Thank you.

Kind regards,

Dorcas Idowu
Ph.D. Candidate
Department of Geology and Geological Engineering
COLORADOSCHOOLOFMINES
EARTH • ENERGY • ENVIRONMENT

Copyright permission from the EEG journal.

APPENDIX B

SUPPLEMENTAL ELECTRONIC FILES

Relevant electronic files are submitted as part of the dissertation. The files contain a collection of geospatial datasets and tables used for analysis. It also includes figures created from the geospatial analysis. These files are available on request. All request may be directed to wzhou@mines.edu.